TECHNISCHE UNIVERSITÄT MÜNCHEN
Fakultät für Medizin
Nuklearmedizinische Klinik des Klinikums rechts der Isar

Innate Cytokine Networks Link Atherosclerosis and Bacterial Sepsis

Philipp J. Rauch

Vollständiger Abdruck der von der Fakultät für Medizin der Technischen Universität München zur Erlangung des akademischen Grades eines

Doktors der Medizin

genehmigten Dissertation.

Vorsitzender:
Univ.-Prof. Dr. Ernst J. Rummeny

Prüfer der Dissertation:
1. Univ.-Prof. Dr. Markus Schwaiger
2. Univ.-Prof. Dr. Hans-Henning Eckstein
3. Univ.-Prof. Dr. Karl-Ludwig Laugwitz

Die Dissertation wurde am 29. Februar 2016 bei der Technischen Universität München eingereicht und durch die Fakultät für Medizin der Technischen Universität München am 12. Oktober 2016 angenommen.

TABLE OF CONTENTS

This publication-based dissertation comprises the following manuscripts enclosed in the appendix: RAUCH ET AL., 2012 and ROBBINS, CHUDNOVSKIY*, RAUCH* ET AL., 2012 (*equal contributions). Passages contained in the original publications have been incorporated into this dissertation, in adapted form or verbatim, where appropriate.*

INTRODUCTION

Atherosclerosis is a chronic inflammatory disease of the vasculature and the primary cause of myocardial infarction and ischemic stroke (Hansson and Libby, 2006). The mortality associated with these complications and the disease's rising incidence, particularly in emerging nations, make it the leading cause of death globally (World Health Organization, 2014).

The pathophysiology of atherosclerosis is characterized by a multifaceted process that most frequently starts to develop at bifurcations of arterial blood vessels, where laminar blood flow becomes interrupted (Swirski et al., 2009b). Resulting turbulent flow conditions and non-laminar shear-stress on the endothelium favor immune cell recruitment into the arterial intima, which marks the beginning of atherosclerotic plaque development (Libby, 2002; Hansson and Libby, 2006). The second major hallmark of atherogenesis is the gradual accumulation of lipid droplets, the most commonly encountered form being low-density lipoproteins (LDL), which become oxidized as the early, streak-like lesion progresses into its mature form, called atheroma (Libby et al., 2011). Atheromatous plaques feature a core region containing lipid-laden foam cells, apoptotic cellular debris and free extra-cellular lipids like cholesterol. This core is encircled by proliferating smooth muscle cells that produce a collagen-rich matrix, which poses a mechanically resilient barrier separating the lipid core from the vessel lumen (Libby et al., 2011; Weber and Noels, 2011).

Despite the chronic nature of the processes building up the atherosclerotic plaque, its evolution does not appear to be a gradual process. Longitudinal studies in humans undergoing up to four coronary angiograms per year (Yokoya et al., 1999; Bruschke et al., 1989) revealed that in the majority of cases, progression occurs in sporadic surges of growth, although gradually increasing luminal obstruction was also observed in some of the lesions studied. Thus, future lesion growth is very hard to predict on the basis of previously gathered morphological information alone, not because of technical limitations, but due to the biological behavior inherent to the

lesions. Mechanistically, the sudden acceleration in development can be ascribed to several distinct types of events (Libby, 2002): First, atherosclerotic plaques exhibit angiogenic activity, likely mediated by vascular endothelial growth factor A (VEGF-A) secreted by lesional macrophages. Newly created, fragile micro-vessels are sites of predilection for intra-plaque hemorrhage and thrombosis (Khurana, 2005). Platelets become activated in this process (Huo and Ley, 2004) and can initiate lesion growth through transforming growth factor beta (TGF-β) production, which is a potent activator of smooth muscle cells (Assoian and Sporn, 1986). On the other hand, there are those events afflicting the plaque-lumen interface: Desquamation of endothelial cells is frequently noted on pathological examination of arterial specimens with atherosclerosis (Ross and Glomset, 1976) and can serve as a root for intraluminal thrombosis through exposure of Von Willebrand Factor (vWF) and other sub-endothelial matrix proteins.

Professional phagocytes, and among them, monocytes in particular, are viewed as central cellular protagonists of atherosclerosis (Swirski et al., 2009b). Circulating monocytes adhere to activated endothelium through very late antigen 4 (VLA-4) interaction with initially exposed vascular cell-adhesion molecule 1 (VCAM-1), and subsequently infiltrate the nascent atherosclerotic lesion along with T lymphocytes (Meerschaert and Furie, 1995). Monocyte accumulation into lesions increases over time and has been found to be proportionate to severity of disease (Swirski et al., 2006). Under the influence of locally produced macrophage colony-stimulating factor (M-CSF), newly recruited monocytes differentiate into inflammatory lesional macrophages (Shi et al., 2000), promoting progression of atherosclerosis: Macrophages ingest oxidized lipoproteins via scavenger receptors such as CD36, lectin-type oxidized low density lipoprotein receptor 1 (LOX1) or scavenger receptor A (SRA), and thus as lipid-rich foam cells, become part of the disease's physical bulk (Swirski et al., 2009b). Foam cells also express several types of Toll-like receptors (TLR), and there is solid evidence that oxidized LDL (oxLDL) can initiate the TLR signaling cascade, eventually leading to translocation of nuclear factor-κB (NF-κB) into the nucleus and production of pro-inflammatory cytokines (Higashimori et al., 2010). Of note, neutrophil granulocytes, the second major type of phagocyte known

to infiltrate atherosclerotic lesions, have been ascribed a role in plaque rupture and, more recently, have also been implicated in early lesional development in a chemokine (C-C motif) ligand 5 (CCL5) dependent manner (Soehnlein, 2012).

Consequentially, leukocytosis in general, and monocytosis in particular, have been identified as key risk factors for atherosclerosis and are thought to be causally linked to disease (Swirski et al., 2009b; 2007; Tacke et al., 2007; An et al., 2008). Understanding how leukocytosis and monocytosis develop is therefore essential to understanding the evolution of atherosclerosis. Recent findings have identified cell-intrinsic mechanisms that link reverse cholesterol transport and ATP-binding cassette transporters, subfamily A and G (ABCA1 and ABCG1) with the proliferation of hematopoietic stem and progenitor cells (Yvan-Charvet et al., 2010). However, little is known about the (micro)-environments in which monocytosis arises or its extrinsic orchestrating components.

The spleen is a secondary lymphoid organ that can be structurally divided into two compartments, the red pulp and the white pulp. The red pulp's cords, created by fibroblasts and reticular fibers, allow for an open blood circulation to develop between themselves, and are also home to vast numbers of macrophages (Mebius and Kraal, 2005). Together with the venous sinuses that retrieve blood from the open circulation, these red pulp macrophages form an efficient filtration and recycling system for old and damaged erythrocytes, and in particular for their heme-bound iron content (MacDonald et al., 1987). The red pulp also harbors plasmablasts and plasma cells, and is thus an important site of antibody production. The spleen is known to be indispensable for effective immune defense against infections with encapsulated bacteria: in splenectomized patients, such infections rapidly progress to septicemia and carry a high mortality (Di Sabatino et al., 2011). Antigen recognition by B cells, which precedes plasma cell differentiation, occurs in the white pulp of the spleen, where B cells pass through the T cell zones surrounding the terminal white pulp arterioles, in order to eventually clonally expand in the B cell follicles (Mebius and Kraal, 2005). They then transit via the splenic marginal zone to exit the follicle and migrate into the red pulp cords in a sphingosine-1-phosphate

receptor-1 (S1PR1)-dependent manner (Arnon et al., 2013). The marginal zone, located between white and red pulp, serves as an interface between innate and adaptive immunity, bringing together marginal-zone (MZ) B cells with MARCO (macrophage receptor with collagenous structure)-positive marginal-zone macrophages. MZ B cells depend on these macrophages for proper localization, and act as first responders to blood-borne pathogens, making use of an opportune hemodynamic architecture allowing first pass of arterial blood through the marginal zone (Cerutti et al., 2013).

Recently, the spleen has been found to contain a reservoir of undifferentiated, bona-fide monocytes that cluster in the red pulp and vastly outnumber their circulating counterparts. The reservoir monocytes are relatively immotile but are distinct from macrophages and dendritic cells. In response to distant injury, splenic monocytes increase their motility, exit the spleen *en masse*, accumulate in acutely injured tissue, and participate in healing (Swirski et al., 2009a). It is not known whether and how the monocyte reservoir participates in chronic diseases such as atherosclerosis. Interestingly, a study on World War II veterans that had undergone splenectomy for trauma revealed an excess mortality from cardiovascular events when compared to a non-splenectomized control group (Robinette and Fraumeni, 1977). As predisposition to such events tends to develop over years, studies into the long-term effects of the presence or absence of the splenic monocyte pool on monocytosis and on the development of atherosclerosis are necessary.

Hematopoietic stem and progenitor cells (HSPC) are capable of exiting the bone marrow (Goodman and Hodgson, 1962; Wright et al., 2001; Méndez-Ferrer et al., 2008). They can accumulate in a variety of suitable extramedullary sites, such as in niches adjacent to the splenic sinusoidal endothelium (Kiel et al., 2005), and either differentiate to tissue-resident myeloid cells or recirculate (Massberg et al., 2007; Si et al., 2010). Among other signals, growth factors such as granulocyte colony-stimulating factor (G-CSF) liberate HSPC from their bone marrow niches (Jaiswal and Weissman, 2009). Sphingosine-1-phosphate (S1P) regulates the balance between retention and recirculation of HSPC once they have accumulated in

extramedullary sites (Massberg et al., 2007). The third step of this cascade, extrinsic signals orchestrating differentiation and proliferation of HSPC in extramedullary sites, remains largely obscure. The second important consideration is one of quantity: Under steady state conditions, small numbers of circulating HSPC are thought to fulfill tissue surveillance functions and can react to inflammatory stimuli, such as gram-negative bacterial endotoxin lipopolysaccharide (LPS), with local differentiation (Massberg et al., 2007). On the other hand, extramedullary hematopoiesis that is quantitatively relevant to the body's circulating leukocyte pool is thought to occur during fetal development and in a number of genetic and myeloproliferative conditions both in rodents and in humans (Freedman and Saunders, 1981; Dzierzak and Medvinsky, 1995; Hassan and Neiman, 1985; Lowell et al., 1996; Snover et al., 1981, Wolber et al., 2002). Under these conditions, the spleen and the liver become secondary hematopoietic organs, where mass production of leukocytes is known to occur. However, the extent to which extramedullary hematopoiesis may be relevant in other, non-developmental and non-neoplastic pathophysiological contexts, acute or chronic, and how it may be regulated, has not been studied systematically.

Consequentially, the first aim of this work was to investigate the potential role of extramedullary hematopoiesis to the development and maintenance of atherosclerosis. The second, interconnected aim was to characterize the molecular mechanisms that regulate myelopoiesis in this setting, with a particular focus on the hematopoietic cytokines granulocyte-macrophage colony-stimulating factor (GM-CSF) and interleukin-3 (IL-3). Together, these two aims comprise the first enclosed manuscript, ROBBINS*, CHUDNOVSKIY*, RAUCH* ET AL, 2012 (*equal contributions).

While the inflammatory nature of atherosclerosis has only been recognized in recent decades (Libby, 2002), sepsis, on the other hand, can be viewed as the prototypic inflammatory response that occurs in response to pathogen associated molecular patterns (PAMP) recognized by the host through a family of dedicated receptors (Mogensen, 2009). The term sepsis was coined by Hippocrates to describe decay of flesh, or more generally, of organic matter. Since then, understanding of sepsis much evolved to incorporate modern germ theory over the course of the late 19th and

early 20th century (Angus and van der Poll, 2013). 1992 marked the introduction of the currently accepted definition of sepsis as systemic inflammation occurring in response to infection (Bone et al., 1992). Along with that definition came the recognition of the host, as opposed to the pathogen, as the preeminent driver of sepsis pathogenesis.

Sepsis is a growing problem especially in critically ill patients, with as many as 2% of patients admitted to U.S. hospitals experiencing an episode of severe sepsis (Angus et al., 2001; Angus and van der Poll, 2013). With the disease's incidence rising over the past 30 years, the currently available therapeutic agents with proven benefit remain targeted solely at the invading pathogen, in the form of antibiotics.

While the insights gained on the self-inflicted nature of sepsis pathophysiology did spur the development of treatment approaches targeting the host response, such alternative strategies, including anti-lipopolysaccharide agents and coagulation modifiers, have failed to gain regulatory approval (Opal et al., 2014) or, in the case of activated protein C, were withdrawn from the market after post-approval studies failed to confirm efficacy of the drug (Martí-Carvajal et al., 2012). Along with these disappointments came the recognition of a more ambiguous nature of the host response in sepsis: while the early, hyper-inflammatory phase, characterized by an overwhelming cytokine storm culminating in end-organ injury and shock, had previously been viewed as the major component of sepsis immunopathogenesis and the prime therapeutic target, experimental and clinical evidence increasingly points towards sepsis-induced immunosuppression, manifesting in a failure to clear the primary and potential secondary pathogens, as a central cause of morbidity and mortality in sepsis (Hotchkiss et al., 2013). On the cellular level, a myriad of changes to elements of both the innate and adaptive immune system have been observed in protracted sepsis, including T cell exhaustion (Boomer et al., 2011), decreased antigen-specific antibody production by B cells (Mohr et al., 2012), decreased HLA-DR expression on monocytes (Döcke et al., 1997), and decreased reactive oxygen species release by neutrophils (Kovach and Standiford, 2012). While these changes

provide a cellular basis for the immune deficiencies observed, the knowledge on their orchestrating cellular and molecular factors remains limited.

Findings derived from the first two aims characterizing the innate immune response in atherosclerosis hinted at striking similarities to some aspects of immune regulation in acute inflammation. This realization prompted me to broaden the scope of the studies and investigate regulation of the innate immune response by GM-CSF in the context of acute inflammation in general, and in an experimental model of polymicrobial sepsis in particular. Results from these studies are described in the second enclosed manuscript, RAUCH ET AL., 2012.

DETAILED METHODS

Animals

Both male and female mice were used in this study, all housed under special pathogen-free conditions according to Massachusetts General Hospital Center for Comparative Medicine (CCM) guidelines. All animal protocols were approved by the Animal Review Committee at Massachusetts General Hospital (MGH).

C57BL/6J (wt)

C57BL/6J was the background strain for all genetically modified animals in this study, and wild-type (wt) mice from this strain were also used as control animals in our experiments. The C57BL/6J strain has a principal role in mouse genetics (Mouse Genome Sequencing Consortium et al., 2002) and was also the first strain to have its entire genome sequenced in the year 2002. In the context of cardiovascular research, the strain is preferred over others because of its inherent susceptibility to mild hyperlipidemia and atherosclerosis when fed a diet high in fat and cholesterol, which can be greatly increased by genetic alterations (Whitman, 2004).

ApoE$^{-/-}$

ApoE$^{-/-}$ (B6.129P2-Apoe^{tm1Unc}) male and female mice used here had been backcrossed to the C57BL/6 background for at least ten generations. ApoE$^{-/-}$ mice are homozygous for a disrupted apolipoprotein E (ApoE) allele and their serum is completely devoid of ApoE protein. The lack of ApoE primarily impairs uptake of chylomicron and VLDL remnants by hepatocytes, which in turn leads to development of LDL-dominated hypercholesterolemia. The phenotype resembles type III hyperlipoproteinemia in humans, which is caused by a missense mutation in the ApoE gene that decreases binding of ApoE to its receptor (Zhang et al., 1992) 50-fold. ApoE$^{-/-}$ mice fed a normal chow diet develop fatty streaks in the proximal aorta starting at three months of age, which then quickly progress to advanced, complex atherosclerotic lesions. The phenotype is exacerbated when the mice are fed an atherogenic diet. In this study, groups of animals were placed on a Western diet

(21.2% fat w/w; 0.2% cholesterol w/w) (Harlan Teklad, Madison, WI) starting at 8-10 weeks of age. The remaining animals continued to consume a regular chow diet.

LDLR$^{-/-}$

(LDLR$^{-/-}$)ApoB48$^{-/-}$ (B6;129S-Apob^{tm2Sgy} Ldlr^{tm1Her}/J) male and female mice had been backcrossed to the C57BL/6 background for at least ten generations. Homozygous LDLR$^{-/-}$ mice lack functional LDL receptor genes, disrupting re-uptake of LDL as well as intermediate density lipoproteins (IDL) from the blood into the liver. As a result, the mice develop hypercholesterolemia, albeit to a lower extent when compared to ApoE$^{-/-}$ mice. The mice are very susceptible to receiving an atherogenic diet, although their atherosclerotic phenotype is milder than that of ApoE$^{-/-}$ mice, develops more slowly, and mainly features lesions with a simple morphology without necrosis or calcification (Getz and Reardon, 2012). In our study, the animals were placed on a Western diet (21.2% fat w/w; 0.2% cholesterol w/w) (Harlan Teklad) starting at 8-10 weeks of age.

CD45.1$^{+/+}$

The B6.SJL-Ptprc^{a}Pep3^{b}/BoyJ strain of mice carries a differential allele of the CD45 antigen (protein tyrosine phosphatase, receptor type C). This allele is referred to as CD45.1, in contrast to the CD45.2 allele normally found in mice of the C57BL/6J background. CD45 is expressed by most hematopoietic cells and it thus suitable for tracking leukocytes in transplantation and adoptive transfer studies using allele-specific antibodies. In the results section of this work, mice carrying two CD45.1 alleles (CD45.1$^{+/+}$) and cells derived from these mice will be referred to as CD45.1, and mice or cells carrying two CD45.2 alleles (CD45.2$^{+/+}$) will be referred to as CD45.2.

CD45.1$^{+/+}$ ApoE$^{-/-}$

CD45.1$^{+/+}$ ApoE$^{-/-}$ mice constitute a novel strain generated in this study after backcrossing ApoE$^{-/-}$ mice to CD45.1$^{+/+}$ mice.

GFP^{+}

Transgenic C57BL/6-Tg(UBC-GFP)30Scha/J (GFP^{+}) mice express enhanced Green Fluorescent Protein (GFP) under the human ubiquitin C promoter in all tissues, which permits cell tracking by flow cytometry and by intravital microscopy. These mice were purchased from Jackson Laboratories.

B cell (subset) deficient mice

B10.129S2(B6)-*Ighm*^{tm1Cgn}/J (μMT), B6(Cg)-*Tnfrsf13c*^{tm1Mass}/J (BAFFR-deficient), B6.129P2(C)-Cd19$^{tm1(cre)Cgn}$/J (CD19-deficient) female mice, purchased from Jackson Laboratories, were used in this study.

TLR signaling pathway component knock-out mice

B6.B10ScN-Tlr4$^{lps-del}$/JthJ (TLR4-deficient) MyD88-deficient and TRIF-deficient (*Ticam1*$^{-/-}$) mice on a C57BL/6 background were a kind gift from Dr. Rodrigo Mora of Massachusetts General Hospital.

GM-CSF-deficient mice

GM-CSF-deficient mice (*Csf2*$^{-/-}$) on a C57BL/6 background were a gift from Dr. Randy Seeley of the University of Cincinnati.

Animal models and in vivo interventions.

Experiments involving microsurgery were performed with expert help from the MGH Center for Systems Biology Animal Surgery Core, led by Dr. Jose Luiz Figueiredo.

Splenectomy

Under isoflurane anesthesia, the peritoneal cavity of mice was opened and the splenic vessels were ligated using a 6.0 silk suture (Ethicon, Albuquerque, NM). The spleen was then carefully removed. For control experiments, the peritoneum was opened, but the spleen was not excised. The procedure itself does not change the number of circulating monocytes and neutrophils in the steady state (Swirski et al., 2009a).

Spleen transplantation

Spleen transplantation was carried out as previously described (Swirski et al., 2009a): Donor mice were anesthetized with a subcutaneous (s.c.) injection of ketamine (90 mg/kg) and xylazine (10 mg/kg), followed by an intravenous (i.v.) injection of 200 units of heparin (American Pharmaceutical, Schaumburg, IL). The complete inhibition of clotting ensures that no vascular or intra-splenic thrombosis occurs. In deep anesthesia, the thorax was then opened and the right atrium sectioned to allow blood to exit during perfusion. Over a period of three minutes, the entire mouse was then perfused with a total of 15 mL of normal endotoxin-free saline (154 mM NaCl) through a 25G needle inserted into the apex of the left ventricle. At the end of this procedure, fluid exiting the right atrium was clear which indicates thorough removal of the donor blood. The pancreas, the spleen and the abdominal vasculature in the epigastric region were identified and ligated with 6.0 cotton (Ethicon). The celiac artery was then isolated, and the hepatic and gastric artery ligated with 10.0 suture (Ethicon). The abdominal aorta was ligated and cut just below the celiac artery with micro-dissection scissors (Roboz Surgical Instrument Co., Rockville, MD), and also dissected above the celiac artery. This approach resulted in an aortic cuff connected to the splenic artery, which allowed vascular anastomosis of the spleen to the recipient. Following ligation of the bile duct, the portal vein was isolated, and the superior and inferior mesenteric and gastric veins were ligated. The portal vein was intersected closely to the liver. The entire organ package containing the vascular connections, spleen and the pancreas was then removed and stored in ice-cold saline for 15 minutes while the recipient was prepared. The recipient (*CD45.1*$^{+/+}$) was anesthetized with isoflurane (1-2% v/v), supplemented with oxygen (1-2 L/min). An abdominal midline incision was made and the inferior vena cava and the descending aorta isolated below the renal arteries. The recipient vessels were clamped with an atraumatic vascular clamp (Accurate Surgical & Scientific Instruments Co., Westbury, NY) and opened with micro-scissors. The portal vein was anastomosed to the inferior vena cava and the donor aortic cuff was connected with an end-to side anastomosis to the recipient aorta using 10.0 suture. The clamp was then opened to restore blood flow.

Endotoxin-induced peritonitis and peritoneal lavage

Mice were administered 10 μg of LPS in PBS (Sigma) daily by i.p. injections over the course of 4 days, unless otherwise stated. For some experiments, different TLR ligands (all Invitrogen) were administered i.p. daily. TLR1/2: Pam3CSK4 (100 μg/mouse), TLR3: Poly(I:C) (200 μg/mouse), TLR5: FLA-ST (10 μg/mouse), TLR2/6: FSL-1 (10 μg/mouse), TLR7: R848 (25 μg/mouse), TLR9: CpG ODN 1668 (10 μg/mouse). Controls received PBS alone. For select experiments, the peritoneal cavity was lavaged with 10 mL of PBS to retrieve infiltrated and resident leukocytes.

Sepsis models

Cecal ligation and puncture (CLP), a rodent model of sepsis, was carried out as previously described (Rittirsch et al., 2009). In brief, the peritoneal cavity was opened during isoflurane anesthesia, the cecum was exteriorized and ligated about 2 mm distal of the ileo-cecal valve using a non-absorbable 6-0 suture. The distal end of the cecum was then perforated using a 23 G needle, and a small drop of feces was extruded through the puncture. The cecum was relocated into the peritoneal cavity, and the peritoneum was closed. Animals were then resuscitated by s.c. injection of 1 mL of saline and closely monitored. For experiments requiring single-pathogen gram-negative infection, animals were injected i.p. with 10^7 CFU of *E. coli.* Age-matched controls receiving sham surgical procedures were included for all procedures.

Parabiosis

The procedure, adapted from (Bunster and Meyer, 1933) was conducted as previously described (Swirski et al., 2009a): After shaving the corresponding lateral aspects of each mouse, matching skin incisions were made from behind the ear to the tail of each mouse, and the subcutaneous fascia was bluntly dissected to create about ½ cm of free skin. The olecranon and knee joints were attached by a mono-nylon 5.0 (Ethicon), and the dorsal and ventral skins were approximated by continuous suture. After an interval of several weeks, mice in parabiosis were surgically separated by a reversal of the procedure. One group was splenectomized, as described above. Chimerism in the blood was defined for gated monocytes,

neutrophils and Lin^+ cells (mostly lymphocytes) as $\frac{\%CD45.1}{\%CD45.1+\%CD45.2}$ in CD45.2 mice, and as $\frac{\%CD45.2}{\%CD45.2+\%CD45.1}$ in CD45.1 mice.

Adoptive transfer of GMP

Donor GFP^+ cells from the bone marrow were first enriched using anti-PE beads (Miltenyi Biotec GmbH, Bergisch-Gladbach, Germany) to deplete Lin^+ cells and then sorted using a BD FACSAria II (BD Biosciences, Franklin Lakes, NJ), as defined in the Cells/Flow Cytometry section. Typically, purity of the sorted population was >99.5%. 5×10^4 GMP were injected into the tail vein of non-irradiated recipient mice.

Anti-GM-CSF and IL-3 treatment

Mice were i.v. injected with 300 μg of blocking antibody against GM-CSF and IL-3 twice daily for four consecutive days. Control animals received 300 μg of anti-mouse IgG2a.

Cells

In vivo

Peripheral blood for flow cytometric analysis was collected by cardiac puncture, using a 50 mM EDTA solution as anticoagulant. Erythrocytes were lysed using BD FACS Lysing Solution (BD Biosciences). Total white blood cell count was determined by preparing a 1:10 dilution of (undiluted) peripheral blood obtained from the orbital sinus using heparin-coated capillary tubes in RBC Lysis Buffer (BioLegend, Inc., San Diego, CA). After organ harvest, single cell suspensions were obtained as follows: for bone marrow, femur and tibia of one leg were flushed with endotoxin-free phosphate-buffered saline (PBS; 154 mM NaCl, 5.60 mM Na_2HPO_4, 1.06 mM KH_2PO_4, pH 7.3-7.5, 287-309 mOsm/kg; Lonza, Basel, Switzerland). Spleens were homogenized through a 40 μm-nylon mesh under repeated flushing with PBS, after which erythrocyte lysis was performed on the spleens using RBC Lysis Buffer (BioLegend). For aortae, tissue was cut in small pieces and subjected to enzymatic digestion with 450 U/mL collagenase I, 125 U/mL collagenase XI, 60 U/mL DNase I and 60 U/mL hyaluronidase (Sigma-Aldrich, St. Louis, MO) in PBS for

1 h at 37°C while shaking. Total viable cell numbers were counted in an Improved Neubauer hemocytometer using Trypan Blue (Cellgro, Mediatech, Inc., Manassas, VA). To determine total bone marrow cellularity, one femur was estimated to represent 5% of total marrow (Colvin et al., 2004). For morphological assessment, cytospins were prepared from 5×10^4 cells and stained using HEMA 3 staining kit (Fisher Scientific, Waltham, MA).

In vitro

Cells were cultured in 96-well round-bottom plates (Corning) and kept in a humidified CO_2 incubator at 37°C for 48 hours. B1a, IRA-B and T-cells were cultured in RPMI-1640 medium supplemented with 10% fetal bovine serum, 25 mM HEPES, 2mM L-glutamine, 100 U/mL penicillin, 100 U/mL streptomycin and 50 µM 2-mercaptoethanol. Human Umbilical Vein Endothelial Cells (HUVEC) were cultured using the EGM-MV Bulletkit (Clonetics). All cell types were seeded at a density of 40,000 cells/100 μL medium.

Where indicated, LPS was added at 10 μg/mL.

Flow cytometry

The antibodies used for flow cytometric analyses in this work are listed in Supplemental Material/Expanded Methods and Results (ROBBINS*, CHUDNOVSKIY*, RAUCH* ET AL., 2012) and Supporting Online Material/Materials and Methods (RAUCH ET AL., 2012), respectively. Streptavidin-PerCP, Streptavidin-APC, Streptavidin-APC-Cy7 and V450-Streptavidin (BD Biosciences) were used to label biotinylated antibodies. Cathepsin activity was assessed using ProSense 680 (PerkinElmer). Cell cycle analysis was carried using FxCycle violet stain (Invitrogen). Apoptotic cells were identified as those cells falling within the subG_1 gate as previously described (Hotz et al., 1994). Contribution of newly-made cells to different cell populations was determined by *in vivo* labeling with 5-bromo-2'-deoxyuridine (BrdU). Mice received 1 mg of BrdU (BD Biosciences) by intraperitoneal (i.p.) injection. Incorporation was measured using either FITC or APC-conjugated anti-BrdU antibodies according to the manufacturer's instructions. Monocytes, macrophages/dendritic cells and neutrophils were identified as described previously (Swirski et al., 2009a).

Hematopoietic stem cells were identified as lineage $(Lin)^{low}$ (Lin = CD90/B220/CD19/CD49b/TER119/NK1.1/Gr-1/CD11b/CD11c) IL-7Rα^{-} CD117^{+} Sca-1^{+}. Myeloid progenitors were identified as Lin^{low} IL-7Rα^{-} CD117^{+} Sca-1^{-}. Within this population, granulocyte/macrophage progenitors (GMP) were CD34^{+} CD16/32^{+}, common myeloid progenitors (CMP) were CD34^{+} $CD16/32^{low}$ and megakaryocyte-erythroid progenitors (MEP) were CD34^{-} CD16/32^{-}. Data were acquired on an LSRII flow cytometer (BD Biosciences) and analyzed with FlowJo v8.8.6 (Tree Star Inc., Ashland, OR). Cells were sorted on a BD FACSAria II cell sorter (BD Biosciences).

Fluorescence reflectance imaging (FRI)

Mice were sacrificed 24 hours after intravenous injection of 5 nmol ProSense 680 (PerkinElmer) and excised aortas were imaged using a planar fluorescent reflectance imaging system (OV-110, Olympus) with an excitation wavelength of 680 nm. Light and near infrared fluorescence (NIRF) images were obtained with respective exposure times between 75 milliseconds and 60 seconds. Imaging procedures were performed with help from the MGH Center for Systems Biology Mouse Imaging Program (MIP).

Histology

Aortae and spleens were excised, embedded in O.C.T. compound (Sakura Finetek), and flash-frozen in isopentane and dry ice. 5 μm-thick frozen sections were used in all staining protocols. Immunofluorescence staining was carried out using the following primary antibodies: anti-CD11b, clone M1/70 (BD Biosciences), biotin anti-CD45.1: clone A20 (BioLegend), and biotin anti-CD45.2: clone 104 (BD Biosciences). In some cases, either streptavidin-Texas Red or streptavidin-fluorescein (GE Healthcare) were directly conjugated to primary antibodies. Biotinylated secondary antibodies were used when required. Cover slips were placed over specimens using mounting medium containing DAPI (Vector Laboratories) to identify cell nuclei. Samples were visualized using an epifluorescence microscope (Nikon Eclipse 80i, Nikon Instruments Inc.) equipped with a Cascade Model 512B camera (Roper Scientific). Immunohistochemical staining was used to detect GM-CSF (clone FL-144, Santa Cruz Biotechnology) and IL-3 (clone MP2-8F8,

BioLegend) on spleen sections. Following application of appropriate biotinylated secondary antibodies, samples were developed using a Vectastain ABC kit (Vector Laboratories) and AEC substrate (DakoCytomation). All sections were counterstained with Harris Hematoxylin. Masson trichrome (Sigma) and Oil Red O (Sigma) staining were performed to visualize collagen and lipid content, respectively. Hematoxylin and eosin (H&E) staining was performed to assess overall tissue morphology. Captured images were digitized automatically at 400x magnification using a Nanozoomer 2.0RS (Hamamatsu) and image analysis was done using IPLab (version 3.9.3; Scanalytics).

Molecular biology

Western blots

10^7 IgM^+ or IgM^- cells were sorted from spleens of LPS-treated mice, and stimulated, or not, in vitro with 1 μg/ml LPS and Golgi Plug for 5 hours. Pellets were then frozen in liquid nitrogen. For protein extraction sample pellets were resuspended in Ripa buffer (Boston Bioproducts, BP-116TX) supplemented with protease and phosphatase inhibitors (Thermo Scientific, PI-87786, PI-78420) and incubated on ice for 30 minutes. Samples were spun down and 15 μL of protein extract was mixed with 15 μL of Laemmli buffer (BioRad) in accordance with the manufacturer's instructions. Samples were developed by electrophoresis on a 4-15% polyacrylamide gel (BioRad). The proteins were transferred to a polyvinylidene difluoride membrane (Fischer) by dry transfer. Membranes were blocked with carnation milk and PBS supplemented with 0.05% Tween 20 overnight. Membranes were washed, stained initially with anti-GM-CSF antibody (MP1-31G6) (Abcam) followed by appropriate secondary antibody. For GAPDH stain the membrane was stripped with Restore buffer (Pierce), and stained with anti-glyceraldehyde-3-phosphate (GAPDH) (Rockland Immunochemicals for Research). Blots were developed with Western Lightning Chemiluminescence reagent (PerkinElmer) and molecular weights were compared to bands for Precision Plus Protein Western C standards (BioRad).

ELISA

ELISA was performed with R&D ELISA kits according to the manufacturer's instructions.

ELISpot

ELISpot was performed with Mabtech Mouse IgG and IgM according the the manufacturer's instructions.

Real-time PCR

Total RNA was isolated from cryostat-prepared 20 μm spleen sections or 3-10x10^4 FACS-sorted cells using the PicoPure RNA Isolation Kit (Arcturus) according to the manufacturer's instructions. cDNA was generated from 50-200 ng of total RNA per sample using the High Capacity cDNA Reverse Transcription Kit (Applied Biosystems). Real time PCR was performed in triplicates using the TaqMan Gene Expression Assay System on a 7300 Real-Time PCR System (Applied Biosystems). Primers Mm01290062_m1 (GM-CSF) were used (Applied Biosystems). Mean normalized expression was calculated using the Q-Gene Application (Simon, 2003) with 18S rRNA (Applied Biosystems) serving as endogenous control. At least three independent samples per group were analyzed.

Microarray gene expression profiling

B cell subsets from spleens or peritoneum of a group of 8-10 mice (per biological replicate) that received 10 μg LPS i.p. daily over the course of 4 days or from steady state were isolated by fluorescence activated cell sorting (FACS) to a purity of >99% in accordance with the Immunological Genome Project standard operating procedures (www.immgen.org). Cells were sorted directly into RLT lysis buffer, and total RNA was isolated using the RNeasy Mini Kit (Qiagen) according to the manufacturer's instructions. RNA quality was assessed using RNA pico lab chips on the Agilent Bioanalyzer. For all samples a RNA integrity number (RIN) above 8 could be achieved. Gene expression datasets were generated on Illumina Mouse Ref-8 gene expression arrays at the Broad Institute Genetic Analysis Platform (Broad Institute, 301 Binney St. Cambridge, MA 02142). Briefly, total RNA from the samples

was normalized to 20 ng/μL and the IlluminaTotalPrep-96 RNA Amplification Kit (Applied Biosystems, PN #4393543) protocol was used for amplification in a semi-automated process. The total RNA underwent reverse transcription to synthesize first-strand cDNA. This cDNA was then converted into a double-stranded DNA template for transcription. *In vitro* transcription synthesized aRNA and incorporated a biotin-conjugated nucleotide. The aRNA was then purified to remove unincorporated NTPs, salts, enzymes, and inorganic phosphate. Labeled cRNA was normalized to 150 ng/μL and hybridized to Illumina's MouseRef-8 v2.0 Expression BeadChip. The labeled RNA strand was hybridized to the bead on the BeadChip containing the complementary gene-specific sequence. After a 16 hour hybridization, the beadchips were washed and stained using a Cy3 streptavidin conjugate. Illumina's BeadArray Reader was used to measure the fluorescence intensity at each addressed bead location. Analysis of expression data was performed using the server hosted version of Gene Pattern (http://genepattern.broadinstitute.org) (Version 3.3.2, build Id: 9695, Java Version 1.6.0_21) (Reich et al., 2006). Illumina IDAT files were uploaded to Genepattern and a background subtracted .gct expression file was generated using the 'IlluminaExpressionFileCreator' with the MouseRef-8_V2_0_R2_11278551_A manifest file followed by quantile normalization (Workman et al., 2002) using the 'IlluminaNormalizer' module. Hierachical clustering was performed by submitting the normalized expression dataset to the 'HierachicalClustering' and 'HierachicalClusteringViewer' modules choosing pairwise complete linkage as clustering method and a Pearson correlation as the column distance measure (Reich et al., 2006). For principal component analysis the expression file was submitted to the 'PCA' and 'PCAViewer' modules choosing columns as the clustering method (Raychaudhuri et al., 2000). The dataset was displayed over principal components 2, 3 and 4. Data were deposited to the Gene Expression Omnibus (GEO) bank under Accesion Number GSE32372. To reveal distinct and common features among IRA-B cells, B1a B cells and plasma cells (PC) gene expression signatures for each B cell subset were defined based on the available gene expression dataset. To this end the Genepattern Comparative Marker Selection module was utilized using default parameters and for each pairwise comparison the cell type of interest was compared to all other available B cell subsets. The top 350 ranking genes were defined as

signature genes for the respective B cell subtype. The following comparisons were performed: IRA-B vs [Fo, B1a, T1, MZ, PC]; PC vs [Fo, B1a, T1, MZ, IRA-B]; B1a vs [Fo, IRA-B, T1, MZ, PC]. Subsequently Gene Set Enrichment Analysis was utilized to quantify the correlation between the IRA-B signature and B1a cells or PC respectively.

Statistics

Results were expressed as arithmetic mean ± standard error of the mean (SEM) or standard deviation, as appropriate. Statistical tests included unpaired, 2-tailed Student's t test using Welch's correction for unequal variances for two groups, and 1-way ANOVA followed by Tukey's or Bonferroni's Comparison Test for three or more groups. Statistical analysis was performed using GraphPad Prism software, version 5.0a. P values of 0.05 or less were considered to denote significance.

SUMMARY OF RESULTS: ROBBINS*, CHUDNOVSKIY*, RAUCH* ET AL. (*equal contributions)

Our studies in apolipoprotein E-deficient (apoE$^{-/-}$) mice consuming a diet high in fat and cholesterol (Western diet) for 20 weeks, a widely used mouse model of atherosclerosis, revealed a dramatic expansion of the myeloid, and specifically, of the monocyte reservoir in the spleen, microscopically expanding the splenic red pulp and macroscopically resulting in splenomegaly. Vascularized, short-term spleen transplantation combined with donor cell tracking using variant CD45 alleles showed a relevant contribution of splenic monocytes to the peripheral blood and atheromatous monocyte pool. The data additionally uncovered a surprisingly rapid lesional cell turnover.

Spleen-derived lesional monocytes and macrophages were found to be inflammatory, as defined by their exclusive belonging to the Ly6C^{hi} subset, proIL-1β expression, proteolytic activity and production of reactive oxygen species (ROS). Comparing lesional evolution in splenectomized and control mice showed that – while lesional size was slightly increased in the splenectomy group – these lesions contained less monocytes, macrophages and foam cells.

To determine whether the spleen is a mere storage, or rather a production site for myeloid cells in atherosclerosis, we quantified colony-forming activity and phenotypically defined hematopoietic stem and progenitor cell populations in the spleen in wild type and apoE$^{-/-}$ mice. As expected, splenic myelopoietic activity was negligible in the steady state, while there was a sizable, continuous and sustained increase in an atherosclerotic context. In contrast, myelopoietic activity in the bone marrow increased only transiently and was in fact outnumbered by splenic activity in many older animals with atherosclerosis. Adoptive transfer of highly purified granulocyte-macrophage progenitors (GMP), the most committed progenitor cell population known to give rise to both granulocytes and monocytes, confirmed active splenic monocytopoiesis *in vivo*. Long-term spleen transplantation experiments exceeding the lifespan of mature monocytes demonstrated infiltration of atheromata

by spleen-produced monocytes that partially differentiated into macrophages. This finding was corroborated by GMP adoptive transfer experiments into splenectomized mice, which accumulated significantly fewer donor-derived monocytes in the aorta than their non-splenectomized counterparts. Parabiosis experiments followed by separation, with or without concomitant splenectomy, substantiated the role of the spleen in maintaining the lesional monocyte pool.

Investigating myelopoietic cytokine production in atherosclerosis revealed significant expansion of IL-3 und GM-CSF producing cells in the spleen, but not in the bone marrow. Targeting these cytokines by neutralizing antibodies attenuated survival and proliferation of myeloid progenitors as well as mature monocytes and neutrophils in the spleen and largely reduced atherosclerosis-associated peripheral blood monocytosis and neutrophilia.

Lastly, we aimed to determine whether splenic myelopoiesis occurs in other forms of inflammation, and whether it can be visualized *in vivo*. Mice that received repeated injections of lipopolysaccharide (LPS) developed visible splenomegaly and splenic myelopoiesis resembling the findings in atherosclerotic animals. Intravital fluorescent microscopy after adoptive transfer of progenitors expressing green-fluorescent protein (GFP) showed formation of progeny clusters outside of blood vessels in the splenic red pulp. Co-transfer of progenitors expressing either GFP or red-fluorescent protein (RFP) led to clusters that were exclusively green or exclusively red, proving local clonal expansion.

The study concluded that extramedullary hematopoiesis supplements – and in certain cases may exceed – the bone marrow's contribution to the inflammatory myeloid cell repertoire in atherosclerosis in particular and in inflammation in general.

SUMMARY OF RESULTS: RAUCH ET AL.

Profiling of GM-CSF producing cells by intracellular flow cytometry in a mouse model of acute inflammation, consisting of daily injections of lipopolysaccharide (LPS) for 4 days, led to the unexpected discovery of a large GM-CSF producing cell population expanding preferentially in the spleen in response to inflammation. These cells were predominantly IgM^+ B lymphocytes. This finding was confirmed by Western blot analysis and quantitative PCR. Spatially, $GM\text{-}CSF^+$ B cells were located in the red pulp of the spleen, in close vicinity of myeloid cell clusters. Emergence of $GM\text{-}CSF^+$ B cells was also observed in *Escherichia coli* infection and in a mouse model of bacterial sepsis.

More detailed phenotypic, ontogenetic and functional analysis led to the conclusion that $GM\text{-}CSF^+$ B cells constitute a distinct subset, that we named IRA (innate response activator). IRA B cells display the distinct surface phenotype IgM^{high} $CD23^{low}$ $CD43^{high}$ $CD93^+$ $CD284^+$ VLA-4^{high}. Whole genome microarray analysis followed by unsupervised hierarchical clustering and principal component analysis grouped IRA B cells in a population separate from other known B1 and B2 cell subsets as well as plasma cells. Ontogenetically, parabiosis experiments demonstrated that IRA B cells derive from a circulating precursor. Detailed fate-mapping studies employing adoptive transfer approaches revealed that IRA B cells are derived from peritoneal B1a B cells that differentiate and relocate to the spleen upon an inflammatory stimulus, in an LFA-1 and VLA-4-dependent manner.

Using knockout mouse strains, we showed emergence of IRA B cells to depend on the TLR-4-MyD88 signaling pathway and on the B cell activating factor receptor (BAFFR). Adoptive transfer of TLR4-sufficient B1a B cells into a TLR-4 deficient environment demonstrated TLR-4 signaling on the B cell side to be sufficient for IRA B cell generation.

To elucidate the functional role of GM-CSF production by IRA B cells in bacterial sepsis, we subjected mixed chimeric mice lacking B cell-derived GM-CSF

production, or their appropriate controls, to cecal ligation and puncture, a faithful murine sepsis model. Mice lacking B cell-derived GM-CSF displayed decreased serum levels of IgM, reduced neutrophil phagocytic activity, and consequently increased bacterial titers. This in turn led to the development of a severe cytokine storm characterized by increased levels of IL-1β and TNFα, prominent hepatic and pulmonary pathologies, and significantly increased mortality.

The study concluded that GM-CSF production by a newly discovered B cell subset termed IRA is central to mounting an effective host response in microbial sepsis.

Statement of Contributions

This publication-based dissertation comprises the following manuscripts enclosed in the appendix and summarized above: RAUCH ET AL., 2012 and ROBBINS, CHUDNOVSKIY*, RAUCH* ET AL., 2012 (*equal contributions). I was involved in all aspects of both studies as first author, including conceptualization of the studies, experimental planning, performance of experiments, data acquisition, interpretation of results, and writing the respective manuscripts.*

DISCUSSION

Atherosclerosis has been one of the major causes of death in industrialized countries for decades and represents a growing problem in developing countries. In addition to causing individual morbidity and mortality, the disease imposes an enormous economic burden on heath care systems. Its direct and indirect costs, which includes expenditures for physicians, hospital and ambulatory services, medications, as well as costs to the general economy incurred by lost productivity, exceeded an estimated $320 billion in the United States alone in 2015 (Mozaffarian et al., 2015) – representing almost 2% of the entire U.S. gross domestic product (GDP). This indicates an urgent need for advanced diagnostic tools (Nahrendorf et al., 2015) in conjunction with improved causal treatment strategies.

Pharmacological preventive and treatment approaches to atherosclerosis currently in clinical use, besides pure antihypertensives, are centered around inhibition of the renin-angiotensin-aldosterone system (RAAS), and modulation of lipid metabolism (Swirski et al., 2009b). Pharmaceuticals limiting RAAS activation, such as angiotensin-converting enzyme (ACE) inhibitors, have been proven to exert effects on the development of atherosclerosis going beyond the achieved reduction in arterial blood pressure (ONTARGET Investigators et al., 2008); the mechanisms behind these blood-pressure independent effects are incompletely understood and may hold potential to identify even more specific therapeutic targets. Statins, inhibitors of 3-hydroxy-3-methyl-glutaryl coenzyme A (HMG-CoA) reductase, the rate-limiting enzyme of cholesterol biosynthesis, are the most notable lipid-targeting class of drugs. They mainly decrease levels of cholesterol contained in low-density lipoprotein particles (LDL cholesterol) through feed-back acceleration of LDL uptake into the liver, which results from the primary inhibition of *de novo* cholesterol synthesis (Tobert, 2003). Statins have been in clinical use since 1987, when lovastatin was first introduced into the market, and can lower the risk for ischemic heart disease by as much as 60% (Law et al., 2003). As such, they are a cornerstone of secondary prevention in atherosclerosis and exert proven benefits in primary prevention, which recently led to recommendations vastly expanding the

number of patients eligible for statin therapy (Stone et al., 2014). In contrast to LDL, raising levels of high-density lipoprotein (HDL) was shown to be atheroprotective in animal trials, and attempts have been made to exploit this characteristic for drug therapy. It was discovered that individuals with mutations in the cholesteryl ester transferase protein (CETP) gene locus have high levels of HDL cholesterol, which led to the development of CETP inhibitors as potential anti-atherosclerotic agents (Agerholm-Larsen et al., 2000). However, phase III trials of torcetrapib, the first drug candidate in this class, were terminated early because of an elevated number of cardiovascular events and a 60% relative increase in overall mortality (Barter et al., 2007). A subsequent molecule in this class, dalcetrapib, also failed to show meaningful clinical efficacy and the respective phase III trial was halted as a result (Schwartz et al., 2012). These experiences underlined the need for a diversification of experimental approaches to atherosclerosis treatment (Rader and Daugherty, 2008; Swirski et al., 2009b); consequentially, the recognition of the inflammatory nature of atherogenesis has spurred the exploration of anti-inflammatory treatment options (Weber and Noels, 2011).

The present study, ROBBINS*, CHUDNOVSKIY*, RAUCH* ET AL., 2012 (*equal contributions), enriches our understanding of the inflammatory component of atherosclerosis in several ways, which may inform and refine present and future drug development efforts.

First, our study identifies the spleen as an unexpected source of lesion-infiltrating leukocytes. Landmark experiments performed almost 50 years ago proposed that the bone marrow is the exclusive monocyte production site in the adult organism under steady state conditions; splenic hematopoiesis occurs in development and in a number of genetic and myeloproliferative conditions in rodents and in humans (Freedman and Saunders, 1981; Dzierzak and Medvinsky, 1995; Hassan and Neiman, 1985; Lowell et al., 1996; Snover et al., 1981; Wolber et al., 2002). We now show that, in chronic inflammation, the spleen can produce circulating myeloid cells such as monocytes and neutrophils. The findings build on previous work exposing the existence of a rapidly mobilizable splenic monocyte reservoir (Swirski et al.,

2009a), by identifying the specific mechanism that can replenish and maintain this monocyte pool; consequently, we now understand the reservoir's influence to be greater in scope than previously assumed. The data also provide further evidence that the production of extramedullary myeloid cells depends on several discrete processes: first, bone marrow HSPC mobilize (Massberg et al., 2007; Méndez-Ferrer et al., 2008; Kiel et al., 2005); second, mobilized HSPC seed extramedullary sites (Massberg et al., 2007; Han et al., 2010); production, i.e. proliferation and differentiation, of myeloid cells is the third step and occurs in response to GM-CSF and IL-3. Thus, HSPC differentiation depends not only on the intrinsic ability of progenitors to proliferate (Hirai et al., 2006; Nagai et al., 2006), but also on extrinsic accessory factors, such as myelopoietic cytokines. Future studies will need to further enrich our understanding of the mechanisms that orchestrate each of these processes.

Among organs, the spleen represents an ideal outsource destination. It has an open circulation, allowing for fast exchange with the blood (Mebius and Kraal, 2005), yet it is capable of cell retention through a myriad of adhesive ligands (Karlsson et al., 2003; Lu and Cyster, 2002). The organ can accommodate vast quantities and fluctuations of cells, especially in the red pulp. It also allows for rapid exit of undifferentiated monocytes, indicating that entry into its fenestrated parenchyma neither forces differentiation nor precludes recirculation (Swirski et al., 2009a). Thus, location, elasticity and architecture render the spleen a perfect seeding ground for the production of myeloid cells in chronic inflammation.

Second, the spleen transplantation data point to a previously unrecognized cellular turnover in atheromata. During atherogenesis, circulating leukocytes accumulate in the intima, ingest lipids, and differentiate into foam cells. According to previous thinking, individual mononuclear phagocytes persist in lesions chronically or depart by efferocytosis (Weber and Noels, 2011). The identification of a rapid leukocyte turnover in experimental atheromata challenges this paradigm. Subsequent studies in the Swirski group identified local proliferation of macrophages as a second major source of lesional macrophages that may dominate accumulation and differentiation in certain settings (Robbins et al., 2013). In a more general sense, the rapid

leukocyte turnover in lesions indicates that atheromata, to a certain degree, resemble sites of acute inflammation.

Whether the observations in mice reported here apply to humans remains uncertain. Splenectomy in humans may heighten the risk of ischemic heart disease (Robinette and Fraumeni, 1977), probably due to multiple mechanisms, although obvious confounders might contribute to this association. The spleen protects against infections that may precipitate atherosclerotic events or aggravate atherogenesis (Caligiuri et al., 2002), but splenic generation of circulating monocytes and neutrophils might help to meet demand for circulating leukocytes and complement the bone marrow production of hematopoietic cells. Our experimental data do reveal an altered lesional evolution in asplenic mice. Whether lesions with fewer macrophages are more or less likely to precipitate clinical events requires further study.

Altogether, the data presented here advance the idea that extramedullary hematopoiesis and dynamic leukocyte turnover can influence atherogenesis; the study's results have biological, diagnostic, and therapeutic implications.

The second part of this work, RAUCH ET AL., 2012, significantly broadens our understanding of acute inflammation in general and the host response in sepsis in particular. Profiling hematopoietic cytokine production led to the surprise discovery of a population of B lymphocytes that arises early in response to an inflammatory insult. This cell population, termed Innate Response Activator (IRA) B cells, was found to be the major producer of granulocyte macrophage colony stimulating factor (GM-CSF) in this setting. Specifically deleting GM-CSF production by these cells in a mouse model of sepsis led to impaired neutrophil phagocytosis, precipitated a cytokine storm and dramatically increased mortality.

This study highlights several novel aspects of innate immunity regulation in response to an inflammatory stimulus:

First, we describe a previously elusive type of B lymphocyte with crucial functions in the early inflammatory response to bacterial infection. At the level of nomenclature, we debated whether to call GM-CSF-producing B cells a distinct B cell subset. Cell subsets are typically delineated according to phenotype, lineage relationships, location and function (Allman and Pillai, 2008; Auffray et al., 2009; Geissmann et al., 2010; Robbins and Swirski, 2010). We reasoned that GM-CSF-producing cells meet all three criteria. IRA B cells are distinct on the level of both surface phenotype and transcriptome. They reside in a specific and exclusive location. They are linked to other B cell subsets through ontogeny but form a discrete population upon differentiation of their precursor, B1a cells, in vitro and in vivo. Most importantly, their function is unique among any yet ascribed to B cells. Thus, we believe that IRA B cells represent a newly identified subset.

Second, the study highlights a previously unrecognized nexus between cell types traditionally belonging to the innate and adaptive immune system, respectively. Namely, IRA B cells – ontogenetically a part of the adaptive arm of the immune system -– serve as sentinels of an inflammatory insult by means of expression of pattern-recognition receptors, a functional role traditionally ascribed to cells of the innate immune system (Takeuchi and Akira, 2010). By way of their GM-CSF expression, IRA B cells then license bacterial phagocytosis by neutrophils. This previously unrecognized mechanism challenges previous assumptions about the directional nature of crosstalk between adaptive and innate immunity during early phases of inflammation. Our findings point to a model in which cells traditionally assigned to innate or adaptive immunity are engaged in bidirectional communication, which may serve to enable feedback control of the immune response tailored towards the type of insult. Our findings complement examples of bidirectional regulation recognized during other phases of inflammation: examples include helper T-cells activating macrophages during Th1 responses by way of INF-γ secretion (Schroder et al., 2004), or B10 cells suppressing macrophages by way of IL-10 expression during the resolution phase (Tedder, 2015).

Third, our study uncovers a previously unrecognized cellular and locational specificity to the actions of GM-CSF, a pleiotropic cytokine that influences production, maturation, function, and survival of its target cells. Previous studies of the cytokine's role in sepsis led to ambiguity with regards to its function: while indiscriminate ablation of GM-CSF protected mice from septic shock (Basu et al., 1997), its supplementation seems to be beneficial (Gennari et al., 1994). The identification of a B cell subset that produces GM-CSF exclusively in the spleen and appears at a defined time after the initial insult may help explain this apparent paradox; our results favor a multidimensional model of GM-CSF action in which source, location and timing are critical determinants of the cytokine's effector functions.

Putting the two manuscripts at the center of my dissertation in context reveals striking similarities in the cytokine regulation of innate immunity in atherosclerosis, on the one hand, and in bacterial sepsis, on the other hand: in ROBBINS*, CHUDNOVSKIY*, RAUCH* ET AL., 2012 (*equal contributions) we show that locally secreted GM-CSF and IL-3 function to maintain splenic hematopoiesis in atherosclerosis, which in turn contributes monocytes to the growing atheromata. We further demonstrate that a surprisingly similar hematopoietic pattern can be elicited by short term endotoxin challenge, and visualize that response *in vivo*. In RAUCH ET AL., 2012 we consequentially describe the novel subset of IRA B lymphocytes, that regulate innate immune cell function in acute endotoxin-induced inflammation by virtue of secreting an array of cytokines, most prominently, GM-CSF and IL-3.

The recruitment of similar cellular and cytokine pathways promoting inflammation in two seemingly unrelated pathophysiological conditions supports a model where chronic vascular inflammation is born out of a string of insults that mimic the immunopathogenesis of acute infection; it may also provide a mechanistic basis for the aforementioned clinical phenomenon of incremental atheromata evolution (Yokoya et al., 1999; Bruschke et al., 1989). Subsequent studies built upon our work to describe additional aspects of IRA B cell action in atherosclerosis, demonstrating that it may aggravate atherosclerosis in part by GM-CSF dependent generation of a

dendritic cell subset that shifts adaptive immunity towards a Th1 response (Hilgendorf et al., 2014).

In summary, the work towards my dissertation first revealed a previously unrecognized and deleterious role of extramedullary myelopoiesis and monocytopoiesis in atherogenesis. Continuative studies by myself and others showed that this phenomenon is mirrored in other conditions accompanied by an inflammatory response, including acute myocardial infarction (Leuschner, Rauch, et al., 2012) and adenocarcinoma of the lung (Cortez-Retamozo et al., 2013; 2012). Future studies should determine to what extent this phenomenon – identified in experimental disease models -– extends to the human system, and whether it may be exploited therapeutically. Second, a search for cellular regulators of the innate immune response in acute inflammation led to the surprise discovery of a subset of B lymphocytes called IRA (innate response activator), that produces GM-CSF and IL-3 and shapes the immune response to acute bacterial infection, both from peritoneal (Rauch et al., 2012) and pleural (Weber et al., 2014) sources, as well as in atherosclerosis (Robbins et al., 2012; Hilgendorf et al., 2014). This gives rise to the question whether IRA B cells are a universal feature of inflammation.

BIBLIOGRAPHY

Agerholm-Larsen, B., A. Tybjaerg-Hansen, P. Schnohr, R. Steffensen, and B.G. Nordestgaard. 2000. Common cholesteryl ester transfer protein mutations, decreased HDL cholesterol, and possible decreased risk of ischemic heart disease: The Copenhagen City Heart Study. *Circulation*. 102:2197–2203.

Allman, D., and S. Pillai. 2008. Peripheral B cell subsets. *Curr Opin Immunol*. 20:149–157.

An, G., H. Wang, R. Tang, T. Yago, J.M. McDaniel, S. McGee, Y. Huo, and L. Xia. 2008. P-selectin glycoprotein ligand-1 is highly expressed on Ly-6Chi monocytes and a major determinant for Ly-6Chi monocyte recruitment to sites of atherosclerosis in mice. *Circulation*. 117:3227–3237.

Angus, D.C., and T. van der Poll. 2013. Severe sepsis and septic shock. *N Engl J Med*. 369:840–851.

Angus, D.C., W.T. Linde-Zwirble, J. Lidicker, G. Clermont, J. Carcillo, and M.R. Pinsky. 2001. Epidemiology of severe sepsis in the United States: analysis of incidence, outcome, and associated costs of care. *Crit Care Med*. 29:1303–1310.

Arnon, T.I., R.M. Horton, I.L. Grigorova, and J.G. Cyster. 2013. Visualization of splenic marginal zone B-cell shuttling and follicular B-cell egress. *Nature*. 493:684–688.

Assoian, R.K., and M.B. Sporn. 1986. Type beta transforming growth factor in human platelets: release during platelet degranulation and action on vascular smooth muscle cells. *J. Cell Biol.* 102:1217–1223.

Auffray, C., D.K. Fogg, E. Narni-Mancinelli, B. Senechal, C. Trouillet, N. Saederup, J. Leemput, K. Bigot, L. Campisi, M. Abitbol, T. Molina, I. Charo, D.A. Hume, A. Cumano, G. Lauvau, and F. Geissmann. 2009. CX3CR1+ CD115+ CD135+ common macrophage/DC precursors and the role of CX3CR1 in their response to inflammation. *J Exp Med*. 206:595–606.

Barter, P.J., M. Caulfield, M. Eriksson, S.M. Grundy, J.J.P. Kastelein, M. Komajda, J. Lopez-Sendon, L. Mosca, J.-C. Tardif, D.D. Waters, C.L. Shear, J.H. Revkin, K.A. Buhr, M.R. Fisher, A.R. Tall, B. Brewer, ILLUMINATE Investigators. 2007. Effects of torcetrapib in patients at high risk for coronary events. *N Engl J Med*. 357:2109–2122.

Basu, S., A.R. Dunn, M.W. Marino, H. Savoia, G. Hodgson, G.J. Lieschke, J. Cebon. 1997. Increased tolerance to endotoxin by granulocyte-macrophage colony-stimulating factor-deficient mice, *J Immunol.* 159:1412–1417.

Bone, R.C., R.A. Balk, F.B. Cerra, R.P. Dellinger, A.M. Fein, W.A. Knaus, R.M. Schein, and W.J. Sibbald. 1992. Definitions for sepsis and organ failure and guidelines for the use of innovative therapies in sepsis. The ACCP/SCCM Consensus Conference Committee. American College of Chest Physicians/Society of Critical Care Medicine. *CHEST*. 101:1644–1655.

Boomer, J.S., K. To, K.C. Chang, O. Takasu, D.F. Osborne, A.H. Walton, T.L. Bricker, S.D. Jarman, D. Kreisel, A.S. Krupnick, A. Srivastava, P.E. Swanson, J.M. Green, and R.S. Hotchkiss. 2011. Immunosuppression in patients who die of sepsis and multiple organ failure. *JAMA*. 306:2594–2605.

Bruschke, A.V., J.R. Kramer, E.T. Bal, I.U. Haque, R.C. Detrano, and M. Goormastic. 1989. The dynamics of progression of coronary atherosclerosis studied in 168 medically treated patients who underwent coronary arteriography three times. *Am. Heart J.* 117:296–305.

Bunster, E., and R.K. Meyer. 1933. An improved method of parabiosis. *The Anatomical Record*. 57:339–343.

Caligiuri, G., A. Nicoletti, B. Poirier, and G.K. Hansson. 2002. Protective immunity against atherosclerosis carried by B cells of hypercholesterolemic mice. *J Clin Invest*. 109:745–753.

Cerutti, A., M. Cols, and I. Puga. 2013. Marginal zone B cells: virtues of innate-like antibody-producing lymphocytes. *Nature Reviews Immunology*. 13:118–132.

Colvin, G.A., J.-F. Lambert, M. Abedi, C.-C. Hsieh, J.E. Carlson, F.M. Stewart, and P.J. Quesenberry. 2004. Murine marrow cellularity and the concept of stem cell competition: geographic and quantitative determinants in stem cell biology. *Leukemia*. 18:575–583.

Cortez-Retamozo, V., M. Etzrodt, A. Newton, **P.J. Rauch**, A. Chudnovskiy, C. Berger, R.J.H. Ryan, Y. Iwamoto, B. Marinelli, R. Gorbatov, R. Forghani, T.I. Novobrantseva, V. Koteliansky, J.-L. Figueiredo, J.W. Chen, D.G. Anderson, M. Nahrendorf, F.K. Swirski, R. Weissleder, and M.J. Pittet. 2012. Origins of tumor-associated macrophages and neutrophils. *Proceedings of the National Academy of Sciences*. 109:2491–2496.

Cortez-Retamozo, V., M. Etzrodt, A. Newton, R. Ryan, F. Pucci, S.W. Sio, W. Kuswanto, **P.J. Rauch**, A. Chudnovskiy, Y. Iwamoto, R. Kohler, B. Marinelli, R. Gorbatov, G. Wojtkiewicz, P. Panizzi, M. Mino-Kenudson, R. Forghani, J.-L. Figueiredo, J.W. Chen, R. Xavier, F.K. Swirski, M. Nahrendorf, R. Weissleder, and M.J. Pittet. 2013. Angiotensin II Drives the Production of Tumor-Promoting Macrophages. *Immunity*.

Di Sabatino, A., R. Carsetti, and G.R. Corazza. 2011. Post-splenectomy and hyposplenic states. *Lancet*. 378:86–97.

Döcke, W.D., F. Randow, U. Syrbe, D. Krausch, K. Asadullah, P. Reinke, H.D. Volk, and W. Kox. 1997. Monocyte deactivation in septic patients: restoration by IFN-gamma treatment. *Nat Med*. 3:678–681.

Drenckhahn, D., T. Gress, and R.P. Franke. 1986. Vascular endothelial stress fibres: their potential role in protecting the vessel wall from rheological damage. *Klin. Wochenschr.* 64:986–988.

Dzierzak, E., and A. Medvinsky. 1995. Mouse embryonic hematopoiesis. *Trends Genet.* 11:359–366.

Freedman, M.H., and E.F. Saunders. 1981. Hematopoiesis in the human spleen. *Am. J. Hematol.* 11:271–275.

Geissmann, F., M.G. Manz, S. Jung, M.H. Sieweke, M. Merad, and K. Ley. 2010. Development of monocytes, macrophages, and dendritic cells. *Science*. 327:656–661.

Gennari, R., J.W. Alexander, L. Gianotti, T. Eaves-Pyles, S. Hartmann. 1994. Granulocyte macrophage colony-stimulating factor improves survival in two models of gut-derived sepsis by improving gut barrier function and modulating bacterial clearance. *Ann Surg.* 220:68–76.

Getz, G.S., and C.A. Reardon. 2012. Animal models of atherosclerosis. *Arteriosclerosis, Thrombosis, and Vascular Biology*. 32:1104–1115.

Goodman, J.W., and G.S. Hodgson. 1962. Evidence for stem cells in the peripheral blood of mice. *Blood*. 19:702–714.

Han, Y.-C., C.Y. Park, G. Bhagat, J. Zhang, Y. Wang, J.-B. Fan, M. Liu, Y. Zou, I.L. Weissman, and H. Gu. 2010. microRNA-29a induces aberrant self-renewal capacity in hematopoietic progenitors, biased myeloid development, and acute myeloid leukemia. *J Exp Med*. 207:475–489.

Hansson, G.K., and P. Libby. 2006. The immune response in atherosclerosis: a double-edged sword. *Nature Reviews Immunology*. 6:508–519.

Hassan, N.M., and R.S. Neiman. 1985. The pathology of the spleen in steroid-treated immune thrombocytopenic purpura. *Am. J. Clin. Pathol.* 84:433–438.

Higashimori, M., J.B. Tatro, K.J. Moore, M.E. Mendelsohn, J.B. Galper, and D. Beasley. 2010. Role of Toll-Like Receptor 4 in Intimal Foam Cell Accumulation in Apolipoprotein E-Deficient Mice. *Arteriosclerosis, Thrombosis, and Vascular Biology*. 31:50–57.

Hilgendorf, I., I. Theurl, L.M.S. Gerhardt, C.S. Robbins, G.F. Weber, A. Gonen, Y. Iwamoto, N. Degousee, T.A.W. Holderried, C. Winter, A. Zirlik, H.Y. Lin, G.K. Sukhova, J. Butany, B.B. Rubin, J.L. Witztum, P. Libby, M. Nahrendorf, R. Weissleder, and F.K. Swirski. 2014. Innate response activator B cells aggravate atherosclerosis by stimulating T helper-1 adaptive immunity. *Circulation*. 129:1677–1687.

Hirai, H., P. Zhang, T. Dayaram, C.J. Hetherington, S.-I. Mizuno, J. Imanishi, K. Akashi, and D.G. Tenen. 2006. C/EBPbeta is required for “emergency” granulopoiesis. *Nat Immunol*. 7:732–739.

Hotchkiss, R.S., G. Monneret, and D. Payen. 2013. Sepsis-induced immunosuppression: from cellular dysfunctions to immunotherapy. *Nature Reviews Immunology*. 13:862–874.

Hotz, M.A., J. Gong, F. Traganos, and Z. Darzynkiewicz. 1994. Flow cytometric detection of apoptosis: comparison of the assays of in situ DNA degradation and

chromatin changes. *Cytometry*. 15:237–244.

Huo, Y., and K.F. Ley. 2004. Role of platelets in the development of atherosclerosis. *Trends Cardiovasc. Med.* 14:18–22.

Jaiswal, S., and I.L. Weissman. 2009. Hematopoietic stem and progenitor cells and the inflammatory response. *Ann. N. Y. Acad. Sci.* 1174:118–121.

Karlsson, M.C.I., R. Guinamard, S. Bolland, M. Sankala, R.M. Steinman, and J.V. Ravetch. 2003. Macrophages control the retention and trafficking of B lymphocytes in the splenic marginal zone. *J Exp Med*. 198:333–340.

Khurana, R. 2005. Role of Angiogenesis in Cardiovascular Disease: A Critical Appraisal. *Circulation*. 112:1813–1824.

Kiel, M.J., O.H. Yilmaz, T. Iwashita, O.H. Yilmaz, C. Terhorst, and S.J. Morrison. 2005. SLAM family receptors distinguish hematopoietic stem and progenitor cells and reveal endothelial niches for stem cells. *Cell*. 121:1109–1121.

Kovach, M.A., and T.J. Standiford. 2012. The function of neutrophils in sepsis. *Curr. Opin. Infect. Dis.* 25:321–327.

Law, M.R., N.J. Wald, and A.R. Rudnicka. 2003. Quantifying effect of statins on low density lipoprotein cholesterol, ischaemic heart disease, and stroke: systematic review and meta-analysis. *BMJ*. 326:1423.

Leuschner, F., **P.J. Rauch**, T. Ueno, R. Gorbatov, B. Marinelli, W.W. Lee, P. Dutta, Y. Wei, C. Robbins, Y. Iwamoto, B. Sena, A. Chudnovskiy, P. Panizzi, E. Keliher, J.M. Higgins, P. Libby, M.A. Moskowitz, M.J. Pittet, F.K. Swirski, R. Weissleder, and M. Nahrendorf. 2012. Rapid monocyte kinetics in acute myocardial infarction are sustained by extramedullary monocytopoiesis. *J Exp Med*. 209:123–137.

Libby, P. 2002. Inflammation in atherosclerosis. *Nature*. 420:868–874.

Libby, P., P.M. Ridker, and G.K. Hansson. 2011. Progress and challenges in translating the biology of atherosclerosis. *Nature*. 473:317–325.

Lowell, C.A., M. Niwa, P. Soriano, and H.E. Varmus. 1996. Deficiency of the Hck and Src tyrosine kinases results in extreme levels of extramedullary hematopoiesis. *Blood*. 87:1780–1792.

Lu, T.T., and J.G. Cyster. 2002. Integrin-mediated long-term B cell retention in the splenic marginal zone. *Science*. 297:409–412.

MacDonald, I.C., D.M. Ragan, E.E. Schmidt, and A.C. Groom. 1987. Kinetics of red blood cell passage through interendothelial slits into venous sinuses in rat spleen, analyzed by in vivo microscopy. *Microvasc. Res.* 33:118–134.

Martí-Carvajal, A.J., I. Solà, D. Lathyris, and A.F. Cardona. 2012. Human recombinant activated protein C for severe sepsis. *Cochrane Database Syst Rev*. 3:CD004388.

Massberg, S., P. Schaerli, I. Knezevic-Maramica, M. Köllnberger, N. Tubo, E.A. Moseman, I.V. Huff, T. Junt, A.J. Wagers, I.B. Mazo, and U.H. von Andrian. 2007. Immunosurveillance by hematopoietic progenitor cells trafficking through blood, lymph, and peripheral tissues. *Cell*. 131:994–1008.

Mebius, R.E., and G. Kraal. 2005. Structure and function of the spleen. *Nature Reviews Immunology*. 5:606–616.

Meerschaert, J., and M.B. Furie. 1995. The adhesion molecules used by monocytes for migration across endothelium include CD11a/CD18, CD11b/CD18, and VLA-4 on monocytes and ICAM-1, VCAM-1, and other ligands on endothelium. *J Immunol*. 154:4099–4112.

Méndez-Ferrer, S., D. Lucas, M. Battista, and P.S. Frenette. 2008. Haematopoietic stem cell release is regulated by circadian oscillations. *Nature*. 452:442–447.

Mogensen, T.H. 2009. Pathogen recognition and inflammatory signaling in innate immune defenses. *Clin. Microbiol. Rev.* 22:240–73, Table of Contents.

Mohr, A., J. Polz, E.M. Martin, S. Griessl, A. Kammler, C. Pötschke, A. Lechner, B.M. Bröker, S. Mostböck, and D.N. Männel. 2012. Sepsis leads to a reduced antigen-specific primary antibody response. *Eur. J. Immunol.* 42:341–352.

Mouse Genome Sequencing Consortium, R.H. Waterston, K. Lindblad-Toh, E. Birney, J. Rogers, J.F. Abril, P. Agarwal, R. Agarwala, R. Ainscough, M. Alexandersson, P. An, S.E. Antonarakis, J. Attwood, R. Baertsch, J. Bailey, K. Barlow, S. Beck, E. Berry, B. Birren, T. Bloom, P. Bork, M. Botcherby, N. Bray, M.R. Brent, D.G. Brown, S.D. Brown, C. Bult, J. Burton, J. Butler, R.D. Campbell, P. Carninci, S. Cawley, F. Chiaromonte, A.T. Chinwalla, D.M. Church, M. Clamp, C. Clee, F.S. Collins, L.L. Cook, R.R. Copley, A. Coulson, O. Couronne, J. Cuff, V. Curwen, T. Cutts, M. Daly, R. David, J. Davies, K.D. Delehaunty, J. Deri, E.T. Dermitzakis, C. Dewey, N.J. Dickens, M. Diekhans, S. Dodge, I. Dubchak, D.M. Dunn, S.R. Eddy, L. Elnitski, R.D. Emes, P. Eswara, E. Eyras, A. Felsenfeld, G.A. Fewell, P. Flicek, K. Foley, W.N. Frankel, L.A. Fulton, R.S. Fulton, T.S. Furey, D. Gage, R.A. Gibbs, G. Glusman, S. Gnerre, N. Goldman, L. Goodstadt, D. Grafham, T.A. Graves, E.D. Green, S. Gregory, R. Guigó, M. Guyer, R.C. Hardison, D. Haussler, Y. Hayashizaki, L.W. Hillier, A. Hinrichs, W. Hlavina, T. Holzer, F. Hsu, A. Hua, T. Hubbard, A. Hunt, I. Jackson, D.B. Jaffe, L.S. Johnson, M. Jones, T.A. Jones, et al. 2002. Initial sequencing and comparative analysis of the mouse genome. *Nature*. 420:520–562.

Mozaffarian, D., E.J. Benjamin, A.S. Go, D.K. Arnett, M.J. Blaha, M. Cushman, S. de Ferranti, J.-P. Després, H.J. Fullerton, V.J. Howard, M.D. Huffman, S.E. Judd, B.M. Kissela, D.T. Lackland, J.H. Lichtman, L.D. Lisabeth, S. Liu, R.H. Mackey, D.B. Matchar, D.K. McGuire, E.R. Mohler, C.S. Moy, P. Muntner, M.E. Mussolino, K. Nasir, R.W. Neumar, G. Nichol, L. Palaniappan, D.K. Pandey, M.J. Reeves, C.J. Rodriguez, P.D. Sorlie, J. Stein, A. Towfighi, T.N. Turan, S.S. Virani, J.Z. Willey, D. Woo, R.W. Yeh, M.B. Turner, American Heart Association Statistics Committee and Stroke Statistics Subcommittee. 2015. Heart disease and stroke statistics--2015 update: a report from the American Heart Association. *Circulation*. 131:e29–322.

Nagai, Y., K.P. Garrett, S. Ohta, U. Bahrun, T. Kouro, S. Akira, K. Takatsu, and P.W. Kincade. 2006. Toll-like receptors on hematopoietic progenitor cells stimulate innate immune system replenishment. *Immunity*. 24:801–812.

Nahrendorf, M., S. Frantz, F.K. Swirski, W.J.M. Mulder, G. Randolph, G. Ertl, V. Ntziachristos, J.J. Piek, E.S. Stroes, M. Schwaiger, D.L. Mann, and Z.A. Fayad. 2015. Imaging systemic inflammatory networks in ischemic heart disease. *J. Am. Coll. Cardiol.* 65:1583–1591.

ONTARGET Investigators, S. Yusuf, K.K. Teo, J. Pogue, L. Dyal, I. Copland, H. Schumacher, G. Dagenais, P. Sleight, and C. Anderson. 2008. Telmisartan, ramipril, or both in patients at high risk for vascular events. *N Engl J Med*. 358:1547–1559.

Opal, S.M., R.P. Dellinger, J.-L. Vincent, H. Masur, and D.C. Angus. 2014. The next generation of sepsis clinical trial designs: what is next after the demise of recombinant human activated protein C?*. *Crit Care Med*. 42:1714–1721.

Rader, D.J., and A. Daugherty. 2008. Translating molecular discoveries into new therapies for atherosclerosis. *Nature*. 451:904–913.

Rauch, P.J., A. Chudnovskiy, C.S. Robbins, G.F. Weber, M. Etzrodt, I. Hilgendorf, E. Tiglao, J.-L. Figueiredo, Y. Iwamoto, I. Theurl, R. Gorbatov, M.T. Waring, A.T. Chicoine, M. Mouded, M.J. Pittet, M. Nahrendorf, R. Weissleder, and F.K. Swirski. 2012. Innate response activator B cells protect against microbial sepsis. *Science*. 335:597–601.

Raychaudhuri, S., J.M. Stuart, and R.B. Altman. 2000. Principal components analysis to summarize microarray experiments: application to sporulation time series. *Pac Symp Biocomput*. 455–466.

Reich, M., T. Liefeld, J. Gould, J. Lerner, P. Tamayo, and J.P. Mesirov. 2006. GenePattern 2.0. *Nat. Genet.* 38:500–501.

Rittirsch, D., M.S. Huber-Lang, M.A. Flierl, and P.A. Ward. 2009. Immunodesign of experimental sepsis by cecal ligation and puncture. *Nat Protoc*. 4:31–36.

Robbins, C.S.*, A. Chudnovskiy*, **P.J. Rauch***, J.-L. Figueiredo, Y. Iwamoto, R. Gorbatov, M. Etzrodt, G.F. Weber, T. Ueno, N. van Rooijen, M.J. Mulligan-Kehoe, P. Libby, M. Nahrendorf, M.J. Pittet, R. Weissleder, and F.K. Swirski. 2012. Extramedullary hematopoiesis generates Ly-6C(high) monocytes that infiltrate atherosclerotic lesions. *Circulation*. 125:364–374. (*equal contributions)

Robbins, C.S., and F.K. Swirski. 2010. The multiple roles of monocyte subsets in steady state and inflammation. *Cell. Mol. Life Sci.* 67:2685–2693.

Robbins, C.S., I. Hilgendorf, G.F. Weber, I. Theurl, Y. Iwamoto, J.-L. Figueiredo, R. Gorbatov, G.K. Sukhova, L.M.S. Gerhardt, D. Smyth, C.C.J. Zavitz, E.A. Shikatani, M. Parsons, N. van Rooijen, H.Y. Lin, M. Husain, P. Libby, M. Nahrendorf, R. Weissleder, and F.K. Swirski. 2013. Local proliferation dominates lesional macrophage accumulation in atherosclerosis. *Nat Med*. 19:1166–1172.

Robinette, C.D., and J.F. Fraumeni. 1977. Splenectomy and subsequent mortality in veterans of the 1939-45 war. *Lancet*. 2:127–129.

Ross, R., and J.A. Glomset. 1976. The pathogenesis of atherosclerosis (second of two parts). *New England Journal of Medicine*. 295:420–425.

Schroder, K., P.J. Hertzog, T. Ravasi, and D.A. Hume. 2004. Interferon-gamma: an overview of signals, mechanisms and functions. *J Leukoc Biol*. 75:163–189.

Schwartz, G.G., A.G. Olsson, M. Abt, C.M. Ballantyne, P.J. Barter, J. Brumm, B.R. Chaitman, I.M. Holme, D. Kallend, L.A. Leiter, E. Leitersdorf, J.J.V. McMurray, H. Mundl, S.J. Nicholls, P.K. Shah, J.-C. Tardif, R.S. Wright, dal-OUTCOMES Investigators. 2012. Effects of dalcetrapib in patients with a recent acute coronary syndrome. *N Engl J Med*. 367:2089–2099.

Shi, W., M.E. Haberland, M.L. Jien, D.M. Shih, and A.J. Lusis. 2000. Endothelial responses to oxidized lipoproteins determine genetic susceptibility to atherosclerosis in mice. *Circulation*. 102:75–81.

Si, Y., C.-L. Tsou, K. Croft, and I.F. Charo. 2010. CCR2 mediates hematopoietic stem and progenitor cell trafficking to sites of inflammation in mice. *J Clin Invest*. 120:1192–1203.

Simon, P. 2003. Q-Gene: processing quantitative real-time RT-PCR data. *Bioinformatics*. 19:1439–1440.

Snover, D.C., G. Frizzera, B.D. Spector, G.S. Perry, and J.H. Kersey. 1981. Wiskott-Aldrich syndrome: histopathologic findings in the lymph nodes and spleens of 15 patients. *Hum. Pathol.* 12:821–831.

Soehnlein, O. 2012. Multiple Roles for Neutrophils in Atherosclerosis. *Circ. Res.* 110:875–888.

Stone, N.J., J.G. Robinson, A.H. Lichtenstein, C.N. Bairey Merz, C.B. Blum, R.H. Eckel, A.C. Goldberg, D. Gordon, D. Levy, D.M. Lloyd-Jones, P. McBride, J.S. Schwartz, S.T. Shero, S.C. Smith, K. Watson, P.W.F. Wilson, K.M. Eddleman, N.M. Jarrett, K. LaBresh, L. Nevo, J. Wnek, J.L. Anderson, J.L. Halperin, N.M. Albert, B. Bozkurt, R.G. Brindis, L.H. Curtis, D. DeMets, J.S. Hochman, R.J. Kovacs, E.M. Ohman, S.J. Pressler, F.W. Sellke, W.-K. Shen, G.F. Tomaselli, American College of Cardiology/American Heart Association Task Force on Practice Guidelines. 2014. 2013 ACC/AHA guideline on the treatment of blood cholesterol to reduce atherosclerotic cardiovascular risk in adults: a report of the American College of Cardiology/American Heart Association Task Force on Practice Guidelines. *Circulation*. 129:S1–45.

Swirski, F.K., M. Nahrendorf, M. Etzrodt, M. Wildgruber, V. Cortez-Retamozo, P. Panizzi, J.-L. Figueiredo, R.H. Kohler, A. Chudnovskiy, P. Waterman, E. Aikawa, T.R. Mempel, P. Libby, R. Weissleder, and M.J. Pittet. 2009a. Identification of splenic reservoir monocytes and their deployment to inflammatory sites. *Science*. 325:612–616.

Swirski, F.K., M.J. Pittet, M.F. Kircher, E. Aikawa, F.A. Jaffer, P. Libby, and R.

Weissleder. 2006. Monocyte accumulation in mouse atherogenesis is progressive and proportional to extent of disease. *Proc Natl Acad Sci USA*. 103:10340–10345.

Swirski, F.K., P. Libby, E. Aikawa, P. Alcaide, F.W. Luscinskas, R. Weissleder, and M.J. Pittet. 2007. Ly-6Chi monocytes dominate hypercholesterolemia-associated monocytosis and give rise to macrophages in atheromata. *J Clin Invest*. 117:195–205.

Swirski, F.K., R. Weissleder, and M.J. Pittet. 2009b. Heterogeneous in vivo behavior of monocyte subsets in atherosclerosis. *Arteriosclerosis, Thrombosis, and Vascular Biology*. 29:1424–1432.

Tacke, F., D. Alvarez, T.J. Kaplan, C. Jakubzick, R. Spanbroek, J. Llodra, A. Garin, J. Liu, M. Mack, N. van Rooijen, S.A. Lira, A.J. Habenicht, and G.J. Randolph. 2007. Monocyte subsets differentially employ CCR2, CCR5, and CX3CR1 to accumulate within atherosclerotic plaques. *J Clin Invest*. 117:185–194.

Takeuchi, O., and S. Akira. 2010. Pattern recognition receptors and inflammation. *Cell*. 140:805–820.

Tedder, T.F. 2015. B10 cells: a functionally defined regulatory B cell subset. *J Immunol*. 194:1395–1401.

Tobert, J.A. 2003. Lovastatin and beyond: the history of the HMG-CoA reductase inhibitors. *Nat Rev Drug Discov*. 2:517–526.

Weber, C., and H. Noels. 2011. Atherosclerosis: current pathogenesis and therapeutic options. *Nat Med*. 17:1410–1422.

Weber, G.F., B.G. Chousterman, I. Hilgendorf, C.S. Robbins, I. Theurl, L.M.S. Gerhardt, Y. Iwamoto, T.D. Quach, M. Ali, J.W. Chen, T.L. Rothstein, M. Nahrendorf, R. Weissleder, and F.K. Swirski. 2014. Pleural innate response activator B cells protect against pneumonia via a GM-CSF-IgM axis. *J Exp Med*. 211:1243–1256.

Whitman, S.C. 2004. A practical approach to using mice in atherosclerosis research. *Clin Biochem Rev*. 25:81–93.

Wolber, F.M., E. Leonard, S. Michael, C.M. Orschell-Traycoff, M.C. Yoder, and E.F. Srour. 2002. Roles of spleen and liver in development of the murine hematopoietic system. *Exp. Hematol.* 30:1010–1019.

Workman, C., L.J. Jensen, H. Jarmer, R. Berka, L. Gautier, H.B. Nielser, H.-H. Saxild, C. Nielsen, S. Brunak, and S. Knudsen. 2002. A new non-linear normalization method for reducing variability in DNA microarray experiments. *Genome Biol.* 3:research0048.

World Health Organization. 2014. The top 10 causes of death (Fact sheet No. 310).

Wright, D.E., S.H. Cheshier, A.J. Wagers, T.D. Randall, J.L. Christensen, and I.L. Weissman. 2001. Cyclophosphamide/granulocyte colony-stimulating factor

causes selective mobilization of bone marrow hematopoietic stem cells into the blood after M phase of the cell cycle. *Blood*. 97:2278–2285.

Yokoya, K., H. Takatsu, T. Suzuki, H. Hosokawa, S. Ojio, T. Matsubara, T. Tanaka, S. Watanabe, N. Morita, K. Nishigaki, G. Takemura, T. Noda, S. Minatoguchi, and H. Fujiwara. 1999. Process of progression of coronary artery lesions from mild or moderate stenosis to moderate or severe stenosis: A study based on four serial coronary arteriograms per year. *Circulation*. 100:903–909.

Yvan-Charvet, L., T. Pagler, E.L. Gautier, S. Avagyan, R.L. Siry, S. Han, C.L. Welch, N. Wang, G.J. Randolph, H.W. Snoeck, and A.R. Tall. 2010. ATP-binding cassette transporters and HDL suppress hematopoietic stem cell proliferation. *Science*. 328:1689–1693.

Zhang, S.H., R.L. Reddick, J.A. Piedrahita, and N. Maeda. 1992. Spontaneous hypercholesterolemia and arterial lesions in mice lacking apolipoprotein E. *Science*. 258:468–471.

ACKNOWLEDGEMENTS

First and foremost, I would like to thank my advisor, University Professor Markus Schwaiger, for his unwavering support and guidance throughout my work on this dissertation. Professor Schwaiger's enthusiasm for science has been truly inspirational to me.

I am also deeply indepted to my mentor PD Dr. Moritz Wildgruber, who has been instrumental to the success of this dissertation project in many ways, starting with his invaluable advice in choosing a laboratory for my studies.

Professor Filip Swirski of Harvard Medical School, Boston, USA, welcomed me into his laboratory and entrusted me with a project at the forefront of cardiovascular immunology early in my career. I am very thankful for the training, mentoring and (last but not least) scientific freedom he provided me with.

Further, I would like to thank Professor Ralph Weissleder, director of the Center for Systems Biology at Massachusetts General Hospital and Harvard Medical School, for providing a perfect infrastructure conducive to productive research, and for offering his advice at important junction points of my project.

I would also like to acknowledge my scientific partners Aleksey Chudnovskiy and Professor Clinton Robbins, who made important contributions to the research described here and were simply fantastic colleagues to work with.

Frutiful collaboration with the groups of Professor Matthias Nahrendorf and Professor Mikael Pittet greatly enriched this work. In particular, I would like to thank Drs. Martin Etzrodt, Florian Leuschner and Virna Cortez-Retamozo for their contributions and stimulating discussion.

Lastly, I am grateful to the Boehringer Ingelheim Fonds, especially Drs. Claudia Walther and Anja Hoffmann, for awarding me with an MD Fellowship that amounted to much more than just monetary support.

Copyright Information for Enclosed Manuscripts

Robbins, C.S.*, A. Chudnovskiy*, **P.J. Rauch***, J.-L. Figueiredo, Y. Iwamoto, R. Gorbatov, M. Etzrodt, G.F. Weber, T. Ueno, N. van Rooijen, M.J. Mulligan-Kehoe, P. Libby, M. Nahrendorf, M.J. Pittet, R. Weissleder, and F.K. Swirski. 2012. Extramedullary hematopoiesis generates Ly-6C(high) monocytes that infiltrate atherosclerotic lesions. *Circulation*. 125:364–374 (*equal contributions). *Copyright © 2012, Wolters Kluwer Health Lippincott Williams & Wilkins. Reuse for purpose of dissertation cleared through the Copyright Clearance Center's RightsLink® service.*

Rauch, P.J., A. Chudnovskiy, C.S. Robbins, G.F. Weber, M. Etzrodt, I. Hilgendorf, E. Tiglao, J.-L. Figueiredo, Y. Iwamoto, I. Theurl, R. Gorbatov, M.T. Waring, A.T. Chicoine, M. Mouded, M.J. Pittet, M. Nahrendorf, R. Weissleder, and F.K. Swirski. 2012. Innate response activator B cells protect against microbial sepsis. *Science*. 335:597–601. *Reprinted with permission from AAAS.*

Extramedullary Hematopoiesis Generates Ly-6C^{high} Monocytes That Infiltrate Atherosclerotic Lesions

Clinton S. Robbins, PhD*; Aleksey Chudnovskiy, MS*; Philipp J. Rauch, BS*; Jose-Luiz Figueiredo, MD; Yoshiko Iwamoto, BS; Rostic Gorbatov, BS; Martin Etzrodt, BS; Georg F. Weber, MD; Takuya Ueno, MD, PhD; Nico van Rooijen, PhD; Mary Jo Mulligan-Kehoe, PhD; Peter Libby, MD; Matthias Nahrendorf, MD, PhD; Mikael J. Pittet, PhD; Ralph Weissleder, MD, PhD; Filip K. Swirski, PhD

Background—Atherosclerotic lesions are believed to grow via the recruitment of bone marrow–derived monocytes. Among the known murine monocyte subsets, Ly-6C^{high} monocytes are inflammatory, accumulate in lesions preferentially, and differentiate. Here, we hypothesized that the bone marrow outsources the production of Ly-6C^{high} monocytes during atherosclerosis.

Methods and Results—Using murine models of atherosclerosis and fate-mapping approaches, we show that hematopoietic stem and progenitor cells progressively relocate from the bone marrow to the splenic red pulp, where they encounter granulocyte macrophage colony-stimulating factor and interleukin-3, clonally expand, and differentiate to Ly-6C^{high} monocytes. Monocytes born in such extramedullary niches intravasate, circulate, and accumulate abundantly in atheromata. On lesional infiltration, Ly-6C^{high} monocytes secrete inflammatory cytokines, reactive oxygen species, and proteases. Eventually, they ingest lipids and become foam cells.

Conclusions—Our findings indicate that extramedullary sites supplement the hematopoietic function of the bone marrow by producing circulating inflammatory cells that infiltrate atherosclerotic lesions. **(*Circulation*. 2012;125:364-374.)**

Key Words: atherosclerosis ■ imaging ■ immune system ■ immunology ■ macrophages

Monocytes are myeloid leukocytes that circulate in the blood and patrol the vascular endothelium.[1–4] During inflammatory diseases, monocytes accumulate in target sites and mature to macrophages or dendritic cells. Although monocytes are thought to arise exclusively in the bone marrow, hematopoietic stem and progenitor cells (HSPCs), which are developmentally upstream, readily mobilize from their bone marrow niches, accumulate in the periphery, and differentiate.[5,6] Although this phenomenon of extramedullary hematopoiesis is known to give rise to erythrocytes, platelets, granulocytes, and dendritic cells, it remains unknown whether HSPCs can yield monocytes outside the bone marrow. Likewise, the mechanisms that govern HSPC proliferation and differentiation and the eventual fate of the various progeny remain elusive.

Clinical Perspective on p 374

Atherosclerosis is a chronic disease characterized by the accumulation of lipids and leukocytes in the arterial vessel wall.[7–10] Among leukocytes, monocytes are essential to the development and exacerbation of the disease.[4,11,12] On lesional accumulation and as a consequence of ingesting lipids abundantly, monocyte-derived macrophages become foam cells, the key culprits of atherosclerotic complications. Of the 2 recognized murine monocyte subsets, Ly-6C^{high} monocytes have been shown to accumulate preferentially in growing lesions and to give rise to macrophages in atheromata.[12,13] Ly-6C^{high} monocytes are also believed to convert to Ly-6C^{low} monocytes,[14,15] but this conversion is compromised during atherosclerosis.[12] It remains unknown whether extramedullary hematopoiesis in general and the extramedullary production of Ly-6C^{high} monocytes specifically contribute to the development of atherosclerosis.

In this study, we focused on experimental atherosclerosis to determine whether lesion-accumulating monocytes can have extramedullary origins. Our data show that the spleen, which

Received August 22, 2011; accepted November 22, 2011.

From the Center for Systems Biology, Massachusetts General Hospital and Harvard Medical School, Boston (C.S.R., A.C., P.J.R., J.-L.F., Y.I., R.G., M.E., G.F.W., T.U., M.N., M.J.P., R.W., F.K.S.); Department of Molecular Cell Biology, Free University Medical Center, Amsterdam, the Netherlands (N.v.R.); Department of Surgery, Dartmouth-Hitchcock Heart and Vascular Research Center, Dartmouth Medical School, Lebanon, NH (M.J.M.-K.); and Cardiovascular Division, Department of Medicine, Brigham and Women's Hospital, Boston, MA (P.L.).

*Dr Robbins, A. Chudnovskiy, and P.J. Rauch contributed equally to this article.

Guest Editor for this article was Donald D. Heistad, MD.

The online-only Data Supplement is available with this article at http://circ.ahajournals.org/lookup/suppl/doi:10.1161/CIRCULATIONAHA.111.061986/-/DC1.

Correspondence to Filip K. Swirski, PhD, or Clinton S. Robbins, PhD, Center for Systems Biology, Massachusetts General Hospital, Harvard Medical School, Simches Research Bldg, 185 Cambridge St, Boston, MA 02114. E-mail fswirski@mgh.harvard.edu or robbins.clinton@mgh.harvard.edu

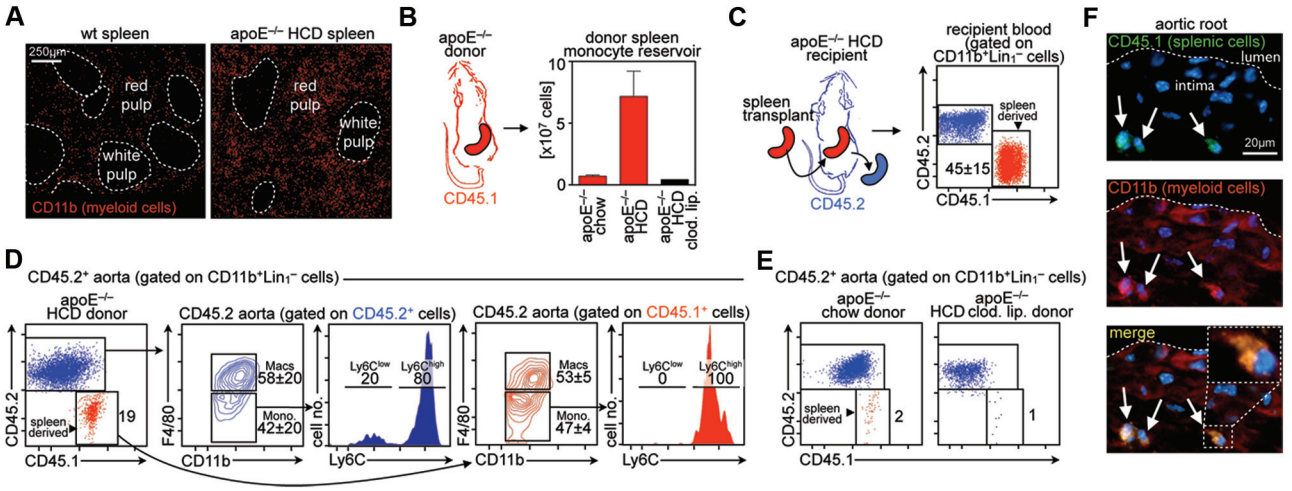

Figure 1. Splenic myeloid cells infiltrate atherosclerotic lesions. **A**, Immunofluorescence (IF) of CD11b cells (red) in spleens of C57BL/6 (wt) and apolipoprotein E–deficient (ApoE$^{-/-}$) mice consuming a high-cholesterol diet (HCD) for 20 weeks. Data show that the red pulp myeloid component enlarges during atherosclerosis and pushes the white pulp clusters away from each other. **B**, Size of the monocyte reservoir in ApoE$^{-/-}$ mice consuming a chow diet for 20 weeks, ApoE$^{-/-}$ mice consuming an HCD 20 weeks, and ApoE$^{-/-}$ mice consuming an HCD for 20 weeks and then injected with clodronate liposomes 1 day earlier (n=2–10). **C**, Presence of CD45.1^{+} cells in the blood of CD45.2^{+} mice that received CD45.1^{+} spleens by transplantation. **D**, Spleen transplantation from CD45.1 ApoE$^{-/-}$ donors consuming an HCD to CD45.2 ApoE$^{-/-}$ recipients. Data show direct accumulation and differentiation of splenic Ly-6C^{high} monocytes in aortic lesions in 1 day. One of 11 representative experiments is shown. **E**, Spleen transplantation from CD45.1 ApoE$^{-/-}$ donors consuming chow and from CD45.1 ApoE$^{-/-}$ donors consuming an HCD and then injected with clodronate liposomes. Data show negligible accumulation of splenic monocytes in aortic lesions in these controls. **F**, IF on the aortic root with antibodies against CD45.1 (green) and CD11b (red) and the merge of the 2 (yellow). DAPI depicts nuclei (blue). Arrows point to CD11b^{+} cells of splenic origin. For all flow cytometric plots, the ticks represent 0, 10^2, 10^3, 10^4, 10^5 fluorescence units, except for axes labeled "cell no." or "SSC," for which the ticks represent 0, 50 000, 100 000, 150 000, 200 000, and 250 000 fluorescence units.

contains a reservoir of undifferentiated monocytes in the steady state,[16–18] becomes monocytopoietic during atherosclerosis.

Methods

Animals

C57BL/6J (wild-type [wt]), B6.SJL-Ptprc^{a}Pep3^{b}/BoyJ (CD45.1^{+}), C57BL/6-Tg(UBC-GFP)30Scha/J (green fluorescent protein–positive [GFP^{+}]), B6.Cg-Tg(ACTB-mRFP1)1F1Hadj/J (red fluorescent protein–positive [RFP^{+}]), apolipoprotein E–deficient (ApoE$^{-/-}$) mice (B6.129P2-Apoe^{tm1Unc}), and low-density lipoprotein receptor–deficient (LDLR$^{-/-}$)ApoB48$^{-/-}$ (B6;129S-Apob^{tm2Sgy} Ldlr^{tm1Her}/J) male and female mice were purchased from The Jackson Laboratories. All protocols were approved by the Animal Review Committee at Massachusetts General Hospital. More details are given in the online-only Data Supplement.

Animal Models and In Vivo Interventions

Splenectomy, spleen transplantation, parabiosis, and adoptive transfer of cells are described in detail in the Experimental Procedures section in the online-only Data Supplement. Mice were injected intravenously with blocking antibodies, with clodronate liposomes, or with oxidized LDL, as described in the online-only Data Supplement.

Flow Cytometry

Antibodies used in the study are listed in the online-only Data Supplement. Data were acquired on an LSRII (BD Biosciences) and analyzed with FlowJo version 8.8.6 (Tree Star, Inc). Cells were sorted on a BD FACSAria II (BD Biosciences).

Histology

Aortas and spleens were excised, embedded in optimal-cutting-temperature compound (Sakura Finetek), and flash-frozen in isopentane and dry ice. Frozen 5-μm-thick sections were used in all staining protocols. Immunofluorescence staining was carried out with the protocols described in the online-only Data Supplement.

Intravital Microscopy

Intravital microscopy was performed on exteriorized spleens of live animals. Time-lapse images were captured to visualize the behavior of cells. Details of the procedure are given in the online-only Data Supplement.

Statistics

Results are expressed as mean±SEM. Statistical tests included unpaired, 2-tailed Student t test with the Welch correction for unequal variances and 1-way ANOVA followed by the Bonferroni comparison test. Values of $P \leq 0.05$ were considered to denote significance.

Results

The Spleen Contributes Ly-6C^{high} Monocytes to the Growing Atheroma

We have previously shown that the spleen contains a monocyte reservoir that mobilizes in response to acute injury,[17] but the role of this reservoir in chronic inflammatory diseases such as atherosclerosis is unknown. We chose to investigate a possible link between the splenic reservoir and atherosclerosis in ApoE$^{-/-}$ mice. Immunofluorescent staining, which provides information on spatial distribution, showed expansion of CD11b^{+} cells throughout the red pulp of ApoE$^{-/-}$ mice (Figure 1A), indicating enlargement of this reservoir. Enumeration of splenic leukocytes in wt C57BL/6 mice and ApoE$^{-/-}$ mice consuming a diet high in fat and cholesterol (HCD) revealed dramatic differences between the groups: ApoE$^{-/-}$ mice had a marked increase in myeloid but not lymphoid cell number (Figure Ia and Ib in the online-only

Data Supplement), a finding that complements previous work.[12] Within the myeloid compartment of the spleen, both monocyte and neutrophil numbers increased (Figure Ic in the online-only Data Supplement). We also detected an expansion of monocytes and neutrophils in the spleens of LDLR$^{-/-}$ApoB48$^{-/-}$ mice consuming a Paigen diet, indicating that the phenomenon is ApoE independent (Figure Id in the online-only Data Supplement).

To address whether the spleen mobilizes monocytes during atherogenesis, we transplanted spleens from CD45.1 ApoE$^{-/-}$ mice to recently splenectomized 30-week-old CD45.2 ApoE$^{-/-}$ mice that had consumed an HCD for 20 weeks. The transplantation procedure anastomoses splenic and recipient vessels, preserves blood flow and organ integrity,[17] and does not alter the relative proportion of endogenous leukocytes in the spleen, bone marrow, and blood (Figure Ie in the online-only Data Supplement). The transplanted spleens resembled endogenous spleens in size and cellularity, had the characteristic purplish-red color, and were well perfused (Figure If in the online-only Data Supplement). Spleens of CD45.1 ApoE$^{-/-}$ mice consuming an HCD for 20 weeks were large and enriched with myeloid cells (Figure 1B). As a control, we also transplanted spleens from CD45.1 ApoE$^{-/-}$ mice consuming a chow diet (chow) because they contained small spleens and relatively small myeloid reservoirs (Figure 1B) and spleens from CD45.1 ApoE$^{-/-}$ mice consuming an HCD that had their reservoirs depleted with clodronate liposomes (Figure 1B).

Transplantation of CD45.1 ApoE$^{-/-}$ mice consuming an HCD for 20 weeks led to a large accumulation of spleen-derived monocytes, but not macrophages, in the recipient blood ($4.7\times10^5\pm2\times10^5$ monocytes in blood; Figure 1C). After 24 hours, 45±15% of the monocytes found in the blood were splenic derived. Although we focused our analysis on monocytes and progeny (CD11b$^+$Lin$_1^-$; Figure Ia in the online-only Data Supplement), other cells such as neutrophils also accumulated (data not shown). In accordance with the blood data, we observed a substantial population of CD45.1$^+$ cells in the recipient aorta consisting of F4/80^{low} monocytes and F4/80^{high} macrophages (Figure 1D), thus indicating that spleen-experienced F4/80^{low} monocytes accumulated in lesions and matured to F4/80^{high} macrophages locally. The observed contribution of 19% in 24 hours is an underestimation given that an endogenous pool of macrophages already reside in the aorta before transplantation. By focusing on monocytes in the aorta that had recently proliferated, we estimated that the spleen contributed ≈30% of monocytes in 1 day. Remarkably, 100% of monocytes arriving from the spleen (ie, CD45.1) were Ly-6C^{high}, whereas monocytes arriving from all other sources (ie, CD45.2) contained a mixture of Ly-6C^{high} and Ly-6C^{low} monocytes. Transplantation of spleens from either of the 2 controls led to a very low accumulation of monocytes and progeny in the aorta (Figure 1E). Importantly, the total number of aortic monocytes was similar in ApoE$^{-/-}$ HCD spleen recipients compared with age- and diet-matched controls that did not receive a spleen by transplantation (Figure Ig in the online-only Data Supplement), indicating that the transplantation procedure did not interfere with cell accumulation in the aorta. The finding is expected because the transplantation experiments consisted of removing the endogenous spleen and thus represented splenic exchange rather than supplementation. The intima of aortic root lesions contained spleen-derived myeloid cells of mixed morphology readily identified by CD45.1 immunofluorescence (Figure 1F). The spleen therefore contributes inflammatory Ly-6C^{high} monocytes to the growing atheromata.

Spleen-Experienced Monocytes Express Pro–Interleukin-1β, Have Proteolytic Capacity, Contribute Reactive Oxygen Species, and Give Rise to Lipid-Laden Macrophages in Atheromata

Monocyte-derived macrophages in atheromata secrete inflammatory cytokines, express proteolytic enzymes, contribute reactive oxygen species, and ingest lipids. Each of these functions profoundly influences lesion evolution. Inflammatory cytokines and reactive oxygen species propagate inflammation; proteolysis remodels the extracellular matrix; and lipid uptake yields foam cells.[7] We therefore sought to determine whether spleen-experienced monocytes and macrophages exhibit these properties. We compared spleen-experienced monocytes and their descendent macrophages with monocytes and macrophages that arrived from all sources by transplanting CD45.1$^+$ ApoE$^{-/-}$ spleens to CD45.2$^+$ ApoE$^{-/-}$ animals for 2 days, as shown in Figure 1. For simplicity, we call these spleen-experienced monocytes and their descendent macrophages "splenic" and those arriving from all sources medullary. It is important to note, however, that at least some of the medullary cells might have experienced the spleen before accumulating in lesions.

Evaluating inflammatory cytokine expression focused on interleukin (IL)-1β, a monocyte product implicated in many aspects of atherogenesis.[19] Aortic cells in ApoE$^{-/-}$ HCD mice expressed a higher proportion of pro–IL-1β$^+$ compared with wt controls (Figure IIa and IIb in the online-only Data Supplement), reflecting the higher inflammatory burden of these animals. Spleen transplantation revealed similar pro–IL-1β expression among splenic (CD45.1$^+$) and medullary (CD45.2$^+$) monocytes, suggesting that the inflammatory capacity of splenic monocytes is comparable to that of their counterparts (Figure 2A). Splenic (CD45.1$^+$) aortic macrophages remained pro–IL-1β$^+$ at proportions similar to those of monocytes but at higher proportions than CD45.2$^+$ macrophages. This indicates that aortic monocytes and macrophages of splenic origin are at least as, if not more, inflammatory as their CD45.2$^+$ counterparts. To investigate proteolysis, we injected spleen recipients with a protease-activatable fluorescent sensor that reports on cysteinyl cathepsin activity in vivo.[20,21] At the cellular level, most lesional monocytes and macrophages of splenic origin (CD45.1$^+$) exhibited proteolytic activity, and comparison with lesional monocytes and macrophages accumulating from the bone marrow (CD45.2$^+$) revealed a similar proportion (83% versus 78%; 98% versus 85% were positive for Prosense-680) of signal (Figure 2B). Monocytes had less proteolytic activity when residing in the bone marrow and spleen, indicating that proteolysis coincides with activation in destination sites (Figure IIc in the online-only Data Supplement). To measure cellular redox states, we used an intracellular probe that measures oxidative stress.[22] Regardless of origin, monocytes and macrophages expressed reactive oxy-

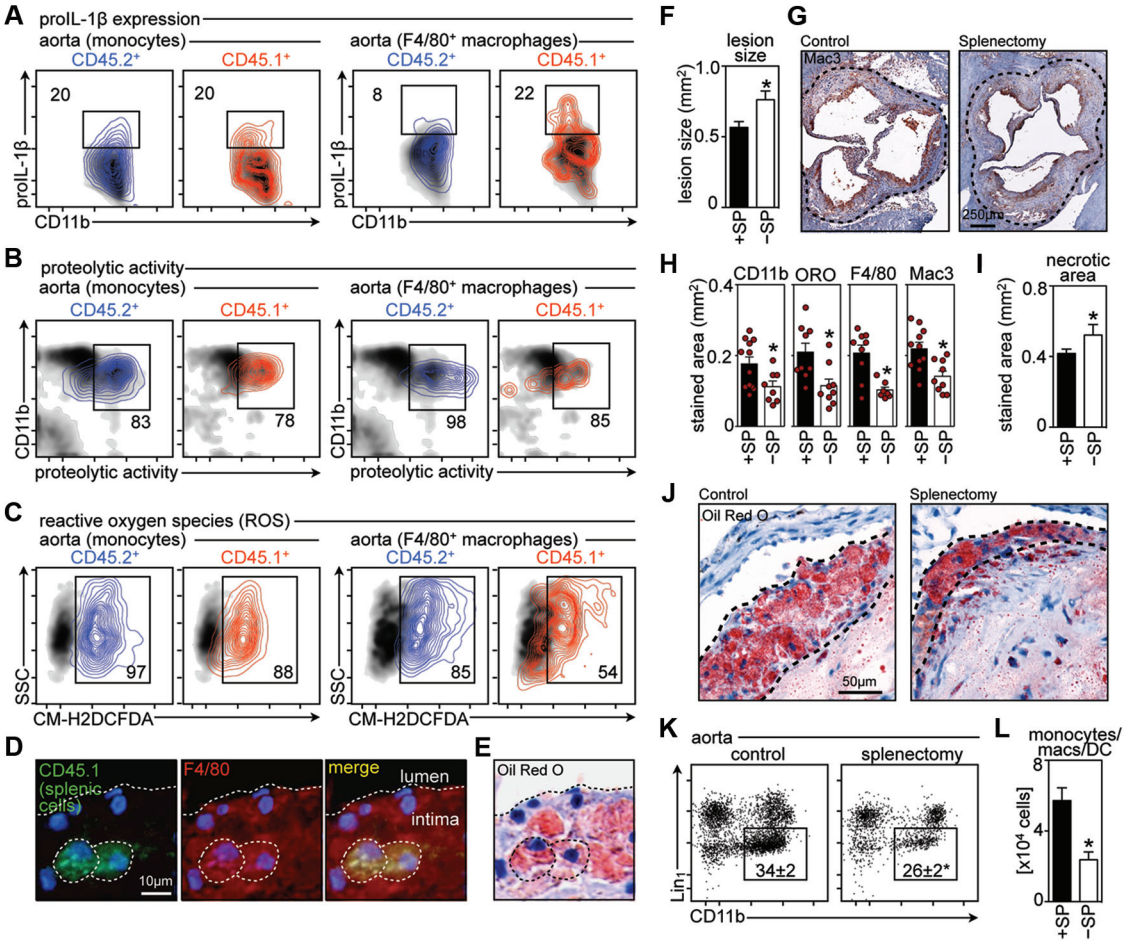

Figure 2. Splenic cells are inflammatory and shape lesional evolution. **A**, Spleen transplantation from CD45.1$^+$ apolipoprotein E–deficient (ApoE$^{-/-}$) to CD45.2$^+$ ApoE$^{-/-}$ mice. Expression of pro–interleukin (IL)-1β on monocytes and macrophages directly ex vivo (ie, unstimulated). Contour plots show pro–IL-1β expression gated on lesional monocytes and macrophages of splenic (CD45.1$^+$, red) or other source (ie, bone marrow) (CD45.2$^+$, blue) origin. The control density plots (black) represent isotype controls. **B**, Contour plots show protease activity gated on lesional monocytes and macrophages of splenic (CD45.1, red) or other source (ie, bone marrow; CD45.2$^+$, blue) origin. The control density plots (black) are gated on all leukocytes. **C**, Contour plots show the presence of reactive oxygen species on lesional monocytes and macrophages of splenic (CD45.1$^+$, red) or other source (ie, bone marrow; CD45.2$^+$, blue) origin. The control density plots (black) are gated on cells that did not receive the probe. Representative plots in **A** through **C** of at least 2 independent experiments are shown. **D**, Spleen transplantation for 10 days. Data show immunofluorescence on the aortic root with antibodies against CD45.1 (splenic cells, green), F4/80 (macrophages, red), and their merge (yellow). DAPI depicts nuclei (blue). Arrows point to F4/80$^+$ cells of splenic origin. **E**, Oil Red O (ORO) staining of the same section as in **D** shows colocalization of ORO with spleen-derived macrophages. **F**, Splenectomy of ApoE$^{-/-}$ high-cholesterol diet (HCD) mice for 12 weeks. Data show enumeration of total lesion size with hematoxylin and eosin. **G**, Representative Mac3 expression on aortic root sections in control and splenectomized ApoE$^{-/-}$ HCD mice. **H**, Enumeration of CD11b, ORO, F4/80, and Mac3 areas on aortic root sections in control and splenectomized ApoE$^{-/-}$ HCD mice. **I**, Enumeration of the necrotic core size in the same groups as above. **J**, Representative ORO staining in the same groups as above. **K**, Flow cytometry of digested aortas. Dot plots show cellular distribution from control and splenectomized ApoE$^{-/-}$ HCD mice. The monocyte/macrophage gate is shown. **L**, Total number of monocytes and macrophages/dendritic cells enumerated by flow cytometry (mean±SEM; n=5–11) *P<0.05.

gen species, although macrophages derived from spleen-experienced monocytes expressed them at somewhat lower levels (Figure 2C). Finally, we asked whether spleen-experienced monocytes can give rise to lesional foam cells. Circulating monocytes of either origin accumulated DiI-oxidized LDL to the same extent (Figure IId in the online-only Data Supplement) and aortic atheromata contained large myeloid cells of splenic origin that took up Oil Red O (Figure 2D and 2E and Figure IIe in the online-only Data Supplement), indicating that the spleen contributes foam cell precursors.

The spleen is a secondary lymphoid organ that supports multiple functions: It contains T and B cells that participate in adaptive immunity and macrophage and dendritic cell subsets that scavenge erythrocytes and screen for blood-borne infections.[23] In animal models, splenectomized mice[24,25] and hamsters depleted of monocytes with clodronate liposomes develop larger lesions.[26] We therefore wondered whether and how splenectomy alters the lesional monocyte/macrophage/foam cell content. As expected, lesions in female mice splenectomized for 12 weeks were larger (Figure 2F) as assessed by hematoxylin and eosin staining (Figure IIf in the online-only Data Supplement). However, the lesions appeared to be less cellular, prompting us to evaluate their content with macrophage markers. Staining for Mac3, CD11b, and F4/80 revealed that aortic root sections in

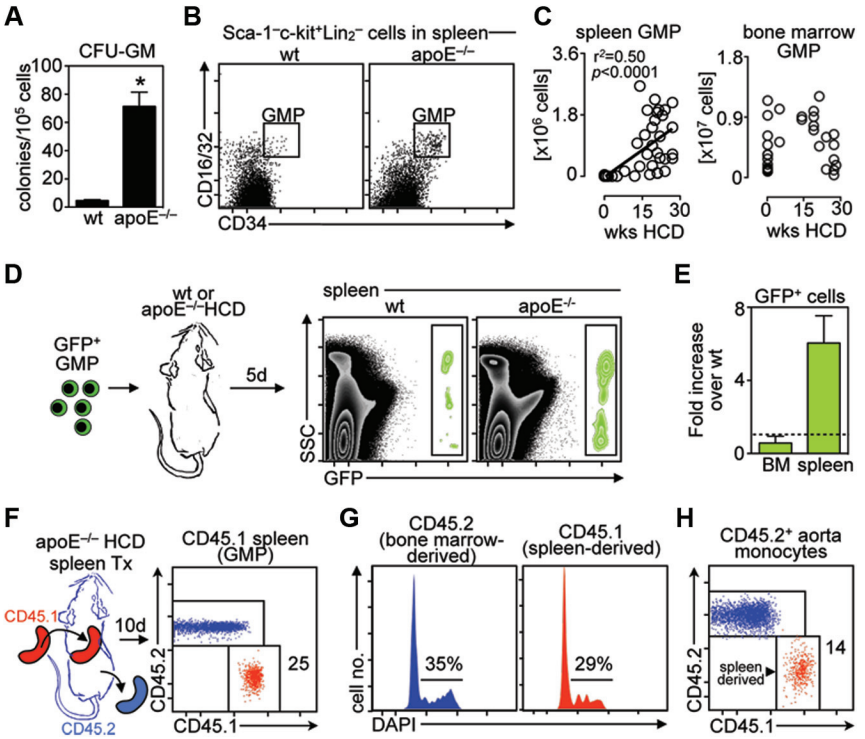

Figure 3. The spleen contains proliferating myeloid cell progenitors that give rise to their progeny in vivo. **A**, Colony-forming units–granulocytes and macrophages (CFU-GM) show colony formation in spleens of wild-type (wt) and apolipoprotein E–deficient ($ApoE^{-/-}$) high-cholesterol diet (HCD) mice (mean±SEM; n=4). *$P<0.05$. **B**, Phenotypic analysis of granulocyte and macrophage progenitors (GMPs) in spleens of wt and $ApoE^{-/-}$ HCD mice. **C**, Enumeration of GMP in spleens and bone marrow of $ApoE^{-/-}$ mice fed an HCD for up to 30 weeks. Linear regression was performed. **D**, Adoptive transfer of green fluorescent protein–positive (GFP^+) GMPs to wt and $ApoE^{-/-}$ HCD mice. Data show GFP cells in spleens 5 days after transfer. **E**, Enumeration of data above. Data show the fold increase from wt to $ApoE^{-/-}$ HCD mice of adoptively transferred GFP^+ cells in the bone marrow (BM) and spleen (data shown are pooled from 2 independent experiments). **F**, $CD45.1^+$ spleens from $ApoE^{-/-}$ HCD mice were transplanted to asplenic $CD45.2^+$ $ApoE^{-/-}$ HCD mice for 10 days. Data show chimerism of GMPs in spleens 10 days after transplantation. **G**, Cell cycle analysis of $CD45.1^+$ and $CD45.2^+$ GMP in transplanted spleens shown in **F**. Numbers indicate percentage of cells in $S/G_2/M$ phase (means±SEM; n=4). **H**, Monocyte accumulation in aortic tissue of the mice described in **F** and **G**. Representatives of 2 independent experiments are shown.

splenectomized mice contained fewer monocyte/macrophages (Figure 2G and 2H and Figure IIg in the online-only Data Supplement) but had larger acellular areas (Figure 2I). Accordingly, cellular Oil Red O areas were smaller in splenectomized mice (Figure 2H and 2J). We detected no differences in collagen content, as measured by Masson trichrome (Figure IIh in the online-only Data Supplement) and no differences in smooth muscle cell content (Figure IIi in the online-only Data Supplement). Flow cytometry of digested aortas confirmed that lesions of splenectomized mice contained fewer monocytes/macrophages (Figure 2K and 2L).Our studies are in accordance with the observation that, when monocyte supply is reduced, lesions become larger and less cellular.[26] Thus, the spleen provides a surplus of cells that serve to shape the evolving lesion.

The Spleen Contains Proliferating Myeloid Cell Progenitors That Give Rise to Their Progeny In Vivo

The cell tracking experiments described thus far may simply reflect production of monocytes in the bone marrow, their circulation through the spleen, and their eventual accumulation in the lesions. We therefore sought to determine whether the spleen can produce monocytes from progenitors. In vitro, splenocytes of $ApoE^{-/-}$ HCD mice formed many more granulocyte/macrophage colonies than wt controls (Figure 3A), indicating clonal myeloid cell proliferation. Compared with wt controls, $ApoE^{-/-}$ HCD mice contained numerous HSPCs, including LSK (Lin_2^- $Sca\text{-}1^+$ $c\text{-}kit^+$) cells and common myeloid progenitors, as well as granulocyte and macrophage progenitors (GMPs), which are the most committed progenitors known to give rise to monocytes and neutrophils[4] (Figure 3B and Figure IIIa in the online-only Data Supplement). Common lymphoid progenitors did not increase in $ApoE^{-/-}$ HCD mice, indicating a preference toward the myeloid lineage in the spleen (Figure IIIa in the online-only Data Supplement). GMP enumeration over 30 weeks of diet showed continued growth in the spleen. The GMP population in the bone marrow also grew, but less markedly and transiently (Figure 3C). Indeed, in many older animals, the GMP population in the spleen exceeded that of the bone marrow. Notably, although the spleen also contained macrophage and dendritic cell progenitors,[27] the aorta and para-aortic lymph nodes were virtually devoid of HSPCs (data not shown). In keeping with the expanded reservoir, the spleens of $LDLR^{-/-}ApoB48^{-/-}$ mice also contained higher numbers of GMPs (Figure IIIb in the online-only Data Supplement). These findings demonstrate that the spleens of atherosclerotic mice contain the requisite myelopoietic cells.

To test for monocytopoiesis in vivo, we injected 1×10^5 highly purified GFP-expressing GMP (Figure IIIc in the online-only Data Supplement) into either ApoE$^{-/-}$ HCD or wt mice and enumerated GFP$^+$ cells 5 days later. Considerably more GFP$^+$ cells accumulated in the spleens of ApoE$^{-/-}$ HCD mice than in the controls (Figure 3D and 3E). Among these cells, we detected progenitors and differentiated CD11b$^+$Gr1$^+$ monocytes and neutrophils (Figure IIId in the online-only Data Supplement), which indicates GMP expansion. The number of GFP$^+$ cells accumulating in the bone marrow, however, was similar in wt and ApoE$^{-/-}$ HCD mice (Figure 3E). This similarity likely reflects a preference for mobilized progenitors to seed the spleen in atherosclerosis (progenitors were injected intravenously).

To demonstrate that the spleen contributes rather than simply collects monocytes, we performed spleen transplantation experiments for longer durations. The monocyte half-life is estimated at a few hours to 1 to 2 days,[11,28] and adoptive transfer of 5×10^6 sorted monocytes by a procedure that allows their retrieval 1 day later[12] failed to yield any cells in lesions, blood, or spleen 5 days later. We therefore reasoned that if monocytes and their progenitors reside in the spleen briefly or simply circulate through its fenestrated parenchyma, spleen transplantation would result in a rapid and complete cell turnover. If, however, the spleen produces monocytes, it should maintain progenitors and monocytes from the original animal for a period exceeding 2 days. In accordance with the second possibility, CD45.2$^+$ ApoE$^{-/-}$ HCD mice that received CD45.1$^+$ ApoE$^{-/-}$ spleens 10 days earlier contained 3.2×10^6 GMPs, of which 25% were still CD45.1$^+$ (Figure 3F), and many were proliferating (Figure 3G). The aortas of these mice also contained numerous CD45.1$^+$ monocytes and macrophages (Figure 3H). Importantly, that 75% of GMPs that were CD45.2$^+$ in these animals indicates that the bone marrow continuously supplies and replenishes the splenic progenitor pool. In contrast, transplantation of naïve spleens, which do not contain progenitors, resulted in complete turnover of the monocyte pool in 2 days. Thus, if the bone marrow is the upstream source of hematopoietic cells, the spleen is a seeding ground for an amplification cascade during inflammation. Together, our findings indicate that the spleen contains proliferating myeloid cell progenitors that give rise to their progeny in vivo.

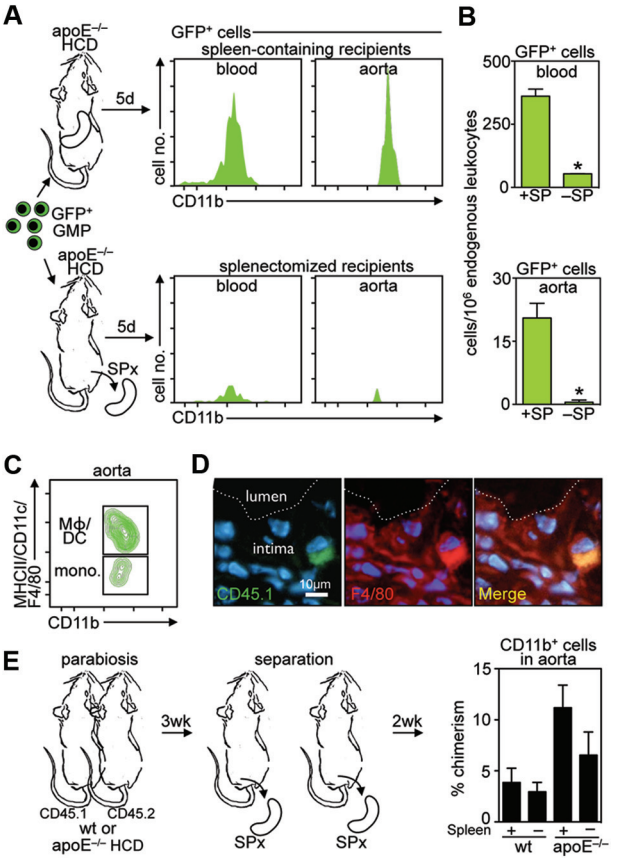

Figure 4. Splenic monocytopoiesis gives rise to lesion-infiltrating monocytes. **A**, Adoptive transfer of green fluorescent protein–positive (GFP$^+$) granulocyte and macrophage progenitors (GMPs) to apolipoprotein E–deficient (ApoE$^{-/-}$) high-cholesterol diet (HCD) mice with or without their spleen. Data show GFP$^+$ CD11b cells retrieved from blood and aorta 5 days after transfer. **B**, Enumeration of data above (data shown are pooled from 2 independent experiments). *$P<0.05$. **C**, Differentiation of GFP$^+$ GMPs into lesional macrophages. A representative contour plot shows that GFP$^+$ cells that were injected as GMPs have accumulated in lesions as monocytes and matured to macrophages. **D**, CD45.1 GMPs were adoptively transferred to ApoE$^{-/-}$ HCD mice, and the aorta was harvested 5 days after transfer. A representative pictograph shows CD45.1 (GMP-derived, green), F4/80 (macrophages, red), and their merge (yellow) in the intima. **E**, CD45.1 and CD45.2 wild-type (wt) or ApoE$^{-/-}$ HCD mice were joined in parabiosis for 3 weeks, separated, splenectomized (or not), and assessed for chimerism 2 weeks later. Data show chimerism for CD11b$^+$ cells in the aorta (mean±SEM; n=4).

Splenic Monocytopoiesis Gives Rise to Lesion-Infiltrating Monocytes

Having established that the spleen contains proliferating hematopoietic progenitors, we next sought to determine more directly whether the spleen supports monocytopoiesis. We injected GFP$^+$ GMPs into age- and diet-matched spleen-containing and asplenic ApoE$^{-/-}$ HCD mice. Compared with controls, asplenic recipients accumulated fewer GFP$^+$ CD11b$^+$ cells in the blood and aorta (Figure 4A and 4B). In the aorta, among the GFP$^+$ cells, we found differentiated monocytes and mature macrophages but not progenitors, which would appear in the lower-left quadrant (CD11b$^-$MHCII/CD11c/F4/80$^-$; Figure 4C), indicating a direct and spleen-dependent link from hematopoietic progenitors to tissue descendants. We confirmed these flow cytometry tracking experiments by detecting adoptively transferred CD45.1$^+$ F4/80$^+$ cells microscopically on tissue sections (Figure 4D).

To confirm the role of the spleen in maintaining the aortic pool of monocytes, we joined CD45.1 to CD45.2 mice by parabiosis (Figure 4E), a technique that establishes a shared circulation by which bone marrow HSPCs can seed partner tissues.[5,6,17,28] Two weeks after parabiont separation, the percent of myeloid cell chimerism in wt aortas was low (≈5%) and spleen independent (Figure 4E). This finding supports the observation that, under normocholesterolemic conditions, the spleen does not produce monocytes.[17] In contrast to wt mice, the aortas of spleen-containing ApoE$^{-/-}$ HCD animals showed a 3-fold increase in chimerism. Strik-

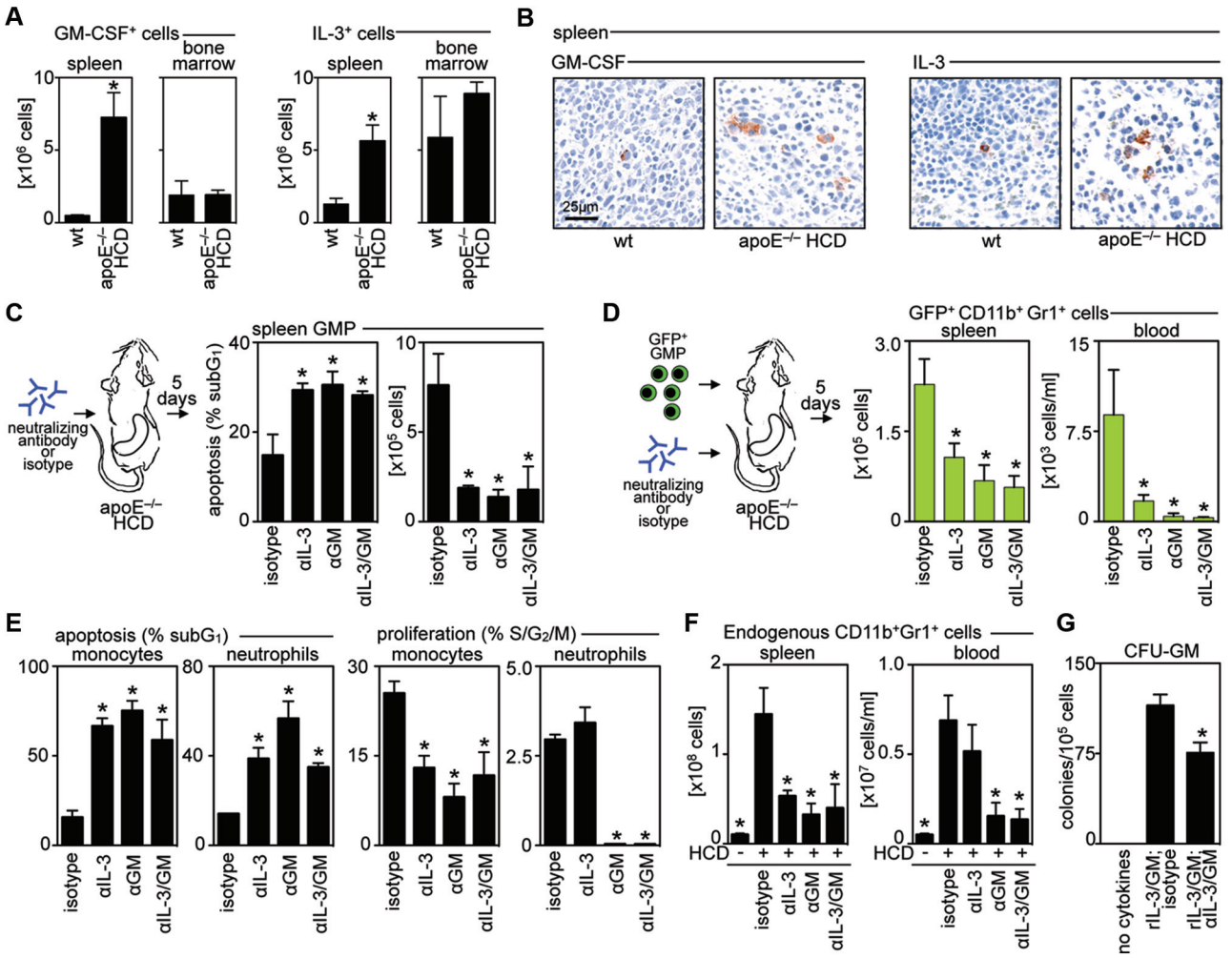

Figure 5. Granulocyte macrophage colony-stimulating factor (GM-CSF) and interleukin (IL)-3 control survival and proliferation of myeloid progenitors and progeny in atherosclerosis. **A**, Enumeration of GM-CSF– and IL-3–producing cells by flow cytometry in the spleen and bone marrow in wild-type (wt) and apolipoprotein E–deficient (ApoE$^{-/-}$) high-cholesterol diet (HCD) mice. Data show a preferential increase of GM-CSF and IL-3–producing cells in the spleen (mean±SEM; n=5). *$P<0.05$. **B**, Presence of GM-CSF– and IL-3–producing cells in the red pulp of wt and ApoE$^{-/-}$ HCD mice. **C**, Effect of IL-3 and GM-CSF neutralization on endogenous splenic granulocyte and macrophage progenitors (GMPs). Data show percent of cells in subG$_1$ and total number of GMPs in spleen (mean±SEM; n=4–5). **D**, Effect of IL-3 and GM-CSF neutralization on the development of myeloid cells after green fluorescent protein—positive (GFP$^+$) GMP pulse chase. Data show GFP$^+$ CD11b$^+$Gr1$^+$ cells in the spleen and blood (mean±SEM; n=4–5). **E**, Effect of IL-3 and GM-CSF neutralization on apoptosis and proliferation of endogenous monocytes and neutrophils in the spleen (mean±SEM; n=4–5). **F**, Effect of IL-3 and GM-CSF neutralization on the endogenous CD11b$^+$Gr1$^+$ repertoire in the spleen and blood (mean±SEM; n=4–5). *$P<0.05$ vs wt (**A**, **B**) or HCD isotype (**C**–**F**). **G**, Colony-forming units granulocyte-macrophage (CFU-GM) in the spleen. Data show that, in the absence of cytokines, colonies do not form in the spleen, that GM-CSF and IL-3 are sufficient for colony formation, and that a single dose of anti–GM-CSF and anti–IL-3 attenuates colony formation in vitro (mean±SEM; n=2).

ingly, splenectomy decreased this chimerism by nearly 50%. These data demonstrate, by an independent approach, that the spleen contributes myeloid cells to the atherosclerotic aorta.

Granulocyte Macrophage Colony-Stimulating Factor and IL-3 Promote Survival and Proliferation of Progenitor Cells and Their Progeny

The growth factors granulocyte macrophage colony-stimulating factor (GM-CSF) and IL-3 can stimulate hematopoiesis, particularly emergency hematopoiesis,[29] but their role in atherosclerosis is poorly understood.[30–32] Recent observations in experimental atherosclerosis that HSPCs increase the common receptor subunit for GM-CSF and IL-3[33] prompted us to investigate the influence of these cytokines on myelopoiesis. GM-CSF– and IL-3–producing cells increased preferentially in the spleen during atherosclerosis (Figure 5A). In the spleen, the red pulp of ApoE$^{-/-}$ HCD mice contained numerous GM-CSF– and IL-3–producing cells that stained specifically for the growth factors on tissue sections (Figure 5B and Figure IVa in the online-only Data Supplement) and costained for the leukocyte marker CD45 by flow cytometry (Figure IVb in the online-only Data Supplement). Negligible levels of GM-CSF and IL-3 cells were detected in the steady-state spleens. Colony-forming assays showed that GM-CSF and IL-3 were sufficient to drive myelopoiesis of splenic progenitors (Figure IVc in the online-only Data Supplement). We therefore injected antibodies

against GM-CSF and IL-3 on 5 consecutive days and evaluated the myeloid lineage in the spleen, bone marrow, and blood in vivo using 4 approaches. First, we analyzed splenic GMPs. Neutralization of IL-3, GM-CSF, or both increased the proportion of GMPs undergoing apoptosis in situ (as measured by DNA content) and correspondingly decreased their total number in the spleen (Figure 5C). Second, we performed pulse-chase experiments that, as in those depicted in Figures 3 and 4, involved the transfer and retrieval of GFP^+ cells. Neutralization of IL-3, GM-CSF, or both prevented the appearance of numerous myeloid cells in the spleen and blood (Figure 5D). Third, we evaluated the survival and proliferation of mature myeloid cells in the spleen. Again, neutralization increased the proportion of in situ dying monocytes and neutrophils and decreased their local proliferation (Figure 5E). Finally, we evaluated the endogenous number of myeloid cells in spleen and blood and found that neutralization attenuated splenic and blood monocytosis and neutrophilia by up to 80% (Figure 5F). In vitro confirmatory experiments showed that myelopoiesis was attenuated with only a single dose of GM-CSF– and IL-3–neutralizing antibodies (Figure 5G). Expectedly, the dramatic decrease in vivo resulted not only from local effects on the spleen, but also from effects on the bone marrow (Figure IVc in the online-only Data Supplement). These data demonstrate that GM-CSF and IL-3 orchestrate the survival and proliferation of myeloid progenitors and their descendants in the bone marrow and spleen in atherosclerosis.

Extramedullary Hematopoiesis Occurs in Response to Peritoneal Endotoxin Challenge and Can Be Visualized In Vivo

Experiments thus far have shown that, in experimental atherosclerosis, HSPCs accumulate in the spleen and proliferate in response to GM-CSF and IL-3 and the spleen contributes monocytes to the growing atheromata. We next sought to determine whether the process occurs in a different model and whether it can be visualized in vivo. Mice that received lipopolysaccharide daily for 4 days developed visibly larger spleens (Figure Va in the online-only Data Supplement) containing plenty of monocytes (11-fold expansion over steady state) and neutrophils (23-fold expansion; Figure Vb in the online-only Data Supplement) that resided in the red pulp (Figure Vc in the online-only Data Supplement). To evaluate whether the spleen contributes newly made neutrophils and monocytes in this model, we first enumerated hematopoietic progenitor cells. In response to lipopolysaccharide, GMPs expanded in the spleen (≈62-fold; Figure Vd in the online-only Data Supplement). The progenitors proliferated vigorously (47% were in S or G_2 phase of the cell cycle at a given time; Figure Ve in the online-only Data Supplement) and gave rise to granulocyte macrophage colony-forming units (Figure Vf in the online-only Data Supplement).

We therefore tested whether splenic GMPs give rise to their progeny. Pulse-chase experiments involving the intravenous transfer of GFP- or RFP-expressing GMPs to nonirradiated (wt) C57BL/6 mice that were naïve or that received lipopolysaccharide permitted us to track cell fate by flow cytometry and intravital microscopy. GMPs injected into naïve mice gave rise to only a few progeny (Figure 6A). Injection of GMP to mice that received lipopolysaccharide, in contrast, led to marked cellular expansion. Three days after transfer, the fluorescent (in this case, GFP^+) cells in the spleen were still mostly $CD11b^-$ $Gr1^-$ progenitors, although a few fluorescent neutrophils and a few Ly-$6C^{high}$ monocytes ($CD11b^+$ $Gr1^+$ cells) emerged in the circulation (Figure 6A). Three to 5 days later (day 6–8), the fluorescent cells in the spleen and blood were almost exclusively $CD11b^+$ $Gr1^+$ neutrophils with a few monocytes but not progenitors, mature macrophages, or dendritic cells (Figure 6A and 6B). Enumeration revealed significant expansion of neutrophils and monocytes in response to lipopolysaccharide in the spleen and blood (Figure 6C). The bone marrow contained numerous GFP progeny, but as reported in the atherosclerosis model, there was no increase in their number in response to lipopolysaccharide. These data show that escalation of the neutrophil and monocyte response in response to endotoxin is associated with an increase in biologically active progenitors in the spleen.

Intravital microscopy showed that GMPs gave rise to clusters of cells that resided outside the blood vessels in the red pulp (Figure 6D). In this pulse-chase experiment, clusters appeared 3 days after adoptive transfer, increased in size by 8 days, and disappeared by 12 days (Figure Vg and Vh in the online-only Data Supplement), which is in keeping with the expected lifespan of GMPs.[34] GFP GMPs and RFP GMPs coinjected in equal numbers (Figure 6E) gave rise to clusters that were exclusively red or exclusively green, indicating that GMPs seeded the spleen, proliferated clonally, and differentiated locally (Figure 6F and Figure Vi–Vk in the online-only Data Supplement). Time-lapse imaging of representative clusters showed that locally produced cells can intravasate and thus contribute to the systemic repertoire (Figure 6G). To enumerate this contribution, mice were subjected either to splenectomy (Figure 6H) or to spleen transplantation (Figure 6I). Both approaches revealed that a substantial number of myeloid cells accumulating in the peritoneum were of splenic origin. The cells were inflammatory, as evidenced by the expression of tumor necrosis factor-α (Figure 6J). Together, these data reveal that extramedullary sites such as the spleen can produce circulating monocytes and neutrophils that accumulate in their respective inflammatory destinations. The model that describes the findings of this study is shown in Figure 7.

Discussion

The motivation for the present study rested on 2 landmark articles published in the 1960s. The first laid the foundation that HSPCs circulate in the blood rather than simply reside in the bone marrow,[35] whereas the second argued that, in the steady state, the bone marrow is the exclusive monocyte production site.[36] Multiple studies since have enriched our understanding of these processes. Extramedullary hematopoiesis occurs in development and in a number of genetic and myeloproliferative conditions.[37–41] It involves several discrete steps: (1) Bone marrow HSPCs mobilize; (2) mobilized HSPCs seed extramedullary sites; and (3) seeded HSPCs proliferate and mature. The cell types that have been described to arise through extramedullary hematopoiesis are terminally differentiated, and many are tissue resident. Mono-

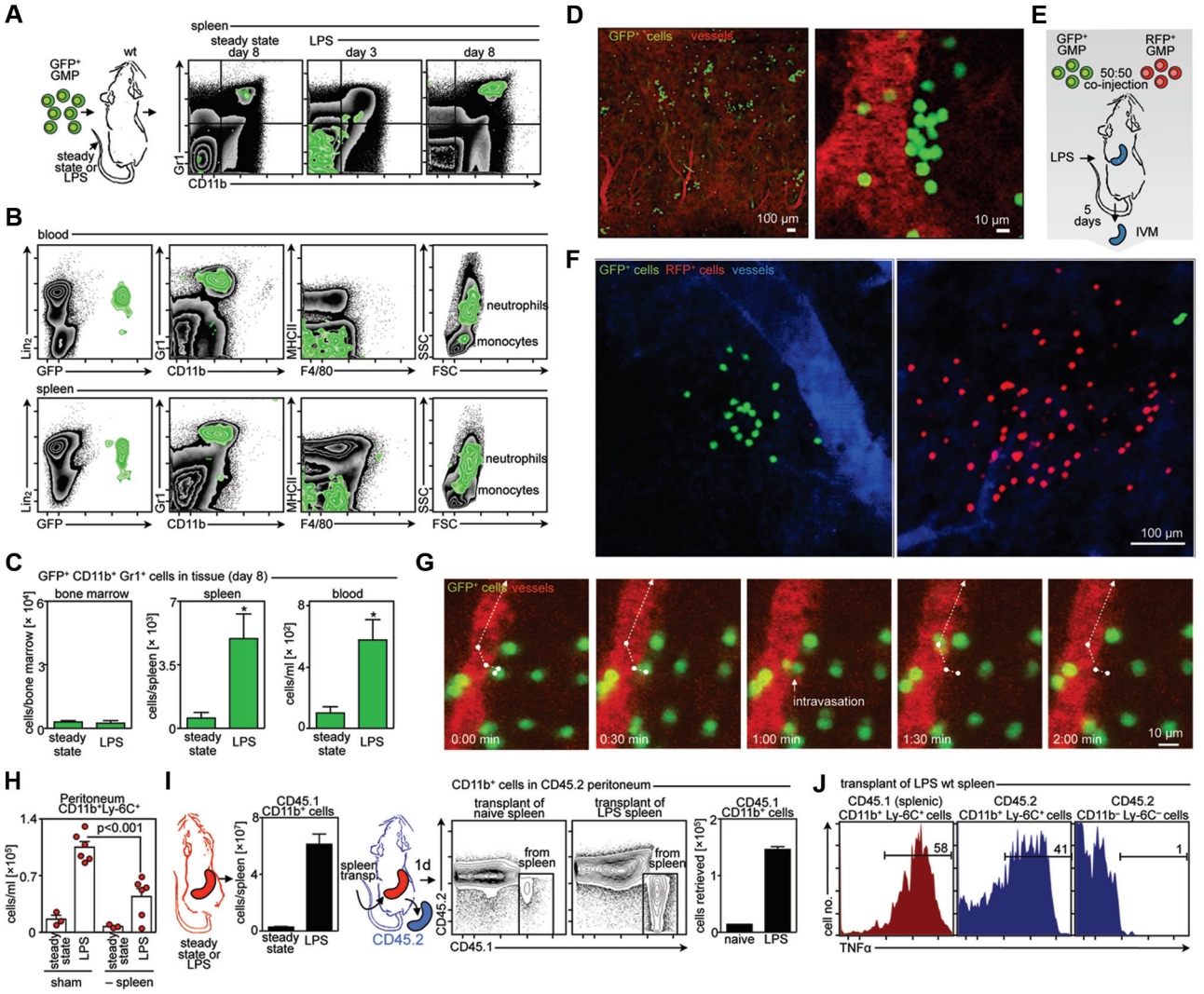

Figure 6. Extramedullary hematopoiesis gives rise to monocytes in response to repeated peritoneal endotoxin challenge. **A**, Cartoon depicts a pulse-chase experiment in which green fluorescent protein—positive (GFP^+) granulocyte and macrophage progenitors (GMPs) were adoptively transferred to wild-type (wt) C57BL/6 mice that remained naïve or were injected with lipopolysaccharide (LPS). A representative plot of at least 3 independent experiments is shown. **B**, GFP^+ GMPs were adoptively transferred to wt C57BL/6 mice injected with LPS. Data are representative of at least 3 independent experiments. **C**, Enumeration of GFP^+ $CD11b^+Gr1^+$ cells adoptively transferred as GFP^+ GMPs 8 days earlier and retrieved from host spleen and blood of naïve or inflammatory mice (mean±SEM; n=3–8). $^*P<0.05$. **D**, Intravital microscopy pictograms of the splenic red pulp depict clusters of GFP^+ cells adoptively transferred intravenously 8 days earlier into inflammatory (LPS-injected) mice. Vasculature is shown in red; the scale is depicted with white bars. Data are representative of at least 3 independent experiments. **E**, Cartoon depicts the experimental design for the coinjection of equal numbers of GFP^+ GMPs and red fluorescent protein–positive (RFP^+) GMPs into C57BL/6 mice injected with LPS. **F**, Green and red clusters in the subcapsular red pulp 5 days after injection of equal numbers of GFP^+ GMPs and RFP^+ GMPs. Vasculature is shown in blue; the scale is depicted by a white bar. Data are representative of at least 3 independent experiments. **G**, A prototypic departing cell is shown to intravasate and enter the circulation. **H**, Accumulation of myeloid cells in splenectomized animals. Mice received LPS and were either splenectomized or subjected to sham surgery. Four days later, peritoneal $CD11b^+Gr1^+$ cells were enumerated. **I**, Spleen transplantation from CD45.1 donors to CD45.2 recipient mice. Donors either were naïve or received LPS. The graph shows the total number of splenic $CD11b^+Gr1^+$ that had accumulated in the peritoneum. **J**, Expression of intracellular tumor necrosis factor-α (TNFα). Histograms show TNFα expression on stimulated cells gated on $CD11b^+Gr1^+$ cells of splenic ($CD45.1^+$, red) or other source (ie, bone marrow) ($CD45.2^+$, blue) origin. Data are representative of at least 2 independent experiments.

cytes, on the other hand, are intermediate, circulating cells, developmentally downstream of HSPCs but upstream of dendritic cells and macrophages.[2] Our study places extramedullary hematopoiesis in a larger context not only because it shows that a GM-CSF– and IL-3–rich splenic environment can produce monocytes and neutrophils that then circulate but also because it illustrates an extramedullary cascade in which HSPC proliferation, differentiation, and terminal maturation are compartmentalized in different organs. In atherosclerosis, our data imply, the bone marrow outsources the production of circulating leukocytes.

Of all the organs, the spleen may be an ideal outsource destination. The organ has an open circulation, allowing fast exchange with the blood,[23] yet it is capable of cell retention through myriad adhesive ligands.[42,43] The organ can accommodate vast quantities and fluctuations of cells, especially in the red pulp. It also allows the rapid exit of undifferentiated monocytes, indicating that entry into its parenchyma neither

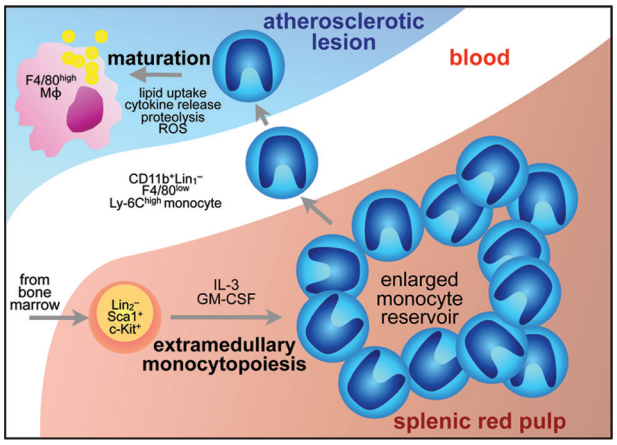

Figure 7. Model depicting the extramedullary generation of monocytes in inflammation. Model shows that mobilized hematopoietic stem and progenitor cells accumulate in the splenic red pulp and give rise to monocytes via interleukin-3 (IL-3) and granulocyte macrophage colony-stimulating factor (GM-CSF). Spleen-derived monocytes infiltrate inflammatory sites and mature to macrophages. The splenic contribution increases as the reservoir enlarges. Monocytes that accumulate from bone marrow directly are omitted in this cartoon. ROS indicates reactive oxygen species.

forces differentiation nor precludes recirculation.[17] Thus, location, elasticity, and architecture render the spleen a perfect seeding ground for the emergency production of inflammatory cells.

It is unknown whether extramedullary hematopoiesis is important in the development of human atherosclerosis. The extent to which the spleen contributes to disease, however, has received some attention. The organ may be dispensable, but it is not unimportant. In humans, splenectomy heightens the risk of infection and ischemic heart disease, probably as a result of multiple mechanisms involving platelets, B cells, T cells, and many of the other components that constitute the organ.[44] The observations made here in response to hypercholesterolemia or endotoxin indicate a role for the spleen in supplying Ly-6C^{high} monocytes, which are known to be inflammatory and proteolytic. We show that, by eliminating this splenic source, lesions become less cellular, although how this particular profile translates to lesion stability requires further study. Future studies also need to elucidate how specific splenic functions can be targeted therapeutically and how other functions such as the protective function of B1 B cells[24] can be spared.

That extramedullary generation of Ly-6C^{high} monocytes occurs during atherosclerosis, when hypercholesterolemia forces a continuous leukocyte supply, is worth further discussion. The steady-state spleen houses a reservoir of undifferentiated monocytes that are, in the absence of neighboring splenic HSPCs, bone marrow derived. The contribution of extramedullary monocytopoiesis during inflammation may be exclusively numeric; with repetitive demand, the organism outsources the production of otherwise identical cells. Alternatively, splenic monocytes, produced in an inflammatory GM-CSF– and IL-3–rich environment, may differ qualitatively from their medullary counterparts. In the present study, we show that monocytes born in extramedullary sites belong to the inflammatory subset and express cytokines, reactive oxygen species, and proteases. They are thus functional and are known to promote the generation of lesions. Future studies need to determine whether splenic birth or experience influences these cells in additional ways.

HSPC mobilization is important to immunosurveillance and likely plays a role in bone marrow niche reconstruction.[5,45] HSPC differentiation in extramedullary sites may be essential to the replenishment of dendritic cells and macrophages.[46] The extramedullary HSPC production of circulating cells, we now show, contributes importantly to inflammatory diseases. This shift in the hematopoietic topographical hierarchy during inflammation is likely to have significant biological, diagnostic, and therapeutic implications.

Acknowledgments

We thank Michael T. Waring and Adam T. Chicoine (Ragon Institute Imaging Core at Massachusetts General Hospital) for sorting cells. We also thank Melissa Greene for secretarial assistance.

Sources of Funding

This work was supported in part by National Institutes of Health grants 1R01 HL095612 (Dr Swirski), U01 HL080731, P50 CA86355, U24 CA092782, P01-A154904 (to Dr Weissleder), and 2R01 HL069948 (to Dr Mulligan-Kehoe). Dr Robbins was supported by the American Heart Association postdoctoral fellowship and the Massachusetts General Hospital ECOR Postdoctoral Award. P.J. Rauch was supported by the Boehringer Ingelheim Fonds. Dr Weber was supported by the German Research Foundation.

Disclosures

None.

References

1. Medzhitov R. Origin and physiological roles of inflammation. *Nature*. 2008;454:428–435.
2. Auffray C, Sieweke MH, Geissmann F. Blood monocytes: development, heterogeneity, and relationship with dendritic cells. *Annu Rev Immunol*. 2009;27:669–692.
3. Nathan C. Neutrophils and immunity: challenges and opportunities. *Nat Rev Immunol*. 2006;6:173–182.
4. Geissmann F, Manz MG, Jung S, Sieweke MH, Merad M, Ley K. Development of monocytes, macrophages, and dendritic cells. *Science*. 2010;327:656–661.
5. Massberg S, Schaerli P, Knezevic-Maramica I, Kollnberger M, Tubo N, Moseman EA, Huff IV, Junt T, Wagers AJ, Mazo IB, von Andrian UH. Immunosurveillance by hematopoietic progenitor cells trafficking through blood, lymph, and peripheral tissues. *Cell*. 2007;131:994–1008.
6. Wright DE, Wagers AJ, Gulati AP, Johnson FL, Weissman IL. Physiological migration of hematopoietic stem and progenitor cells. *Science*. 2001;294:1933–1936.
7. Hansson GK, Libby P. The immune response in atherosclerosis: a double-edged sword. *Nat Rev Immunol*. 2006;6:508–519.
8. Libby P. Inflammation in atherosclerosis. *Nature*. 2002;420:868–874.
9. Swirski FK, Weissleder R, Pittet MJ. Heterogeneous in vivo behavior of monocyte subsets in atherosclerosis. *Arterioscler Thromb Vasc Biol*. 2009;29:1424–1432.
10. Nathan C, Ding A. Nonresolving inflammation. *Cell*. 2010;140:871–882.
11. Swirski FK, Pittet MJ, Kircher MF, Aikawa E, Jaffer FA, Libby P, Weissleder R. Monocyte accumulation in mouse atherogenesis is progressive and proportional to extent of disease. *Proc Natl Acad Sci U S A*. 2006;103:10340–10345.
12. Swirski FK, Libby P, Aikawa E, Alcaide P, Luscinskas FW, Weissleder R, Pittet MJ. Ly-6Chi monocytes dominate hypercholesterolemia-associated monocytosis and give rise to macrophages in atheromata. *J Clin Invest*. 2007;117:195–205.
13. Tacke F, Alvarez D, Kaplan TJ, Jakubzick C, Spanbroek R, Llodra J, Garin A, Liu J, Mack M, van Rooijen N, Lira SA, Habenicht AJ, Randolph GJ. Monocyte subsets differentially employ CCR2, CCR5, and

CX3CR1 to accumulate within atherosclerotic plaques. *J Clin Invest*. 2007;117:185–194.
14. Sunderkotter C, Nikolic T, Dillon MJ, Van Rooijen N, Stehling M, Drevets DA, Leenen PJ. Subpopulations of mouse blood monocytes differ in maturation stage and inflammatory response. *J Immunol*. 2004;172:4410–4417.
15. Varol C, Landsman L, Fogg DK, Greenshtein L, Gildor B, Margalit R, Kalchenko V, Geissmann F, Jung S. Monocytes give rise to mucosal, but not splenic, conventional dendritic cells. *J Exp Med*. 2007;204:171–180.
16. Leuschner F, Panizzi P, Chico-Calero I, Lee WW, Ueno T, Cortez-Retamozo V, Waterman P, Gorbatov R, Marinelli B, Iwamoto Y, Chudnovskiy A, Figueiredo JL, Sosnovik DE, Pittet MJ, Swirski FK, Weissleder R, Nahrendorf M. Angiotensin-converting enzyme inhibition prevents the release of monocytes from their splenic reservoir in mice with myocardial infarction. *Circ Res*. 2010;107:1364–1373.
17. Swirski FK, Nahrendorf M, Etzrodt M, Wildgruber M, Cortez-Retamozo V, Panizzi P, Figueiredo JL, Kohler RH, Chudnovskiy A, Waterman P, Aikawa E, Mempel TR, Libby P, Weissleder R, Pittet MJ. Identification of splenic reservoir monocytes and their deployment to inflammatory sites. *Science*. 2009;325:612–616.
18. Oakley OR, Kim H, El-Amouri I, Lin PC, Cho J, Bani-Ahmad M, Ko C. Periovulatory leukocyte infiltration in the rat ovary. *Endocrinology*. 2010;151:4551–4559.
19. Fearon WF, Fearon DT. Inflammation and cardiovascular disease: role of the interleukin-1 receptor antagonist. *Circulation*. 2008;117:2577–2579.
20. Nahrendorf M, Swirski FK, Aikawa E, Stangenberg L, Wurdinger T, Figueiredo JL, Libby P, Weissleder R, Pittet MJ. The healing myocardium sequentially mobilizes two monocyte subsets with divergent and complementary functions. *J Exp Med*. 2007;204:3037–3047.
21. Nahrendorf M, Waterman P, Thurber G, Groves K, Rajopadhye M, Panizzi P, Marinelli B, Aikawa E, Pittet MJ, Swirski FK, Weissleder R. Hybrid in vivo FMT-CT imaging of protease activity in atherosclerosis with customized nanosensors. *Arterioscler Thromb Vasc Biol*. 2009;29:1444–1451.
22. Eruslanov E, Kusmartsev S. Identification of ROS using oxidized DCFDA and flow-cytometry. *Methods Mol Biol*. 2010;594:57–72.
23. Mebius RE, Kraal G. Structure and function of the spleen. *Nat Rev Immunol*. 2005;5:606–616.
24. Kyaw T, Tay C, Krishnamurthi S, Kanellakis P, Agrotis A, Tipping P, Bobik A, Toh BH. B1a B lymphocytes are atheroprotective by secreting natural IgM that increases IgM deposits and reduces necrotic cores in atherosclerotic lesions. *Circ Res*. 2011;109:830–840.
25. Caligiuri G, Nicoletti A, Poirier B, Hansson GK. Protective immunity against atherosclerosis carried by B cells of hypercholesterolemic mice. *J Clin Invest*. 2002;109:745–753.
26. Calin MV, Manduteanu I, Dragomir E, Dragan E, Nicolae M, Gan AM, Simionescu M. Effect of depletion of monocytes/macrophages on early aortic valve lesion in experimental hyperlipidemia. *Cell Tissue Res*. 2009;336:237–248.
27. Fogg DK, Sibon C, Miled C, Jung S, Aucouturier P, Littman DR, Cumano A, Geissmann F. A clonogenic bone marrow progenitor specific for macrophages and dendritic cells. *Science*. 2006;311:83–87.
28. Liu K, Waskow C, Liu X, Yao K, Hoh J, Nussenzweig M. Origin of dendritic cells in peripheral lymphoid organs of mice. *Nat Immunol*. 2007;8:578–583.
29. Hamilton JA. Colony-stimulating factors in inflammation and autoimmunity. *Nat Rev Immunol*. 2008;8:533–544.
30. Ditiatkovski M, Toh BH, Bobik A. GM-CSF deficiency reduces macrophage PPAR-gamma expression and aggravates atherosclerosis in ApoE-deficient mice. *Arterioscler Thromb Vasc Biol*. 2006;26:2337–2344.
31. Haghighat A, Weiss D, Whalin MK, Cowan DP, Taylor WR. Granulocyte colony-stimulating factor and granulocyte macrophage colony-stimulating factor exacerbate atherosclerosis in apolipoprotein E-deficient mice. *Circulation*. 2007;115:2049–2054.
32. Shaposhnik Z, Wang X, Weinstein M, Bennett BJ, Lusis AJ. Granulocyte macrophage colony-stimulating factor regulates dendritic cell content of atherosclerotic lesions. *Arterioscler Thromb Vasc Biol*. 2007;27:621–627.
33. Yvan-Charvet L, Pagler T, Gautier EL, Avagyan S, Siry RL, Han S, Welch CL, Wang N, Randolph GJ, Snoeck HW, Tall AR. ATP-binding cassette transporters and HDL suppress hematopoietic stem cell proliferation. *Science*. 2010;328:1689–1693.
34. Kondo M, Wagers AJ, Manz MG, Prohaska SS, Scherer DC, Beilhack GF, Shizuru JA, Weissman IL. Biology of hematopoietic stem cells and progenitors: implications for clinical application. *Annu Rev Immunol*. 2003;21:759–806.
35. Goodman JW, Hodgson GS. Evidence for stem cells in the peripheral blood of mice. *Blood*. 1962;19:702–714.
36. van Furth R, Cohn ZA. The origin and kinetics of mononuclear phagocytes. *J Exp Med*. 1968;128:415–435.
37. Dzierzak E, Medvinsky A. Mouse embryonic hematopoiesis. *Trends Genet*. 1995;11:359–366.
38. Hassan NM, Neiman RS. The pathology of the spleen in steroid-treated immune thrombocytopenic purpura. *Am J Clin Pathol*. 1985;84:433–438.
39. Lowell CA, Niwa M, Soriano P, Varmus HE. Deficiency of the Hck and Src tyrosine kinases results in extreme levels of extramedullary hematopoiesis. *Blood*. 1996;87:1780–1792.
40. Snover DC, Frizzera G, Spector BD, Perry G Sr, Kersey JH. Wiskott-Aldrich syndrome: histopathologic findings in the lymph nodes and spleens of 15 patients. *Hum Pathol*. 1981;12:821–831.
41. Wolber FM, Leonard E, Michael S, Orschell-Traycoff CM, Yoder MC, Srour EF. Roles of spleen and liver in development of the murine hematopoietic system. *Exp Hematol*. 2002;30:1010–1019.
42. Karlsson MC, Guinamard R, Bolland S, Sankala M, Steinman RM, Ravetch JV. Macrophages control the retention and trafficking of B lymphocytes in the splenic marginal zone. *J Exp Med*. 2003;198:333–340.
43. Lu TT, Cyster JG. Integrin-mediated long-term B cell retention in the splenic marginal zone. *Science*. 2002;297:409–412.
44. Robinette CD, Fraumeni JFJ. Splenectomy and subsequent mortality in veterans of the 1939–45 war. *Lancet*. 1977;2:127–129.
45. Lymperi S, Ferraro F, Scadden DT. The HSC niche concept has turned 31: has our knowledge matured? *Ann N Y Acad Sci*. 2010;1192:12–18.
46. Swirski FK. The spatial and developmental relationships in the macrophage family. *Arterioscler Thromb Vasc Biol*. 2011;31:1517–1522.

CLINICAL PERSPECTIVE

Atherosclerosis is an inflammatory disease characterized by the accumulation of lipids and leukocytes in the arterial wall. Monocytes are large circulating leukocytes believed to be essential to the development and exacerbation of atherosclerosis. As disease worsens, the number of circulating monocytes rises, whereas in models with monocyte depletion, atherosclerosis neither develops nor evolves. It is believed that hematopoietic progenitors give rise to circulating monocytes exclusively in the bone marrow. These medullary monocytes circulate, accumulate in tissue, and differentiate to macrophages or dendritic cells. Extramedullary sites such as the spleen maintain reservoirs of undifferentiated monocytes that can exit en masse in response to acute inflammation. In this study, we show that during atherosclerosis the bone marrow outsources the production of monocytes to the spleen. These extramedullary monocytes accumulate in the growing atheromata. From a clinical perspective, this finding is important because it identifies the spleen as a possible biomarker organ and therapeutic target for cardiovascular disease, and it proposes that inflammatory hematopoiesis could be targeted therapeutically in atherosclerosis.

Extramedullary Hematopoiesis Generates Ly-6C^{high} Monocytes That Infiltrate Atherosclerotic Lesions

Clinton S. Robbins, Aleksey Chudnovskiy, Philipp J. Rauch, Jose-Luiz Figueiredo, Yoshiko Iwamoto, Rostic Gorbatov, Martin Etzrodt, Georg F. Weber, Takuya Ueno, Nico van Rooijen, Mary Jo Mulligan-Kehoe, Peter Libby, Matthias Nahrendorf, Mikael J. Pittet, Ralph Weissleder and Filip K. Swirski

Circulation. 2012;125:364-374; originally published online December 5, 2011;
doi: 10.1161/CIRCULATIONAHA.111.061986
Circulation is published by the American Heart Association, 7272 Greenville Avenue, Dallas, TX 75231

Print ISSN: 0009-7322. Online ISSN: 1524-4539

Supplemental Material

Expanded Methods and Results

Animals. The LDLR$^{-/-}$ApoB48$^{-/-}$ mouse was selected because it is reported to more closely mimic human atherosclerosis than other models.[1] ApoE$^{-/-}$ animals had been backcrossed to the C57BL/6 background for at least ten generations. ApoE$^{-/-}$ CD45.1$^{+/+}$ were generated after backcrossing ApoE$^{-/-}$ mice to C57BL/6 CD45.1$^{+/+}$. At 10 wk of age, ApoE$^{-/-}$ mice were placed on a Western diet (21.2% fat/weight; 0.2% cholesterol) (Harlan Teklad, Madison, WI) or remained on a chow diet for durations listed in the manuscript. The LDLR$^{-/-}$ApoB48$^{-/-}$ mice were placed on Paigen's high fat diet without cholate (Research Diets, New Brunswich, NJ).[2] for 16 wk at 8 weeks of age. The remaining animals consumed a regular chow diet.

Animal models and in vivo interventions. Splenectomy: Under isofluorane anesthesia, the peritoneal cavity of mice was opened and the splenic vessels were ligated using a 6.0 silk suture. The spleen was then carefully removed. For control experiments, the peritoneum was opened, but the spleen was not excised. The procedure itself does not change the number of circulating monocytes and neutrophils in the steady state [3]. Spleen transplantation: Spleen transplantation was conducted as previously described [3]. Briefly, spleen donor mice were anesthetized with a subcutaneous injection of ketamine (90 mg/kg) and xylazine (10 mg/kg), followed by an intravenous injection of 200 units of heparin (American Pharmaceutical, Schaumburg, Il). The complete inhibition of clotting ensures that no vascular or intrasplenic thrombosis occurs. In deep anesthesia, the thorax was then opened and the right atrium sectioned to allow blood to exit during perfusion. Over a period of 3 minutes, the entire mouse was then perfused with a total of 15 ml of normal saline through a 25G needle inserted into the apex of the left ventricle. At the end of this procedure, fluid exiting the right atrium was clear which indicates thorough removal of the donor blood. Under isofluorane (1-2%), supplemented with oxygen (1-2 L) anesthesia, the abdomen of the recipient mouse was then opened with a longitudinal incision. The pancreas, the spleen and the abdominal vasculature in the epigastric region were identified and ligated with 6.0 cotton (Ethicon). The celiac artery was then isolated, and the hepatic and gastric artery ligated with 10.0 suture (Ethicon). The abdominal aorta was ligated and cut just below the celiac artery with micro-dissection scissors (ROBOZ, Rockville, MD), and also dissected above the celiac artery. This approach resulted in an aortic cuff

connected to the splenic artery, which allowed vascular anastomosis of the spleen to the recipient. Following ligation of the bile duct, the portal vein was isolated, and the superior and inferior mesenteric and gastric veins were ligated. The portal vein was intersected closely to the liver. The entire organ package containing the vascular connections, spleen and the pancreas was then removed and stored in ice-cold saline for 15 minutes while the recipient was prepared. The recipient (CD45.1) was anesthetized with isofluorane (1-2%), supplemented with oxygen (1-2 L). An abdominal midline incision was made and the inferior vena cava and the descending aorta isolated below the renal arteries. The recipient vessels were clamped with an atraumatic vascular clamp (ASSI, Westbury, NY) and opened with micro-scissors. The portal vein was anastomosed to the inferior vena cava and the donor aortic cuff was connected with an end-to side anastomosis to the recipient aorta using 10.0 suture. The clamp was then opened to restore blood flow. Blood flow was confirmed using a blood pool agent (AngioSense-680, VisEn Medical, MA) and imaging as described previously [3]. Parabiosis: The procedure, adapted from [4] was conducted as previously described[3]. Briefly, after shaving the corresponding lateral aspects of each mouse, matching skin incisions were made from behind the ear to the tail of each mouse, and the subcutaneous fascia was bluntly dissected to create about ½ cm of free skin. The scapulas were sutured using a mono-nylon 5.0 (Ethicon, Albuquerque, NM), and the dorsal and ventral skins were approximated by continuous suture. After an interval of three weeks, parabiosed mice were surgically separated by a reversal of the procedure. One group was splenectomized, as described above. Percent chimerism in the blood was defined for gated monocytes, neutrophils and Lin_1^+ cells (mostly lymphocytes) as %CD45.1 / (%CD45.1 + %CD45.2) in CD45.2 mice, and as %CD45.2 / (%CD45.2 + %CD45.1) in CD45.1 mice. Adoptive transfer of GMP: Donor $CD45.1^+$ or GFP^+ cells from the bone marrow were first enriched using anti-PE beads to deplete Lin_2^+ cells (Miltenyi) and then sorted using a BD FACSAria II (BD Biosciences). Typically, purity of the sorted population was 99.5 %. 5×10^4 GMPs were injected into the tail vein of non-irradiated recipient mice. Anti-GM-CSF and IL-3 treatment: Mice were i.v. injected with blocking antibody against GM-CSF (MP1-22E9, eBioscience; 300µg) twice daily for four consecutive days. Control animals received anti-mouse IgG2a (eBR2a, eBioscience; 300µg). Monocyte reservoir depletion: Mice were i.v. injected with 250 µl clodronate loaded liposomes once. Clodronate was a gift from Roche and was incorporated into liposomes are described previously [5]. Injection of oxLDL: Mice were i.v. injected once with DiI-oxLDL (Biomedical Technologies, Inc., Stoughton, MA; 100µg). Endotoxin-induced peritonitis and peritoneal lavage: Mice were administered 10 µg of LPS

(Sigma), unless otherwise stated, daily by i.p. injections in PBS over the course of 4 days. Controls received PBS alone. For select experiments, the peritoneal cavity was lavaged with 10 ml of PBS to retrieve infiltrated and resident leukocytes.

Cells. Peripheral blood for flow cytometric analysis was collected by cardiac puncture, using a 50 mM EDTA solution as anticoagulant. Erythrocytes were lysed using BD FACS Lysing Solution (BD Biosciences). Total white blood cell count was determined by preparing a 1:10 dilution of (undiluted) peripheral blood obtained from the orbital sinus using heparin-coated capillary tubes in RBC Lysis Buffer (BioLegend). After organ harvest, single cell suspensions were obtained as follows: for bone marrow, femur and tibia of one leg were flushed with PBS. Spleens were homogenized through a 40 µm-nylon mesh, after which erythrocyte lysis was performed on the spleens using RBC Lysis Buffer (BioLegend). For the flow cytometry experiments, the entire aorta was digested (from the root to the iliac bifurcation) according to a method previously published.[6] The procedure involves perfusion of the aorta (20 ml PBS) prior to digestion. Aortic tissue was cut in small pieces and subjected to enzymatic digestion with 450 U/ml collagenase I, 125 U/ml collagenase XI, 60 U/ml DNase I and 60 U/ml hyaluronidase (Sigma-Aldrich, St. Louis, MO) for 1 h at 37°C while shaking. Total viable cell numbers were obtained using Trypan Blue (Cellgro, Mediatech, Inc, VA). To determine total bone marrow cellularity, one femur was estimated to represent 5% of total marrow according to[7]. For morphological assessment, cytospins were prepared from 5 $\times 10^4$ cells and stained using HEMA 3 staining kit (Fisher Scientific). Tissue colony forming cell assay: To determine the number of myeloid colony-forming units in the steady state and in atherosclerosis, a single cell suspension was prepared from spleens and $1x10^5$ splenocytes were plated in triplicates in complete methylcellulose medium (MethoCult GF M3434, Stemcell Technologies) or methylcellulose medium lacking growth factors (MethoCult M3234, Stemcell Technologies) supplemented with 100ng recombinant murine GM-CSF and IL-3 according to the manufacturer's instructions. In one set of experiments anti-GM-CSF and anti-IL-3 were added once to cultures at 10 µg/ml. Counts were performed after 8 days of culture. At least three independent samples per group were analyzed.

Flow Cytometry. Anti-CD90-PE, anti-CD90-FITC, 53-2.1 (BD Biosciences); anti-B220-PE, anti B220-FITC, RA3-6B2 (BD Biosciences); anti-CD49b-PE, anti CD49b-FITC, DX5 (BD Biosciences); anti-NK1.1-PE, anti-NK1.1-FITC, PK136 (BD Biosciences); anti-Ly-6G-PE, anti-Ly-6G-FITC, 1A8

(BD Biosciences); anti-TER119-PE, Anti-TER119-FITC, anti-TER119- APC, TER119 (BD Biosciences); anti-NK1.1-PE, anti-NK1.1-FITC, anti-NK1.1-PerCP, PK136 (BD Biosciences); anti-CD11b-APC, M1/70 (BD Biosciences); anti-CD11b-PE (ED8) (Abcam); anti-CD11b-APC-Cy7 M1/70 (BD Biosciences); anti-F4/80-biotin, anti-F4/80-FITC, C1:A3-1 (BioLegend); anti-CD11c-biotin, anti-CD11c-FITC, anti-CD11c-APC, HL3 (BD Biosciences); anti-I-A^b-biotin, anti-I-A^b-FITC, AF6-120.1 (BD Biosciences); anti-F4/80-biotin, C1:A3-1 (BioLegend); anti-F4/80-PE-Cy7, BM8 (BioLegend); anti-Ly-6C-FITC, anti-Ly-6C-biotin, AL-21 (BD Biosciences); anti-Gr-1-PeCy7, RB6-8C5 (BD Biosciences); anti-CD45.2-FITC 104,anti-CD45.2-PerCP 104, anti-CD45.2-Alexa Fluor 700 (BD Biosciences); anti-CD45.1-biotin A20, anti-CD45.1-APC A20, anti-CD45.1-PeCy7 A20 (BD Biosciences);anti-CD34-FITC, anti-CD34-Alexa Fluor 700, RAM34 (BD Biosciences); anti-CD117-APC (BD Biosciences), anti-CD117-PE-Cy7 (eBioscience), 2B8; anti-Sca-1-PE-Cy7, anti-Sca-1-Alexa Fluor 700, D7 (eBioscience); anti-CD16/32-APC-Cy7, 2.4G2 (BD Biosciences); were used for flow cytometric analyses in this study. Streptavidin-PerCP was (BD Biosciences) were used to label biotinylated antibodies. Cathepsin activity was assessed using Prosense-680 (PerkinElmer). Cell cycle analysis was carried using FxCycle violet stain (Invitrogen). Apoptotic cells were identified as those cells falling within the subG_1 gate as previously described[8]. Contribution of newly-made cells to different cell populations was determined by in-vivo labeling with bromodeoxyuridine (BrdU). Mice received 1 mg of BrdU (BD Biosciences) by i.p. injection. Incorporation was measured using either FITC or APC-conjugated anti-BrdU antibodies according to the manufacturer's instructions. Monocytes, macrophages/dendritic cells and neutrophils were identified as described previously.[3] Specifically, monocytes were identified as $CD11b^{hi}$ Lin_1^- (Lin_1 = CD90/B220/CD49b/NK1.1/Ly-6G/Ter119) (F4/80/I-A^b/CD11c)^{lo}. Monocyte subsets were identified as either Ly-$6C^{high\ or}$ Ly-$6C^{low}$. Macrophages/dendritic cells were identified as $CD11b^{hi}$ Lin_1^{lo} (F4/80/I-A^b/CD11c)^{hi} or on the basis of F4/80 expression only. Neutrophils were identified as $CD11b^{hi}$ Lin_1^{hi} (F4/80/I-A^b/CD11c)^{lo} Ly-$6C^{int}$. Monocyte and macrophage/dendritic cell numbers were calculated as total cells multiplied by percent cells within the monocyte/ macrophage gate. Hematopoietic stem cells were identified as Lin_2^{low} (Lin_2 = CD90/B220/CD19/ CD49b/Ter119/NK1.1/Gr-1/CD11b/CD11c) IL-7Rα$^-$ $CD117^+$ $Sca\text{-}1^+$. Myeloid progenitors were identified as Lin_2^{low} IL-7Rα$^-$ $CD117^+$ $Sca\text{-}1^-$. Within this population, granulocyte/macrophage progenitors (GMP) were $CD34^+$ $CD16/32^+$, common myeloid progenitors (CMP) were $CD34^+$ $CD16/32^{low}$ and megakaryocyte/erythroid progenitors (MEP) were $CD34^-$ $CD16/32^-$. Data were acquired on an LSRII (BD Biosciences) and analyzed with FlowJo v8.8.6 (Tree Star, Inc.). Cells were sorted on a BD FACSAria II (BD Biosciences).

Histology. Aortae and spleens were excised, embedded in O.C.T. compound (Sakura Finetek), and flash-frozen in isopentane and dry ice. Aortic roots were sectioned into 5 um slices, generating ~30-40 sections that spanned the entirety of the aortic root. For comparison of lesion size between the groups, the sections that captured the maximum lesion area were used. Sections adjacent to this were used for other histological staining. Immunofluorescence staining was carried out using the following primary antibodies: anti-CD11b: clone M1/70 (BD Biosciences), biotin anti-CD45.1: clone A20 (BioLegend), and anti-F480: clone CI:A3-1 (Abcam). In some cases, either streptavidin-Texas Red or streptavidin-fluorescein (GE Healthcare) were directly conjugated to primary antibodies. Biotinylated secondary antibodies were used when required. Specificity of staining was confirmed using relevant isotype controls. Cover slips were placed over specimens using mounting medium containing DAPI (Vector Laboratories) to identify cell nuclei. Samples were visualized using an epifluorescence microscope (Nikon Eclipse 80i, Nikon Instruments Inc.) equipped with a Cascade Model 512B camera (Roper Scientific). Immunohistochemical staining was used to detect GM-CSF (clone FL-144, Santa Cruz Biotechnology) and IL-3 (clone MP2-8F8, BioLegend) for spleen sections, and anti-CD11b (clone M1/70, BD Biosciences), anti-Mac3: clone M3/84 (BD Biosciences), anti-F4/80: clone CI:A3-1 (Abcam), and actin smooth muscle (NeoMarkers) for aortic roots. Specificity of staining was confirmed using relevant isotype controls. In order to block endogenous peroxidase activity, tissue sections were pre-treated with 0.3% hydrogen peroxide solution. Following application of appropriate biotinylated secondary antibodies, samples were developed using a Vectastain ABC kit (Vector Laboratories) and AEC substrate (DakoCytomation). All sections were counterstained with Harris Hematoxylin. Masson trichrome (Sigma) and Oil Red O (Sigma) staining were performed to visualize collagen and lipid content, respectively. Hematoxylin and eosin (H&E) staining was performed to assess overall tissue morphology. Captured images were digitized automatically using a Nanozoomer 2.0RS (Hamamatsu).

Intravital microscopy

Animal preparation: During isoflurane anesthesia, the peritoneal cavity was opened with a transverse incision in the disinfected abdominal wall. The gastro-splenic ligament was dissected and the spleen carefully exteriorized. Robust blood flow was observed in the splenic artery during the duration of each experiment and splenic perfusion was confirmed by inspection through fluorescence microscopy upon tail vein injection of an intravascular imaging agent. The

exteriorized spleen was completely submerged in temperature-controlled lactated Ringer's solution. Temperature near the spleen was carefully monitored using an Omega HH12A thermometer with fine wire thermocouples (Omega Engineering Inc., Stamford, CT) and kept at 37ºC. Confocal Microscopy: Images were collected with an intravital laser scanning microscope (IV100 vers. 1.2, Olympus Corporation, Tokyo, Japan[9] using an Olympus 4x UPlanSApo (NA 0.16), 10x UPlanFl (NA 0.3), 20x UPlanFl (NA 0.5) objective and the Olympus IV10-ASV 1.2 program. Samples were excited at 488 nm with an air-cooled argon laser (Melles Griot, Carlsbad, CA) for visualization of the GFP^+ cells, at 561 nm with a solid state yellow laser (Melles Griot) for visualization of RFP, and at 748 nm with a red diode laser (Model FV10-LD748, Olympus Corporation, Tokyo, Japan) for visualization of the blood pool agent (AngioSense-750, VisEn Medical, MA). Light was collected using custom-built dichroic mirrors SDM-560 and SDM-640, and emission filters BA 505-550, 585-615 nm, and BA 770 nm IF (Olympus Corporation, Tokyo, Japan). The 488 nm and 750 nm channels were collected simultaneously. The 561 nm channel was collected line-sequentially to avoid bleed through between channels. Time-lapse recordings were made by collecting a z-stack of ten 512x512 pixels images at 10 μm interval every 30s. A cluster was defined as a group of cells (at least 5) in close proximity to one another (typically no more than 100 μm apart).

Additional Figures

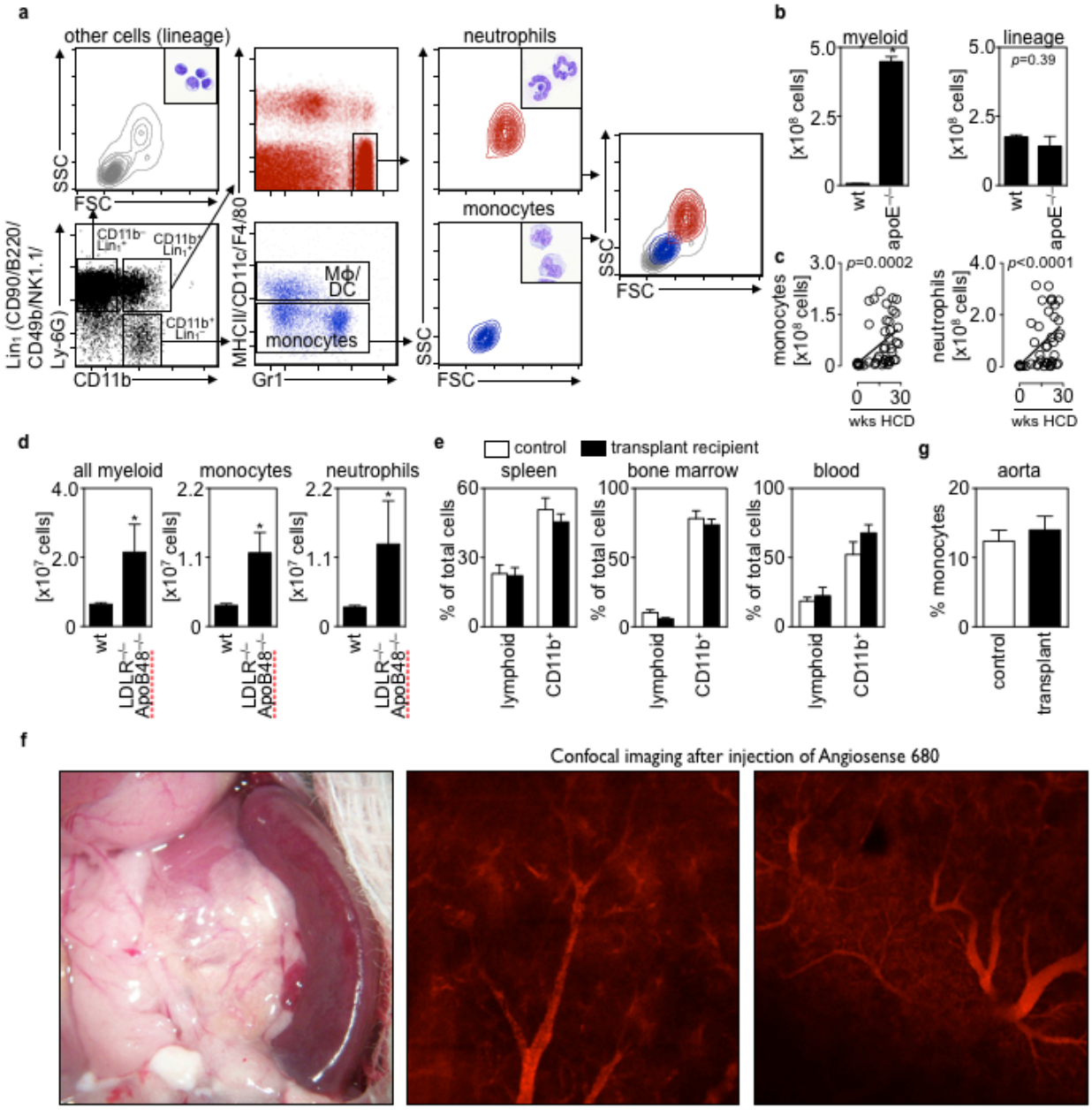

Supplemental Figure I

(a) Schematic for gating on monocytes, macrophages, neutrophils and other cells analyzed in this manuscript. **(b)** Enumeration of myeloid and lineage cells in spleens of C57BL/6 (wt) and apoE$^{-/-}$ mice consuming a high cholesterol diet (HCD) for 20 weeks. Data show that myeloid, but not lineage cells increase in number in apoE$^{-/-}$ mice consuming a HCD (means ± SEM, n =

6) *P< 0.0001. **(c)** Enumeration of monocytes and neutrophils in spleens of mice consuming HCD for up to 30 weeks. Data show that the number of monocytes and neutrophils increase over time in mice consuming HCD. (n= 51). Linear regression was performed on all data. **(d)** Enumeration of myeloid cells, monocytes and neutrophils in the spleens of $LDLR^{-/-}ApoB48^{-/-}$ mice consuming Paigen's diet for 30 weeks (means ± SEM, n = 5) *P< 0.0001. **(e)** Distribution of lymphoid and myeloid cells in the spleen, bone marrow and blood in animals that were splenectomized and received a spleen by transplantation and in control animals that were not splenectomized and did not receive a spleen by transplantation. Data show that spleen transplantation does not affect cell distribution in the various compartments. (means ± SEM, n = 8). **(f)** Pictures showing that the transplanted spleen is perfused. After transplant, Angiosense-680, a fluorescent blood pool agent, was injected and the spleen was imaged by near infrared imaging (NIR) and with a confocal microscope. A picture also shows the characteristic purplish red of the transplanted spleen.

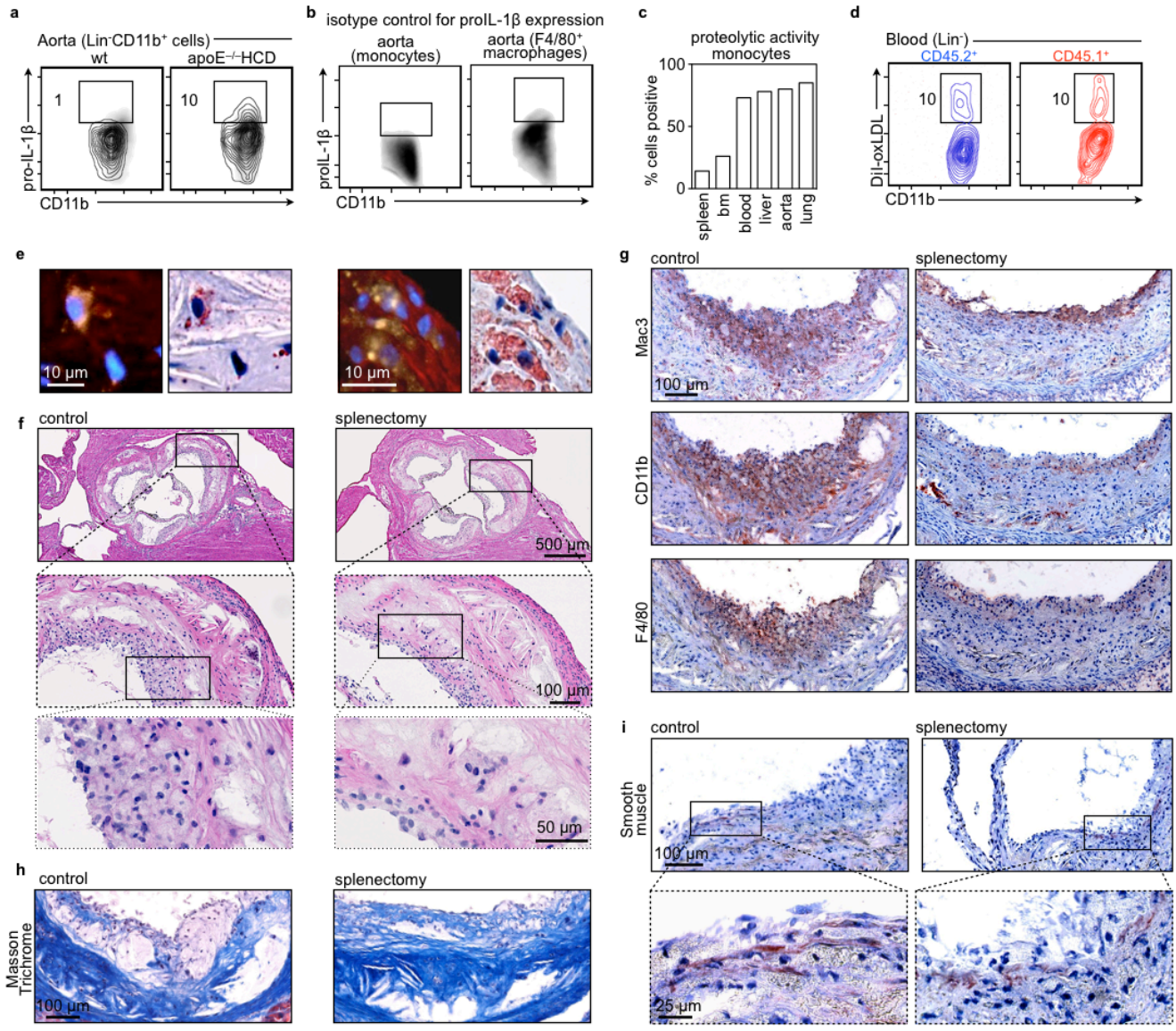

Supplemental Figure II.

(a) Expression of pro-IL-1β on in vitro-unstimulated $Lin_1^-CD11b^+$ cells from the aorta of wt and $apoE^{-/-}$ mice consuming (HCD) for 20 weeks. Staining for the cytokine is shown as a contour plot and isotype staining is shown as a density plot in the back. Data are representative of at least three independent experiments and show that expression of pro-IL-1β increases in an inflammatory context. **(b)** Isotype staining controls for pro-IL-1β antibody staining in aortic monocytes and macrophages. **(c)** Proteolytic activity on monocytes retrieved from different organs. Data show that monocytes residing in the spleen and bone marrow (bm) have little proteolytic activity. This activity increases when monocytes accumulate in different sites. **(d)**

Uptake of DiI-oxLDL by circulating $Lin_1^-CD11b^+$ cells. Data show that $CD45.2^+$ (i.e., bone marrow) and $CD45.1^+$ (i.e. splenic) monocytes take up ox-LDL similarly. DiI-oxLDL was injected i.v. once. **(e)** Spleen transplantation for 10 days. Data show IF (left panels) on the aortic root with antibodies against CD45.1 (green) and F4/80 (red). DAPI depicts nuclei (blue). Yellow cells represent $F480^+$ cells of splenic origin. Oil red O staining (right panels) of the same aortic root tissue section reveals co-localization of lipid accumulation and lesional cells of splenic origin. **(f)** H&E staining of aortic root lesions of spleen-containing and asplenic $apoE^{-/-}$ HCD mice. **(g)** Immunohistochemical staining for macrophage/monocyte markers in aortic root sections from mice in (f). Depicted is representative staining for Mac3, CD11b, and F4/80. **(h)** Masson trichrome staining of aortic roots from representative control and splenectomized mice. **(i)** Actin smooth muscle staining.

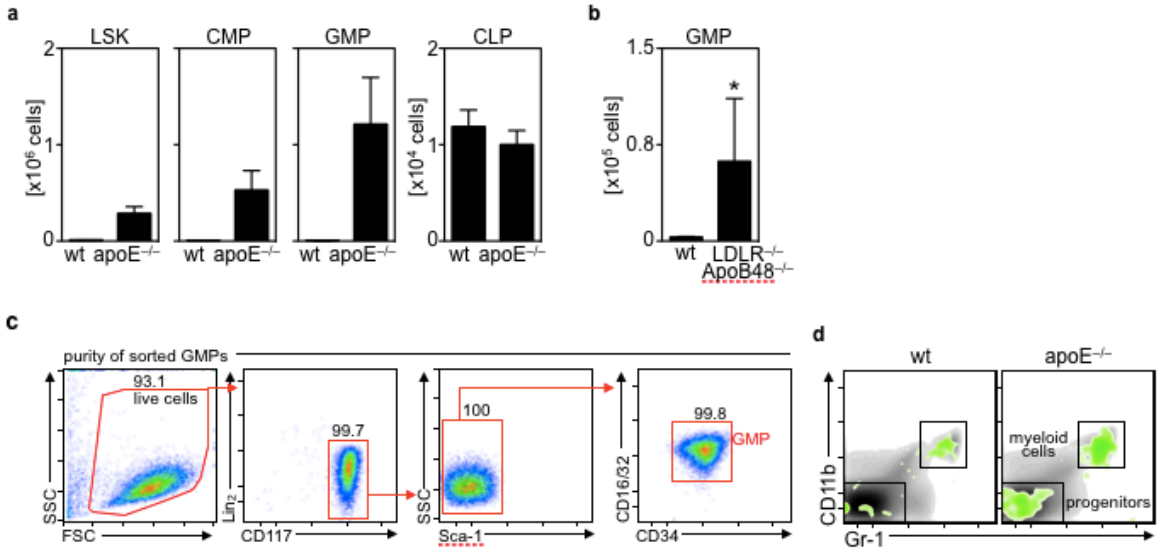

Supplemental Figure III

(a) Enumeration of $Lin_2^-Sca^-c\text{-}kit^+$ (LSK), common myeloid progenitor (CLP), granulocyte-macrophage precursors (GMP), and common lymphoid progenitor cells (CLP) in spleens of C57BL/6 (wt) and $apoE^{-/-}$ mice consuming a high cholesterol diet (HCD) for 8 weeks. Data show that myeloid progenitor populations, but not lineage progenitor cells increase in number in $apoE^{-/-}$ mice consuming a HCD. **(b)** Enumeration of GMP in the spleens of $LDLR^{-/-}ApoB48^{-/-}$ mice consuming Paigen's diet. (means ± SEM, n = 5-8) *P< 0.05. **(c)** Representative post-sort

flow cytometric analysis of GMPs that were used for adoptive transfer. Overall purity of GMPs within the living population was 99.5%. This is a quality control experiment showing that the GFP$^+$ GMP that are injected are sorted to high purity. **(d)** Adoptive transfer of GFP$^+$ GMP to wt and apoE$^{-/-}$ HCD mice. Data show GFP cells in spleens 3 days after transfer. Increased percentage of GFP$^+$ progenitors and myeloid cells was observed in spleens of apoE$^{-/-}$ HCD mice.

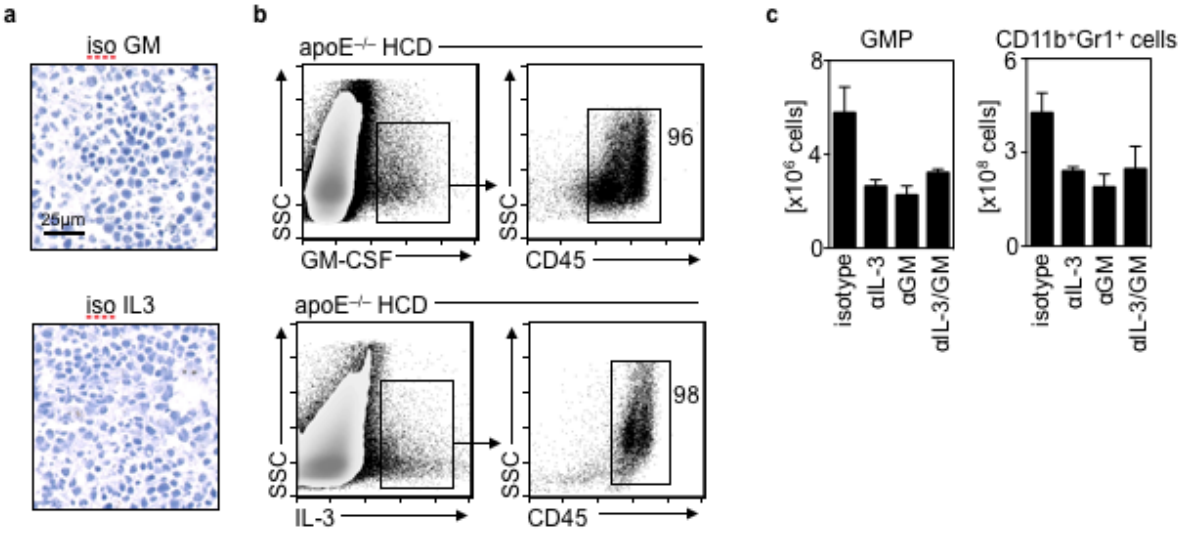

Supplemental Figure IV.

(a) Isotype staining for GM-CSF and IL-3 on spleens from apoE$^{-/-}$ mice consuming HCD for 20 weeks. **(b)** Flow cytometry intracellular staining for GM-CSF, IL-3 and CD45 in spleens of apoE$^{-/-}$ mice consuming HCD for 20 weeks. Representative plots of at least three independent experiments are shown. Isotype controls were used to determine positive staining. **(c)** Effect of IL-3 and GM-CSF neutralization on the endogenous GMP and CD11b$^+$Gr1$^+$ repertoires in the bone marrow (means ± SEM, n = 5).

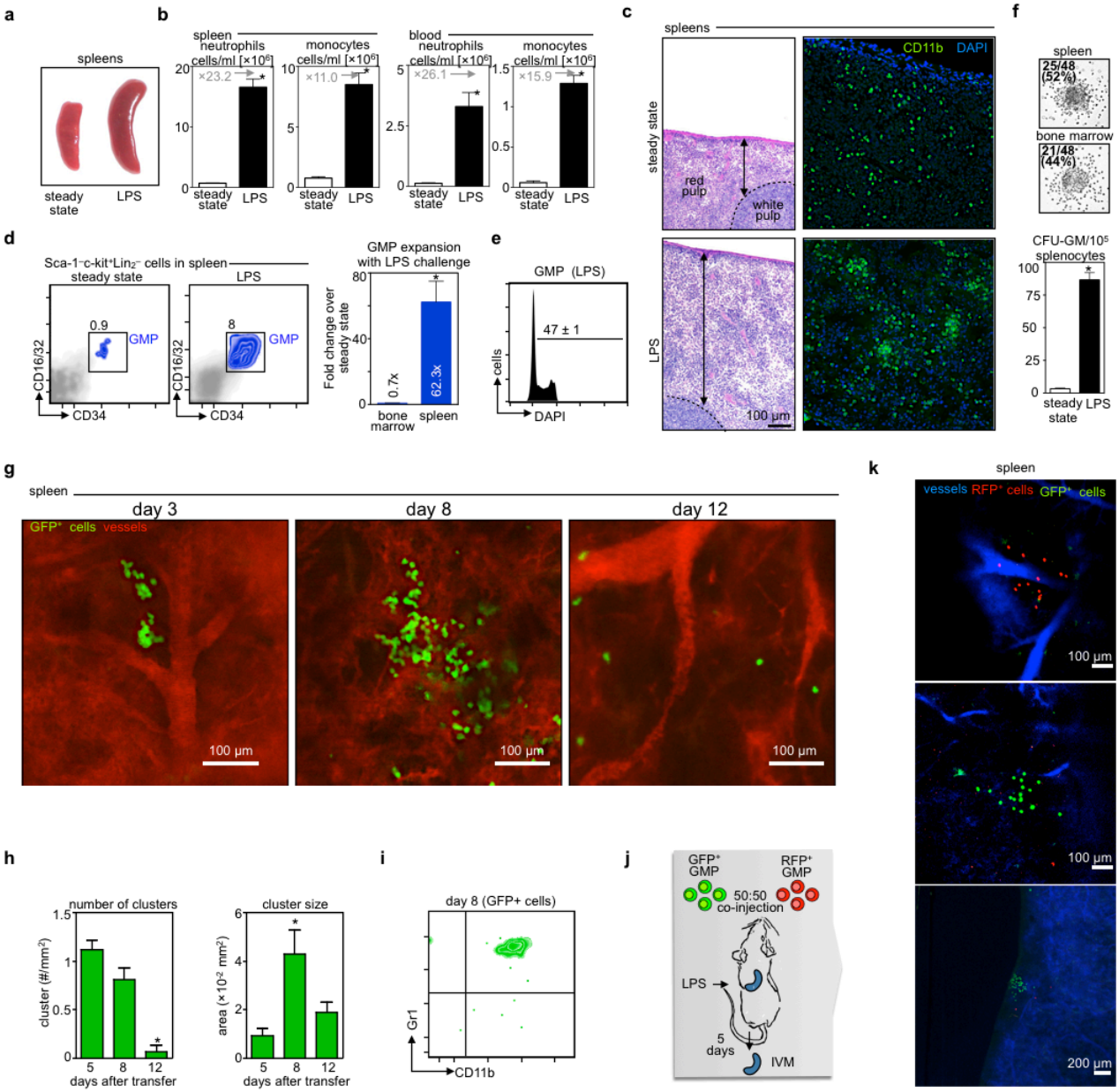

Supplemental Figure V.

(a) Picture of spleens retrieved from animals in the steady state and 4 days after daily injection of lipopolysaccharide (LPS). **(b)** Enumeration of neutrophils and monocytes in the blood and spleen in the steady state and in response to LPS. Numbers in gray show the fold increase for a given population (means ± SEM, n = 3-9).*P< 0.05. **(c)** H&E staining and IF on CD11b on spleen sections from naïve mice or mice that received LPS. Data show that in response to LPS

the red pulp increases in size and this increase is associated with a higher number of $CD11b^+$ cells. Clusters can be detected in the red pulp of the LPS-treated mice. **(d)** Representative flow cytometric plots and enumeration depict the phenotype and fold increase of granulocyte macrophage progenitors (GMP) in spleens of C57BL/6 mice in the steady state and 4 days after daily injection of lipopolysaccharide (LPS). Bars show the fold increase over steady state in spleen and bone marrow (means ± SEM, n = 3 to 5). *P< 0.05. **(e)** DAPI staining shows the percentage of GMPs that are in the S/G_2 phase of the cell cycle. A representative plot of at least three independent experiments is shown. **(f)** Clonal efficiency and colony formation. Single progenitors were sorted into 96-well plates and scored for colonies after 8 days. Percentages of positive wells are shown in parentheses. The data show that GMPs isolated from the spleen and the bone marrow have a similar clonal efficiency. The graph depicts number of CFU-GM in spleen in the steady state and after LPS (means ± SEM, n = 3 to 5).*P< 0.05. **(g)** Intravital microscopy pictograms of the spleen red pulp depict clusters of GFP^+ cells adoptively transferred i.v. 3, 8 and 12 days earlier into inflammatory (LPS-injected) mice. Vasculature is shown in red and the scale is depicted with white bars. The large panels show clusers on day 8 **(h)** Enumeration of cluster number and cluster size in the subcapsular red pulp 5, 8 and 12 days after transfer of GFP^+ GMPs (means ± SEM, n = 4 to 9). **(i)** Phenotype of injected GFP^+ cells in the spleen on day 8. Data show that on day 8 after injection of GFP^+ GMP all the cells detected in the spleen are neutrophils and monocytes and not GMPs. **(j)** Cartoon depicts experimental design for the co-injection of equal numbers of GFP^+ GMPs and RFP^+ GMPs into C57BL/6 mice injected with LPS. **(k)** Green and red clusters in the subcapsular red pulp 5 days after injection of equal numbers of GFP^+ GMPs and RFP^+ GMPs. Vasculature is shown in blue and the scale is depicted by a white bar. Data are representative of at least three independent experiments. Data show that GMPs clonally expand in the spleen. If they did not clonally expand, a mixture of green and red cells would be expected. However, the clusters are either exclusively green or exclusively red and never mixed, thus showing that monocytes and neutrophils are made in the spleen.

References (to Expanded Methods)

1. Farese RVJ, Veniant MM, Cham CM, Flynn LM, Pierotti V, Loring JF, Traber M, Ruland S, Stokowski RS, Huszar D, Young SG. Phenotypic analysis of mice expressing exclusively apolipoprotein B48 or apolipoprotein B100. Proc Natl Acad Sci U S A. 1996;93:6393-6398.

2. Paigen B, Morrow A, Brandon C, Mitchell D, Holmes P. Variation in susceptibility to atherosclerosis among inbred strains of mice. Atherosclerosis. 1985;57:65-73.
3. Swirski FK, Nahrendorf M, Etzrodt M, Wildgruber M, Cortez-Retamozo V, Panizzi P, Figueiredo JL, Kohler RH, Chudnovskiy A, Waterman P, Aikawa E, Mempel TR, Libby P, Weissleder R, Pittet MJ. Identification of splenic reservoir monocytes and their deployment to inflammatory sites. Science. 2009;325:612-616.
4. Bunster E, Meyer RK. An improved method of parabiosis. Anat Rec. 1933;57:339-343.
5. Van Rooijen N, Sanders A. Liposome mediated depletion of macrophages: mechanism of action, preparation of liposomes and applications. J Immunol Methods. 1994;174:83-93.
6. Galkina E, Kadl A, Sanders J, Varughese D, Sarembock IJ, Ley K. Lymphocyte recruitment into the aortic wall before and during development of atherosclerosis is partially L-selectin dependent. J Exp Med. 2006;203:1273-1282.
7. Colvin GA, Lambert JF, Abedi M, Hsieh CC, Carlson JE, Stewart FM, Quesenberry PJ. Murine marrow cellularity and the concept of stem cell competition: geographic and quantitative determinants in stem cell biology. Leukemia. 2004;18:575-583.
8. Hotz MA, Gong J, Traganos F, Darzynkiewicz Z. Flow cytometric detection of apoptosis: comparison of the assays of in situ DNA degradation and chromatin changes. Cytometry. 1994;15:237-244.
9. Alencar H, Mahmood U, Kawano Y, Hirata T, Weissleder R. Novel multiwavelength microscopic scanner for mouse imaging. Neoplasia. 2005;7:977-983.

Published in final edited form as:
Science. 2012 February 3; 335(6068): 597–601. doi:10.1126/science.1215173.

Innate Response Activator B Cells Protect Against Microbial Sepsis

Philipp J. Rauch[1,*], **Aleksey Chudnovskiy**[1,*], **Clinton S. Robbins**[1,†,*], **Georg F. Weber**[1], **Martin Etzrodt**[1], **Ingo Hilgendorf**[1,5], **Elizabeth Tiglao**[1], **Jose-Luiz Figueiredo**[1], **Yoshiko Iwamoto**[1], **Igor Theurl**[1,6], **Rostic Gorbatov**[1], **Michael T. Waring**[3], **Adam T. Chicoine**[3], **Majd Mouded**[4], **Mikael J. Pittet**[1], **Matthias Nahrendorf**[1], **Ralph Weissleder**[1,2], and **Filip K. Swirski**[1,†]

[1]Center for Systems Biology, Massachusetts General Hospital and Harvard Medical School, Boston, MA 02114, USA

[2]Department of Systems Biology, Harvard Medical School, Boston, MA 02115, USA

[3]Ragon Institute Imaging Core, Massachusetts General Hospital and Harvard Medical School, Boston, MA 02114, USA

[4]Division of Pulmonary, Allergy, and Critical Care Medicine, University of Pittsburgh School of Medicine, Pittsburgh, PA 15213, USA

[5]Department of Cardiology, University Hospital Freiburg, 79106 Freiburg, Germany

[6]Department of General Internal Medicine, Clinical Immunology and Infectious Diseases, University Hospital of Innsbruck, A-6020, Innsbruck, Austria

Abstract

Recognition and clearance of bacterial infection is a fundamental property of innate immunity. Here we describe an effector B cell population that protects against microbial sepsis. Innate response activator (IRA)-B cells are phenotypically and functionally distinct, develop and diverge from B1a B cells, depend on pattern recognition receptors, and produce GM-CSF. Specific deletion of IRA-B cell activity impairs bacterial clearance, elicits a cytokine storm, and precipitates septic shock. These observations enrich our understanding of innate immunity, position IRA-B cells as gatekeepers of bacterial infection, and identify new treatment avenues for infectious diseases.

Sepsis is characterized by whole-body inflammation to overwhelming infection (1). Over the last thirty years, sepsis' incidence has risen, indicating a need for a better understanding of its complex pathophysiology (2, 3). The growth factor granulocyte macrophage colony stimulating factor (GM-CSF) elicits multiple changes in cells expressing its cognate receptor. Yet, despite GM-CSF's multiple functions and known relationship with innate leukocytes, its in vivo cellular source and role in sepsis remain uncertain (4).

†To whom correspondence should be addressed. fswirski@mgh.harvard.edu (F.K.S.); robbins.clinton@mgh.harvard.edu (C.S.R.).
*These authors contributed equally to this work.

Supporting Online Material
www.sciencemag.org/cgi/content/full/science.1215173/DC1
Materials and Methods
Figs. S1 to S12
Table S1
References (29–36)

Profiling of GM-CSF expression by flow cytometry led to a surprising observation. Among the organs, the bone marrow and spleen contained the majority of GM-CSF$^+$ cells in the steady state ($1.0 \pm 0.1 \times 10^6$ and $2.9 \pm 0.8 \times 10^5$ cells, respectively) (Fig. 1A) (5). In response to lipopolysaccharide (LPS), a component of gram negative bacteria, GM-CSF$^+$ cells increased in number preferentially in the spleen ($3.2 \pm 0.2 \times 10^6$ cells), and were predominantly B220$^+$ MHCII$^+$ CD19$^+$ IgM$^+$ B cells (Fig. 1B and fig. S1, A and B). This is surprising because GM-CSF is believed to be produced in vivo by non-hematopoietic cells, macrophages, and, in some cases, T cells (4, 6). Nevertheless, B cells constituted the largest GM-CSF$^+$ population under these conditions (fig. S1C), a finding that we confirmed by Western blot analysis (Fig. 1C). We named these B cells innate response activator (IRA) B cells because of GM-CSF's known role in activating innate leukocytes. Numerous IRA-B cells accumulated in the spleen in a mouse model of sepsis (fig. S2, A and B) (7) and in response to *Escherichia coli* infection (fig. S2C), indicating that IRA-B cell expansion is a general feature of the body's response to bacteria. In humans, we detected CD19$^+$ CD20$^+$ IRA-B cells expressing varying levels of CD43, CD27 (fig. S2, D and E), and CD284 (TLR4) (fig. S2F) (8). We therefore elected to characterize murine IRA-B cells in more detail.

Immunofluorescence of spleen sections from LPS recipients co-localized the GM-CSF signal with round mononuclear cells expressing IgM, B220, PAX5, and CD19 (Fig. 1D and fig. S1D) in the red pulp (Fig. 1, E and F). RT-PCR experiments conducted on sorted cells and unprocessed tissue from wild type or B cell-deficient μMT mice indicated that B cells produce GM-CSF (Fig. 1G). Serum GM-CSF levels were negligible (i.e., below the 7.8 pg/ml detection limit of the assay), a finding that is consistent with the observation that GM-CSF is rapidly removed through receptor-mediated clearance (9). Collectively, these data indicate that inflammation expands the IRA-B cell population in vivo.

B cells are linked developmentally, reside in different regions, and mediate distinct functions (10–14). We profiled IRA-B cells according to several well-established methods (13, 15, 16). Our experiments revealed that (CD19$^+$ B220$^+$ MHCII$^+$ GM-CSF$^+$) IRA-B cells are phenotypically unique. They are: IgM^{high} CD23^{low} CD43^{high} CD93$^+$ (Fig. 2, A and B, and fig. S3A); IgD^{low} CD21^{low} (fig. S3B); CD138$^+$ VLA4^{high} LFA1^{high} CD284$^+$ (Fig. 2C and fig. S3, C and D); and CD5^{int} (fig. S3, E and F). IRA-B cells contained large stores of intracellular IgM (fig. S4A) and spontaneously secreted IgM, but not IgA or IgG_1 (fig. S4, B and C). In addition to GM-CSF, IRA-B cells produced IL-3 but not pro-IL-1β, IL-6, and TNFα (fig. S4D). We failed to detect IL-10 expression by IRA-B cells in any of the conditions. Thus, IRA-B cells have a unique B cell phenotype and are functionally distinct from other B cells, including the recently described IL-10-producing B10 B cells (17).

The ability to sort IRA-B cells according to their surface phenotype (fig. S5A) allowed us to profile their transcriptome. Unsupervised hierarchical clustering (Fig. 2D) and principal component analysis (PCA) (Fig. 2E) grouped IRA-B cells in a separate population from T1, FO, MZ, B1a and PC. IRA-B cells also gave rise to a unique transcriptome signature (fig. S5, B to D, and table S1), and expressed genes relevant to B cell biology (fig. S5D).

To decipher where IRA-B cells fit in the B cell lineage we performed several parabiosis and fate-mapping studies. First, we reasoned that if IRA-B cells derive from a circulating precursor they should have high chimerism in a parabiosis setting. Joining CD45.1$^+$ with CD45.2$^+$ mice revealed high chimerism among IRA-B cells (Fig. 3A), T1 and FO B cells (fig. S6A), but markedly lower chimerism for the spleen-resident MZ B cells and their precursors (fig. S6A). Thus, IRA-B cells derive from a circulating cell.

Second, to identify the IRA-B cell precursor, we adoptively transferred B cell subsets to mice receiving LPS for 3 days (fig. S6, B to E). Among the subsets (splenic T1, FO, MZ, B1 and peritoneal B1a, B1b, B2) only peritoneal B1 B cells (Fig. 3B) gave rise to IRA-B cells. Of these, B1a B cells were the dominant precursor. B1a-derived IRA-B cells readily proliferated (fig. S6E), and developed in the spleen after relocating from the peritoneum (fig. S7). These findings confirm that B1a B cells travel to the spleen in response to peritoneal TLR stimuli (18, 19), and indicate that, upon splenic accumulation, B1a B cells can differentiate to IRA-B cells.

The ontogenic relationship between B1a and IRA-B cells raised the question whether IRA-B cells constitute a distinct subset. To elucidate this, we first placed peritoneal B1a B cells in culture. In response to LPS, B1a B cells separated into three discrete populations: $CD138^{-}$ cells resembling "unchanged" B1a B cells, and two populations of $CD138^{+}$ cells, IRA-B cells among them (fig. S8A). In vitro, IRA-B cells spontaneously secreted GM-CSF (fig. S8B). Second, we sorted peritoneal B1a B cells, IRA-B cells, and splenic $CD43^{+}$ $CD138^{+}$ cells, and followed their fate in vivo. B1a B cells gave rise to multiple cell types (fig. S9A), including IRA-B and $CD43^{+}CD138^{+}$ cells, whereas ($CD43^{high}$ $CD138^{+}$) IRA-B and $CD43^{+}$ $CD138^{+}$ cells remained phenotypically segregated (fig. S9, B and C). The data suggest that B1a B cells give rise to distinct cells. IRA-B cells are a subset of this group.

Surface phenotype and fate-mapping studies, though important, reveal little about function. How IRA-B cells arise was our next question. Expectedly, B cell-deficient μMT (20) and *Cd19*$^{-/-}$ (21) mice did not develop IRA-B cells (Fig. 3, C and D). Surprisingly, *Tnfrsf13c*$^{-/-}$ mice lacking the B-cell activating factor receptor (BAFFR) failed to generate IRA-B cells; BAFFR is believed to be dispensable to B1 B cells (22). At the level of microbial recognition, mice lacking the LPS receptor TLR4 or its adaptor MyD88, but not TRIF, did not generate IRA-B cells (Fig. 3, C and D), indicating a specific MyD88-dependent pathway. The process could depend on direct B1a binding to LPS via TLR4, or on indirect, extrinsic factors such as TLR4-expressing macrophages. To discriminate between these two possibilities, we adoptively transferred B1a B cells from wt mice into *Tlr4*$^{-/-}$ mice (Fig. 3E). B1a wt B cells, but not endogenous *Tlr4*$^{-/-}$ B cells, differentiated to IRA-B cells, indicating that direct TLR4 signaling on B1a B cells is sufficient to generate IRA-B cells.

To test whether IRA-B cells are restricted to TLR4-mediated recognition, we injected TLR ligands Pam3CSK4 (ligand for TLR1/2), Poly(I:C) (TLR3), FLA-ST (TLR5), FSL-1 (TLR2/6), R848 (TLR7/8), and CpG ODN1668 (TLR9). The ligands Pam3CSK4, FSL-1 and R848 yielded IRA-B cells (fig. S10A), a finding that we confirmed in vitro (fig. S10B). We also wondered whether GM-CSF can play an autocrine role for B1a-IRA-B cell conversion (23). B1a cells expressed Csf2Rβ (CD131) (fig. S11A) and, when placed in culture with antibodies against CD131, failed to give rise to IRA-B cells (fig. S11, B and C), but remained alive and gave rise to $CD43^{+}$ $CD138^{+}$ cells. Thus, IRA-B cells develop via MyD88-dependent pathways and use GM-CSF as an autocrine factor.

The spleen's open circulation (24) allows blood leukocytes to enter and exit easily. To reside in the spleen, leukocytes resort to adhesive ligands; MZ B cells, for example, rely on VLA-4 and LFA-1 (25). We wondered whether splenic IRA-B cells, which express VLA-4 and LFA-1 at high levels, might behave similarly. Injection of neutralizing antibodies to VLA-4 and LFA-1 diminished IRA-B cell numbers, revealing that, indeed, the two integrins are responsible for retention (Fig. 3F).

Are IRA-B cells functionally important? To answer this, we focused on the cecal ligation and puncture (CLP) sepsis model (26). We generated mixed chimeras by reconstituting lethally irradiated mice with μMT and GM-CSF-deficient (*Csf2*$^{-/-}$) bone marrow cells. In

these mice (called GM/μMT chimeras), the μMT marrow contributed all leukocytes except B cells whereas the *Csf2*$^{-/-}$ marrow contributed only *Csf2*$^{-/-}$ cells. Consequently, the only population completely lacking the capacity to produce GM-CSF in the reconstituted mice were B cells. We tested the quality of the chimeras and their controls by PCR (fig. S11, A and B) and by flow cytometry (fig. S11, C and D).

In response to severe CLP, 40% of control mice survived and recovered, but every GM/μMT chimera died within 2 days (Fig. 4, A and B). To characterize this phenotype further, we profiled GM/μMT chimeras and controls for several sepsis-relevant indices 20 hours after CLP, prior to any mortalities. Compared to IRA-B cell-containing controls (fig. S11E), the peritoneal cavity of GM/μMT chimeras had more leukocytes, mostly neutrophils (Fig. 4C), and experienced a severe IL-1β, IL-6 and TNFα cytokine storm in the serum (Fig. 4D) and peritoneum (Fig. 4E). This inflammatory signature typically associates with a defect in bacterial clearance. Indeed, neutrophils from the GM/μMT chimeras phagocytosed bacteria poorly (Fig. 4F). The GM/μMT chimeras, moreover, had a modest reduction of serum IgM but not IgG (Fig. 4G), and developed severe liver and lung pathologies (Fig. 4H). Finally, bacterial titre measurements revealed that GM/μMT chimeras were more infected than controls (Fig. 4, I and J). Although it is possible that other bone marrow cells contribute GM-CSF for the protection against sepsis in this setting, the most likely explanation is that IRA-B cells protect against septic shock by controlling the organism's ability to clear bacteria.

GM-CSF is a pleiotropic cytokine that influences the production, maturation, function, and survival of its target cells. GM-CSF's role in sepsis has remained elusive because its indiscriminate ablation is protective (27) but its supplementation can be beneficial (28). The in vivo identification of GM-CSF-producing B cells illustrates a previously unrecognized locational specificity that dictates the cytokine's function. IRA-B cells differ from other subsets because their pathogen recognition pathways and tissue distribution license GM-CSF expression. The function is important in sepsis and gives rise to questions as to how IRA-B cells participate in other infectious and inflammatory diseases.

Supplementary Material

Refer to Web version on PubMed Central for supplementary material.

Acknowledgments

This work was supported in part by NIH grants 1R01HL095612 (to F.K.S.), U01 HL080731, P50 CA86355, R24 CA69246, and P01-A154904 (to R.W.). P.J.R. was supported by the Boehringer Ingelheim Fonds. C.S.R. was supported by an American Heart Association (AHA) postdoctoral fellowship. The authors thank K. Rajewsky, D. Scadden, A. Luster, and K. Otipoby (Harvard Medical School) for helpful discussions and critical reading of the manuscript. The authors thank M. Greene for secretarial assistance. The data reported in this paper are tabulated in the main paper and in the supporting online material. MIAME (minimum information about a microarray experiment)-compliant exression data have been deposited under the accession no. GSE32372.

References and Notes

1. Cohen J. The immunopathogenesis of sepsis. Nature. 2002; 420:885. [PubMed: 12490963]
2. Martin GS, Mannino DM, Eaton S, Moss M. The epidemiology of sepsis in the United States from 1979 through 2000. N Engl J Med. 2003; 348:1546. [PubMed: 12700374]
3. Hotchkiss RS, Opal S. Immunotherapy for sepsis—A new approach against an ancient foe. N Engl J Med. 2010; 363:87. [PubMed: 20592301]
4. Hamilton JA. Colony-stimulating factors in inflammation and autoimmunity. Nat Rev Immunol. 2008; 8:533. [PubMed: 18551128]
5. Materials and methods are available as supporting material on *Science* Online.

6. Sonderegger I, et al. GM-CSF mediates autoimmunity by enhancing IL-6–dependent Th17 cell development and survival. J Exp Med. 2008; 205:2281. [PubMed: 18779348]
7. Rittirsch D, Huber-Lang MS, Flierl MA, Ward PA. Immunodesign of experimental sepsis by cecal ligation and puncture. Nat Protoc. 2009; 4:31. [PubMed: 19131954]
8. Griffin DO, Rothstein TL. A small CD11b^{+} human B1 cell subpopulation stimulates T cells and is expanded in lupus. J Exp Med. 2011; 208:2591. [PubMed: 22110167]
9. Metcalf D, Nicola NA, Mifsud S, Di Rago L. Receptor clearance obscures the magnitude of granulocyte-macrophage colony-stimulating factor responses in mice to endotoxin or local infections. Blood. 1999; 93:1579. [PubMed: 10029586]
10. LeBien TW, Tedder TF. B lymphocytes: How they develop and function. Blood. 2008; 112:1570. [PubMed: 18725575]
11. Allman D, Pillai S. Peripheral B cell subsets. Curr Opin Immunol. 2008; 20:149. [PubMed: 18434123]
12. Martin F, Kearney JF. Marginal-zone B cells. Nat Rev Immunol. 2002; 2:323. [PubMed: 12033738]
13. Pillai S, Cariappa A. The follicular versus marginal zone B lymphocyte cell fate decision. Nat Rev Immunol. 2009; 9:767. [PubMed: 19855403]
14. Hao Z, Rajewsky K. Homeostasis of peripheral B cells in the absence of B cell influx from the bone marrow. J Exp Med. 2001; 194:1151. [PubMed: 11602643]
15. Allman D, et al. Resolution of three nonproliferative immature splenic B cell subsets reveals multiple selection points during peripheral B cell maturation. J Immunol. 2001; 167:6834. [PubMed: 11739500]
16. Montecino-Rodriguez E, Dorshkind K. New perspectives in B-1 B cell development and function. Trends Immunol. 2006; 27:428. [PubMed: 16861037]
17. Yanaba K, et al. A regulatory B cell subset with a unique CD1d^{hi}CD5^{+} phenotype controls T cell-dependent inflammatory responses. Immunity. 2008; 28:639. [PubMed: 18482568]
18. Ha SA, et al. Regulation of B1 cell migration by signals through Toll-like receptors. J Exp Med. 2006; 203:2541. [PubMed: 17060475]
19. Kawahara T, Ohdan H, Zhao G, Yang YG, Sykes M. Peritoneal cavity B cells are precursors of splenic IgM natural antibody-producing cells. J Immunol. 2003; 171:5406. [PubMed: 14607944]
20. Kitamura D, Roes J, Kuhn R, Rajewsky K. A B cell-deficient mouse by targeted disruption of the membrane exon of the immunoglobulin μ chain gene. Nature. 1991; 350:423. [PubMed: 1901381]
21. Rickert RC, Rajewsky K, Roes J. Impairment of T-cell-dependent B-cell responses and B-1 cell development in CD19-deficient mice. Nature. 1995; 376:352. [PubMed: 7543183]
22. Schiemann B, et al. An essential role for BAFF in the normal development of B cells through a BCMA-independent pathway. Science. 2001; 293:2111. [PubMed: 11509691]
23. Harris RJ, et al. Granulocyte-macrophage colony-stimulating factor as an autocrine survival factor for mature normal and malignant B lymphocytes. J Immunol. 2000; 164:3887. [PubMed: 10725751]
24. Mebius RE, Kraal G. Structure and function of the spleen. Nat Rev Immunol. 2005; 5:606. [PubMed: 16056254]
25. Lu TT, Cyster JG. Integrin-mediated long-term B cell retention in the splenic marginal zone. Science. 2002; 297:409. [PubMed: 12130787]
26. Doi K, Leelahavanichkul A, Yuen PS, Star RA. Animal models of sepsis and sepsis-induced kidney injury. J Clin Invest. 2009; 119:2868. [PubMed: 19805915]
27. Basu S, et al. Increased tolerance to endotoxin by granulocyte-macrophage colony-stimulating factor-deficient mice. J Immunol. 1997; 159:1412. [PubMed: 9233638]
28. Gennari R, Alexander JW, Gianotti L, Eaves-Pyles T, Hartmann S. Granulocyte macrophage colony-stimulating factor improves survival in two models of gut-derived sepsis by improving gut barrier function and modulating bacterial clearance. Ann Surg. 1994; 220:68. [PubMed: 8024361]
29. Bunster E, Meyer RK. An improved method of parabiosis. Anat Rec. 1933; 57:339.
30. Swirski FK, et al. Identification of splenic reservoir monocytes and their deployment to inflammatory sites. Science. 2009; 325:612. [PubMed: 19644120]

31. Colvin GA, et al. Murine marrow cellularity and the concept of stem cell competition: Geographic and quantitative determinants in stem cell biology. Leukemia. 2004; 18:575. [PubMed: 14749701]
32. Simon P. Q-Gene: Processing quantitative real-time RT-PCR data. Bioinformatics. 2003; 19:1439. [PubMed: 12874059]
33. Reich M, et al. GenePattern 2.0. Nat Genet. 2006; 38:500. [PubMed: 16642009]
34. Workman C, et al. A new non-linear normalization method for reducing variability in DNA microarray experiments. Genome Biol. 2002; 3:research0048. [PubMed: 12225587]
35. Eisen MB, Spellman PT, Brown PO, Botstein D. Cluster analysis and display of genome-wide expression patterns. Proc Natl Acad Sci USA. 1998; 95:14863. [PubMed: 9843981]
36. Raychaudhuri S, Stuart JM, Altman RB. Principal components analysis to summarize microarray experiments: Application to sporulation time series. Pac Symp Biocomput. 2000; 455

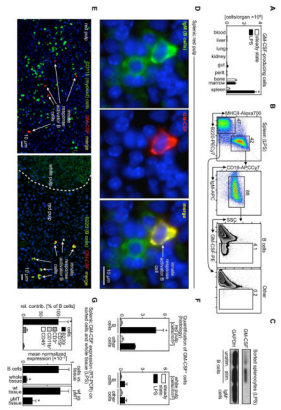

Fig. 1.

Innate response activator (IRA) B cells are GM-CSF-producing B cells that increase in number during inflammation. (**A**) Quantification of GM-CSF-producing cells retrieved from tissues in the steady state and in response to 4 daily i.p. injections of LPS (means ± SEM, n = 3–5). *$P < 0.05$. (**B**) Identification of GM-CSF-producing cells in the spleen. Representative plots show percentage of B cells and their production of GM-CSF retrieved from spleens during inflammation. Data represent at least ten independent experiments. (**C**) Western blot for GM-CSF conducted on sorted cells. One of three independent experiments is shown. (**D**) Co-localization of representative GM-CSF-producing cells with IgM. (**E**) Red pulp sections with markers against CD11b (green) and GM-CSF (red) (left panel) and B220 (green) and GM-CSF (red) (right panel). Co-localization of green and red cells is yellow and the scale bar is shown in white. (**F**) Quantification of GM-CSF^{+} B cells and other cells on histological sections of the spleen in the red pulp and white pulp in the steady state and after LPS (means ± SEM, n = 3–4). *$P < 0.05$. (**G**) Splenic GM-CSF expression detected by RT-PCR and conducted on sorted cells and on unprocessed spleen tissue taken from wild type and B cell knockout (μMT) mice (means ± SEM, n = 3–4). *$P < 0.05$.

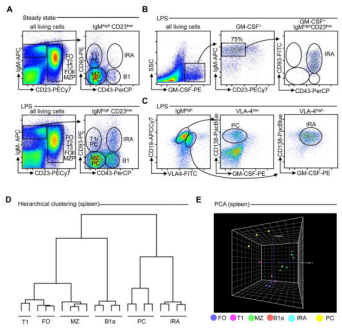

Fig. 2.

IRA-B cells are a distinct subset with a unique phenotypic signature. (**A**) Flow cytometric analysis of the phenotype of IRA-B cells. Plots show B cell phenotypes retrieved from spleens during steady state and inflammation. Representative from $n > 10$ is shown. (**B**) Plots show the phenotype of GM-CSF-producing cells in the spleens during inflammation. IRA-B cells are IgM^{high}, $CD23^{low}$ $CD43^{+}$ $CD93^{+}$. (**C**) Plots show the phenotype of IRA-B cells with respect to VLA4 and CD138 expression as determined by flow cytometry. Representative from $n > 5$ is shown. (**D**) Hierarchical clustering dendrogram based on whole-genome microarray data of sorted samples of B cell subsets retrieved from LPS-treated animals and steady-state B1a. (**E**) Principal Component Analysis (PCA) of the different cell subsets shown in (D).

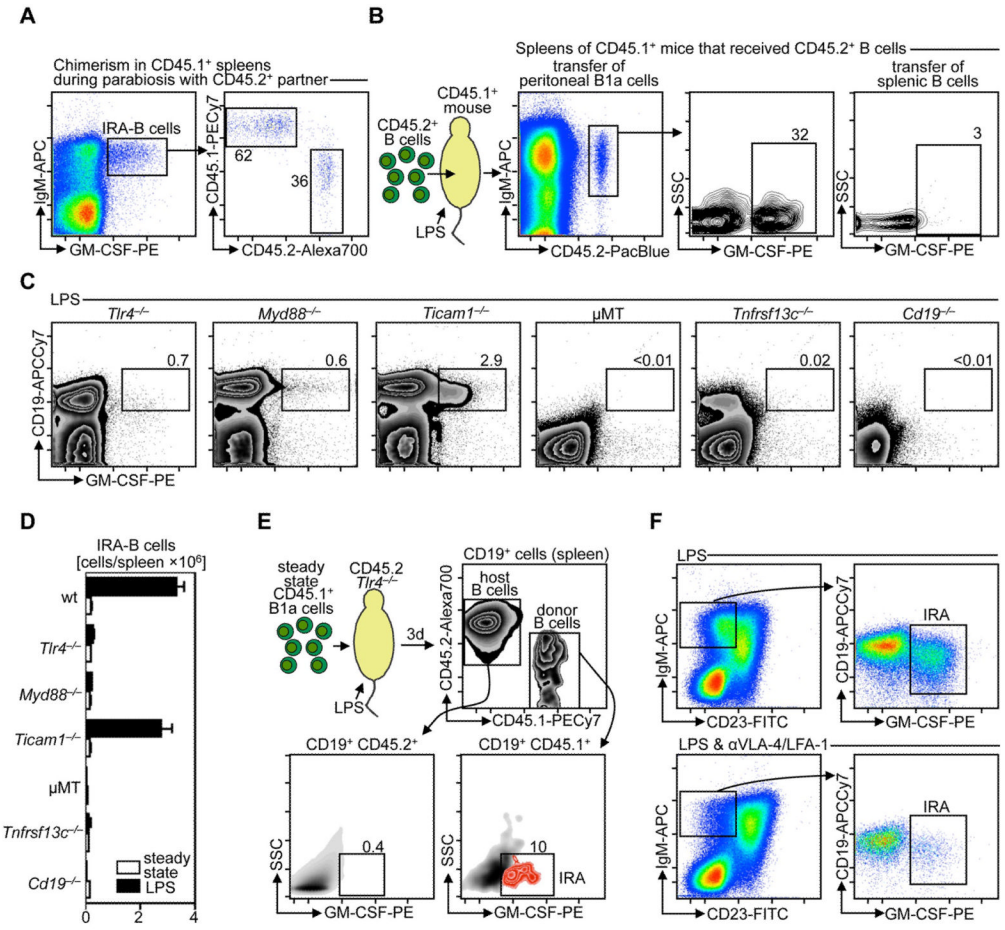

Fig. 3.

IRA-B cells develop from B1a B cells via TLR4/MyD88 and reside in tissue through LFA-1/VLA-4. (**A**) Flow cytometric analysis of the percent chimerism is shown in spleens of CD45.1$^+$ mice that had been in parabiosis with CD45.2$^+$ mice for 3 weeks prior to LPS injection. Mice were sacrificed 2 days after LPS injection. Representative plots from two independent experiments are shown. (**B**) Adoptive transfer of peritoneal B1a B cells yields IRA-B cells. Cells from steady state CD45.2$^+$ mice were transferred to CD45.1$^+$ mice that then received LPS for 3 days. Animals were analyzed 72 hours after transfer. Representative plots from flow cytometric analysis of $n = 4$–5 mice are shown. (**C**) Flow cytometric analysis of the development of IRA-B cells in *Tlr4*$^{-/-}$, *Myd88*$^{-/-}$, *Ticam1*$^{-/-}$ (the gene the encodes TRIF), μMT, *Tnfrsf13c*$^{-/-}$ (the gene that encodes BAFFR), and *Cd19*$^{-/-}$ mice. Representative plots from $n = 4$ mice are shown. (**D**) Enumeration of IRA-B cells in steady state and inflammation in wt (C57BL/6) mice and in the mice shown in (D) (means ± SEM, $n = 4$–10). *$P < 0.05$. (**E**) Flow cytometric analysis of the adoptive transfer of CD45.1$^+$ B1a cells into congenic *Tlr4*$^{-/-}$ CD45.2$^+$ mice injected with LPS. Representative from $n = 3$ mice is shown. (**F**) Flow cytometric analysis of the effect of blocking VLA-4/LFA-1 on IRA-B cell retention in the spleen. Representative from $n = 3$ mice is shown.

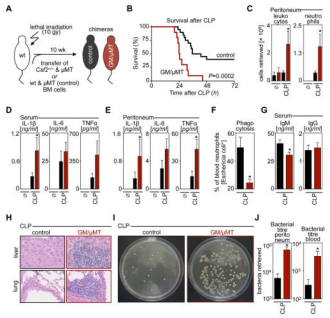

Fig. 4.

IRA-B cells protect against polymicrobial sepsis. (**A**) Generation of mixed chimeras (GM/μMT). (**B**) Kaplan-Meier curve showing survival of GM/μMT and control animals after cecal ligation and puncture (CLP). *n* = 10–20/group. (**C**) Enumeration of total leukocytes and neutrophils in the peritoneum of GM/μMT (dark red) and control (black bars) mice 20 h after CLP. (**D**) Serum levels and (**E**) peritoneal levels of inflammatory cytokines in GM/μMT (dark red) and control (black bars) mice 20 h after CLP. (**F**) Ex vivo phagocytosis assay showing capacity of neutrophils to phagocytose *E. coli* from GM/μMT (dark red) and control (black bars) mice 20 h after CLP. (**G**) serum levels of IgM and IgG 20 h after CLP in same groups as above. (**H**) Representative H&E stain of liver and lung sections 20 h after CLP in same groups as above. (**I**) Blood from GM/μMT and control mice 20 h after CLP was plated for 1 day. Representative plate shows bacterial colonies. (**J**) Enumeration of bacteremia in the peritoneum and blood of GM/μMT (dark red) and control (black bars) mice 20 h after CLP. **P* < 0.05 [means ± SEM, *n* = 10–20/group for (C)–(G), (J). Four independent experiments were performed and data were grouped].

Supporting Online Material

Materials and Methods

Animals. C57BL/6J (wt), B6.SJL-Ptprc^{a}Pepc^{b}/BoyJ (CD45.1^{+}), C57BL/6-Tg(UBC-GFP)30Scha/J (GFP^{+}), B10.129S2(B6)-*Ighm*^{tm1Cgn}/J (μMT), B6(Cg)-*Tnfrsf13c*^{tm1Mass}/J (BAFFR-deficient), B6.129P2(C)-Cd19$^{tm1(cre)Cgn}$/J (CD19-deficient), and B6.B10ScN-Tlr4$^{lps\text{-}del}$/JthJ (TLR4-deficient) female mice (from Jackson Laboratories) were used in this study. GM-CSF-deficient mice (*Csf2*$^{-/-}$) on a C57BL/6 background were a kind gift from Dr. Randy Seeley of the University of Cincinnati. MyD88-deficient and TRIF-deficient (*Ticam1*$^{-/-}$) mice on a C57BL/6 background were a kind gift from Dr. Rodrigo Mora of Massachusetts General Hospital. Mice were 8-12 weeks of age at the time of sacrifice. All protocols were approved by the Animal Review Committee at Massachusetts General Hospital.

Animal models and in vivo interventions. *Endotoxin-induced peritonitis and peritoneal lavage:* Mice were administered 10 μg of LPS (Sigma), unless otherwise stated, daily by i.p. injections in PBS over the course of 4 days. For some experiments different TLR ligands (all Invivogen) were administered i.p. daily. TLR1/2: Pam3CSK4 (100 μg/mouse), TLR3: Poly(I:C) (200 μg/mouse), TLR5: FLA-ST (10 μg/mouse), TLR2/6: FSL-1 (10 μg/mouse), TLR7: R848 (25 μg/mouse), TLR9: CpG ODN 1668 (10 μg/mouse). Controls received PBS alone. For select experiments, the peritoneal cavity was lavaged with 10 ml of PBS to retrieve infiltrated and resident leukocytes. *Cecal ligation and puncture (CLP):* This rodent model of sepsis was carried out as previously described (7). In brief, the peritoneal cavity was opened during isoflurane anesthesia, and the cecum was exteriorized and ligated about 2 mm distal of the ileo-cecal valve using a non-absorbable 6-0 suture. The distal end of the cecum was then perforated using a 23 G needle, and a small drop of feces was extruded through the puncture. The cecum was relocated into the peritoneal cavity, and the peritoneum was closed. Animals were resuscitated by s.c. injection of 1 mL of saline. Age-matched controls were included for all procedures. *Infection with E. coli:* Animals were injected i.p. with 10^7 CFU of E. coli. *Parabiosis:* The procedure, adapted from (29) was conducted as previously described (30). Briefly, after shaving the corresponding lateral aspects of each mouse, matching skin incisions were made from behind the ear to the tail of each mouse, and the subcutaneous fascia was bluntly dissected to create about ½ cm of free skin. The olecranon and knee joints were attached by a mono-nylon 5.0 (Ethicon, Albuquerque, NM), and the dorsal and ventral skins were approximated by continuous suture. Percent chimerism was defined as %CD45.1 / (%CD45.1 + %CD45.2) in CD45.2 mice, and as %CD45.2 / (%CD45.2 + %CD45.1) in CD45.1 mice. *Adoptive transfer of B cell subsets:* B cell subsets were sorted from spleens or peritoneum of naïve CD45.1^{+} or CD45.2^{+} donor mice. IRA-B cells were sorted from the spleens of LPS-treated CD45.1^{+} or CD45.2^{+} donor mice. Equal cell numbers of each subset (5×10^5 cells) were injected into the tail vein or peritoneum of LPS-stimulated CD45.1^{+} or CD45.2^{+} recipients. *Mixed bone marrow chimeras:* Naïve wild type mice were lethally irradiated (10 Gy). 4-7 hours after irradiation, animals were reconstituted with a 1:1 mixture of total bone marrow cells from μMT and wt or GM-CSF knock-out mice, respectively. A total of 4×10^6 cells were injected intravenously. Animals were allowed to recover for a minimum of 10 weeks.

Cells. *Isolation and ex vivo methods:* Peripheral blood for flow cytometric analysis was collected by cardiac puncture, using a 50 mM EDTA solution as anticoagulant. Erythrocytes were lysed using BD FACS Lysing Solution (BD Biosciences). Total white blood cell count was determined by preparing a 1:10 dilution of (undiluted) peripheral blood obtained from the orbital sinus using heparin-coated capillary tubes in RBC Lysis Buffer (BioLegend). After organ harvest, single cell suspensions were obtained as follows: for bone marrow, the femur and tibia of one leg were flushed with PBS. Spleens were homogenized through a 40 μm-nylon mesh, after which erythrocyte lysis was performed on the spleens using RBC Lysis Buffer (BioLegend). For liver, lung, kidney and gut, tissue was cut into small pieces and subjected to enzymatic digestion with 450 U/ml collagenase I, 125 U/ml collagenase XI, 60 U/ml DNase I and 60 U/ml hyaluronidase (Sigma-Aldrich, St. Louis, MO) for 1 h at 37°C while shaking. Total viable cell numbers were obtained using Trypan Blue (Cellgro, Mediatech, Inc, VA). To determine total bone marrow cellularity, one femur and one tibia were estimated to represent 7% of total marrow (31). For morphological assessment, cytospins were prepared from 5×10^4 cells and stained using HEMA 3 staining kit (Fisher Scientific). Human cells were obtained from fresh spleens of patients undergoing

splenectomies at Massachusetts Hospital. Single-cell suspension were prepared. *In vitro:* Cells were cultured in 96-well round-bottom plates (Corning) and kept in a humidified CO_2 incubator at 37°C for 48 hours. B1a, IRA-B and T-cells were cultured in RPMI-1640 supplemented with 10% fetal bovine serum, 25 mM HEPES, 2mM L-glutamine, 100 U/ml penicillin, 100 U/ml streptomycin and 50 μM 2-mercaptoethanol. Human Umbilical Vein Endothelial Cells (HUVEC) were cultured using the EGM-MV Bulletkit (Clonetics). All cell types were seeded at a density of 40,000 cells/100 μL medium. Where indicated, LPS was added at 10 μg/ml.

Flow Cytometry. The following antibodies were used for flow cytometric analyses: anti-MHC Class II-Alexa Fluor 700, anti-MHC Class II-APC, M5/114.15.2 (eBioscience); anti-B220-PE-Cy7, anti-B220-PerCP, RA3-6B2 (BD Biosciences); anti-CD19-APC-Cy7, 6D5 (BioLegend); anti-CD19-FITC, HIB19 (BD Biosciences); anti-IgM-FITC, anti-IgM-APC, anti-IgM-PerCP-Cy5.5, II/41 (BD Biosciences); anti-GM-CSF-PE, MP1-22E9 (BD Biosciences); anti-CD23-FITC, anti-CD23-PECy7, B2B4 (BD Biosciences); anti-CD93-APC, (eBioscience), anti-CD93-PE, anti-CD93-FITC, all AA4.1 (BD Biosciences*)*; anti-CD43-biotin, anti-CD43-FITC, anti-CD43-APC, S7 (BD Biosciences); anti-CD49d/VLA4-FITC, R1-2 (BioLegend); anti-CD138-biotin, 281-2 (BD Biosciences); anti-CD45.2-Pacific Blue (BioLegend), anti-CD45.2-Alexa Fluor 700, 104 (BD Biosciences); anti-CD45.1-PECy7, A20 (BD Biosciences); anti-ratIgG2a-biotin, RMG2a-62 (BioLegend), anti-ratIgG2a-PE, RTK2758 (BD Biosciences); anti-TER119-PE, TER119 (BD Biosciences); anti-CD45-biotin, 30-F11 (BD Biosciences)*;* anti-Ly-6G-FITC, 1A8 (BD Biosciences); anti-CD11b-Alexa Fluor 700 (eBioscience), anti-CD11b-APC, anti-CD11b-APCCy7, M1/70 (BD Biosciences); anti-F4/80-PECy7, BM8 (BioLegend); anti-CD11c-APC, anti-CD11c-biotin, HL3 (BD Biosciences); anti-CD16/32-APCCy7, 2.4G2 (BD Biosciences); anti-CD49b-PE, anti CD49b-FITC, DX5 (BD Biosciences); anti-CD41-PE-Cy7, eBioMWReg30 (eBioscience); anti-CD4-Alexa Fluor 700, GK1.5 (eBioscience); anti-CD3-APCCy7, 17A2 (BD Biosciences); anti-CD3e-FITC, 145-2C11 (BD Biosciences); anti-CD8-PerCP, 53-6.7 (BD Biosciences); anti-HLA-DR-APC, LN3 (eBioscience)*;* anti-CD20-PE-Cy7, 2H7 (eBioscience); anti-CD27-APC, O323 (BioLegend); anti-CD284-biotin, HTA125 (BioLegend); anti-CD284-FITC, MTS510 (BioLegend); anti-IgD-Pacific Blue, anti-IgD-FITC, 11-26c.2a (BioLegend); anti-CD21-PerCP, 7E9 (BioLegend); anti-LFA-1-FITC, H155-78 (BioLegend); anti-CD5-PECy7 (eBioscience), anti-CD5-PerCP, 53-7.3 (BD Biosciences); anti-IgA-FITC, mA-6E1 (eBioscience); anti-IgG1-APC, RMG1-1 (BD Biosciences); anti-IgG2b-biotin, RMG2b-1 (eBioscience); anti-IgG3-FITC, J606 (BD Biosciences); anti-ratIgG1-FITC, MOPC-21 (BD Biosciences); anti-ratIgG1-APC, anti-ratIgG1-Alexa Fluor 700, A85-1 (BD Biosciences); anti-IL3-PE, MP2-8F8 (BD Biosciences); anti-IL6-APC, MP5-20F3 (BD Biosciences); anti-proIL-1b-APC, NJTEN3 (eBioscience); anti-TNFa-APC, MP6-XT22 (BD Biosciences); anti-BrdU-FITC, 3D4 (BD Biosciences); anti-CD131-PE, JORO50 (BD Biosciences); anti-CD25-APC, PC61 (BD Biosciences); anti-CD115-biotin, AFS98 (eBioscience); anti-CD90-PE, 53-2.1 (BD Biosciences); anti-NK1.1-PE, PK136 (BD Biosciences); anti-Ly-6C-FITC, AL-21 (BD Biosciences); anti-F4/80-biotin, C1:A3-1 (BioLegend). Streptavidin-PerCP, Streptavidin-APC, Streptavidin-APC-Cy7 and V450-Streptavidin (BD Biosciences) and Streptavidin-Alexa Fluor 700 (Invitrogen) were used to label biotinylated antibodies. Staining for intracellular cytokines was performed using BD Cytofix/Cytoperm Plus Kit (BD Biosciences) according to the manufacturer's instructions. Cell cycle analysis was carried using FxCycle violet stain (Invitrogen). Contribution of newly-made cells to different cell populations was determined by in-vivo labeling with bromodeoxyuridine (BrdU). Mice received 1 mg of BrdU (BD Biosciences) by i.p. injection. Incorporation was measured using a FITC-conjugated antibody according to the manufacturer's instructions. Splenic B cell populations were identified based on (13, 15, 16). In particular, for purposes of fate mapping and microarray profiling, the following subsets were defined: Splenic marginal zone (MZ) B cells ($CD19^+$ $MHCII^+$ $CD93^-$ IgM^+ $CD23^-$ $CD21^{hi}$); splenic follicular (FO) B cells ($CD19^+$ MHC Class II^+ $CD93^-$ IgM^{low} $CD23^+$); peritoneal or splenic B1a B cells ($CD19^+$ $MHCII^+$ $CD93^-$ IgM^{high} $CD23^-$ $CD43^+$ $CD5^{high}$); peritoneal or splenic B1b cells ($CD19^+$ $MHCII^+$ $CD93^-$ IgM^{high} $CD23^-$ $CD43^+$ $CD5^-$), splenic transitional type 1 (T1) B cells: ($CD19^+$ $MHCII^+$ $CD93^+$ IgM^+ $CD23^-$ $CD43^-$); plasma cells (IgM^+ $CD138^+$ $CD19^+$ $CD43^{-/low}$), innate response activator (IRA) cells (IgM^{high} $CD23^{low}$ $CD43^{high}$ $CD93^+$; and $CD19^+$ $MHCII^+$ VLA-4^{hi} $CD138^+$ $CD5^{int}$). Other B cell types are defined in Figures. Data were acquired on an LSRII (BD Biosciences) and analyzed with FlowJo v8.8.6 (Tree Star, Inc.). Cells were sorted on a BD FACSAria II (BD Biosciences).

Histology. Spleens from wild type C57BL/6 mice and C57BL/6 mice that received LPS were excised, rinsed in PBS, and embedded in OCT (Sakura Finetek). Fresh-frozen serial 6 μm thick sections were used for

immunofluorescence staining. Sections were incubated with anti-CD11b-biotin, M1/70 (BD Biosciences); anti-B220-biotin, RA3-6B2 (BD Biosciences); anti-IgM-biotin, II/41 (BD Biosciences); anti-CD19, 1D3 (BD Biosciences); anti-PAX5, 1H9 (eBioscience); or anti-GM-CSF, FL-144 (Santa Cruz Biotechnology, Inc). Biotinylated primary antibodies were followed by Texas Red-conjugated streptavidin (GE Healthcare) alone while anti-CD19, anti-PAX5, and anti-GM-CSF were followed by the appropriate biotinylated secondary antibodies and Texas Red-conjugated streptavidin or FITC-conjugated streptavidin (GE Healthcare). Mounting medium with DAPI (Vector Laboratories, Inc.) was used to identify cell nuclei. Livers and lungs from control and GM/μMT mice were fixed in 10% formalin solution, paraffin embedded, and stained with hematoxylin and eosin for overall histological analysis. The images were captured and processed using an epifluorescence microscope, Nikon Eclipse 80i (Nikon Instruments Inc.) and Nanozoomer 2.0RS (Hamamatsu). Image analysis was done using IPLab (version 3.9.3; Scanalytics, Inc., Fairfax, VA).

Molecular Biology. *Western blots:* 10^7 IgM^+ or IgM^- cells were sorted from spleens of LPS-treated mice, and stimulated, or not, in vitro with 1μg/ml LPS and Golgi Plug for 5h. Pellets were then frozen in liquid nitrogen. For protein extraction sample pellets were resuspended in Ripa buffer (Boston Bioproducts, BP-116TX) supplemented with protease and phosphatase inhibitors (Thermo Scientific, PI-87786, PI-78420) and incubated on ice for 30 min. Samples were spun down and 15 μl of protein extract was mixed with 15 μl of Laemmli buffer (BioRad) in accordance with the manufacturer's instructions. Samples were developed by electrophoresis on a 4-15% polyacrylamide gel (BioRad). The proteins were transferred to a polyvinylidene difluoride membrane (Fischer) by dry transfer. Membranes were blocked with carnation milk and PBS supplemented with 0.05 % Tween 20 overnight. Membranes were washed, stained initially with anti-GM-CSF antibody (MP1-31G6) (Abcam) followed by appropriate secondary antibody. For GAPDH stain the membrane was stripped with Restore buffer (Pierce), and stained with anti-glyceraldehyde-3-phosphate (GAPDH) (Rockland Immunochemicals for Research). Blots were developed with Western Lightning Chemiluminescence reagent (PerkinElmer Instruments) and molecular weights were compared to bands for Precision Plus Protein Western C standards (BioRad). *ELISA:* ELISA was performed with R&D ELISA kits according to the manufacturer's instructions. *ELISpot:* ELISpot was performed with Mabtech Mouse IgG and IgM according the the manufacturer's instructions. *Real-time PCR:* Total RNA was isolated from cryostat-prepared 20 μm spleen sections or 3-10 x 10^4 FACS-sorted cells using the PicoPure RNA Isolation Kit (Arcturus) according to the manufacturer's instructions. cDNA was generated from 50-200 ng of total RNA per sample using the High Capacity cDNA Reverse Transcription Kit (Applied Biosystems). Real time PCR was performed in triplicates using the TaqMan Gene Expression Assay System on a 7300 Real-Time PCR System (Applied Biosystems). Primers Mm01290062_m1 (GM-CSF)were used (Applied Biosystems). Mean normalized expression was calculated using the Q-Gene Application (32) with 18S rRNA (Applied Biosystems) serving as endogenous control. At least three independent samples per group were analyzed.

Bacteria. *Enumeration of bacterial infection:* Whole blood and peritoneal lavage samples were diluted, plated on tryptic soy agar (BD Difco), and incubated at 37°C. The number of bacterial colonies was assessed 24 hours later. *Phagocytosis assay:* Neutrophil phagocytosis was assessed using a pHrodo™ *E. coli* BioParticles® Phagocytosis Kit (invitrogen) as instructed by the manufacturer.

Microarray gene expression profiling. B cell subsets from spleens or peritoneum of a group of 8-10 mice (per biological replicate) that received 10 μg LPS i.p. daily over the course of 4 days or from steady state were isolated by fluorescence activated cell sorting (FACS) to a purity of >99% in accordance with the Immunological Genome Project standard operating procedures (www.immgen.org). Cells were sorted directly into RLT lysis buffer, and total RNA was isolated using the RNeasy Mini Kit (Qiagen) according to the manufacturer's instructions. RNA quality was assessed using RNA pico lab chips on the Agilent Bioanalyzer. For all samples a RNA integrity number (RIN) above 8 could be achieved. Gene expression datasets were generated on Illumina Mouse Ref-8 gene expression arrays at the Broad Institute Genetic Analysis Platform (Broad Institute, 301 Binney St. Cambridge, MA 02142). Briefly, total RNA from the samples was normalized to 20 ng/ μl and the IlluminaTotalPrep-96 RNA Amplification Kit (Applied Biosystems, PN #4393543) protocol was used for amplification in a semi automated process. The total RNA underwent reverse transcription to synthesize first-

strand cDNA. This cDNA was then converted into a double-stranded DNA template for transcription. *In vitro* transcription synthesized aRNA and incorporated a biotin-conjugated nucleotide. The aRNA was then purified to remove unincorporated NTPs, salts, enzymes, and inorganic phosphate. Labeled cRNA was normalized to 150 ng/µl and hybridized to Illumina's MouseRef-8 v2.0 Expression BeadChip. The labeled RNA strand was hybridized to the bead on the BeadChip containing the complementary gene-specific sequence. After a 16 hour hybridization, the beadchips were washed and stained using a Cy3 streptavidin conjugate. Illumina's BeadArray Reader was used to measure the fluorescence intensity at each addressed bead location. Analysis of expression data was performed using the server hosted version of Gene Pattern (http://genepattern.broadinstitute.org) (Version 3.3.2, build Id: 9695, Java Version 1.6.0_21) (33). Illumina IDAT files were uploaded to Genepattern and a background subtracted .gct expression file was generated using the 'IlluminaExpressionFileCreator' with the MouseRef-8_V2_0_R2_11278551_A manifest file followed by quantile normalization (34) using the 'IlluminaNormalizer' module. Hierachical clustering was performed by submitting the normalized expression dataset to the 'HierachicalClustering' and 'HierachicalClusteringViewer' modules choosing pairwise complete linkage as clustering method and a Pearson correlation as the column distance measure (35). For principal component analysis the expression file was submitted to the 'PCA' and 'PCAViewer' modules choosing columns as the clustering method (36). The dataset was displayed over principal components 2, 3 and 4. Data were deposited to the Gene Expression Omnibus (GEO) bank under Accesion Number GSE32372. http://www.ncbi.nlm.nih.gov/geo/query/acc.cgi?token=flktxaccekgwsdq&acc=GSE32372. To reveal distinct and common features among IRA-B cells, B1a B cells and plasma cells (PC) gene expression signatures for each B cell subset were defined based on the available gene expression dataset. To this end the Genepattern Comparative Marker Selection module was utilized using default parameters and for each pairwise comparison the cell type of interest was compared to all other available B cell subsets. The top 350 ranking genes were defined as signature genes for the respective B cell subtype. The following comparisons were performed: IRA-B vs [Fo, B1a, T1, MZ, PC]; PC vs [Fo, B1a, T1, MZ, IRA-B]; B1a vs [Fo, IRA-B, T1, MZ, PC]. Subsequently Gene Set Enrichment Analysis was utilized to quantify the correlation between the IRA-B signature and B1A cells or PC respectively.

Statistics. Results were expressed as mean ± SEM. Statistical tests included unpaired, 2-tailed Student's *t* test using Welch's correction for unequal variances and 1-way ANOVA followed by Tukey's or Newman-Keuls Multiple Comparison Test. P values of 0.05 or less were considered to denote significance.

Supporting Figures

Figure S1. Phenotype of Innate Response Activator (IRA) B cells. (A) Presence of IRA-B cells in the bone marrow in response to LPS. **(B)** Istoype control for GM-CSF. **(C)** Different GM-CSF$^-$ (blue) cell subpopulations overlaid with GM-CSF$^+$ (red) cell subpopulations in steady state and after LPS treatment. Erythrocytes (Ter119$^+$), non-leukocytes (CD45$^-$), neutrophils (Ly-6G$^+$), dendritic cells (CD11c$^+$), macrophages (F4/80$^+$), platelets/megakaryocytes (CD41$^+$), and T cells (CD4$^+$, CD8$^+$ CD3$^+$) do not express GM-CSF in large amounts. Representative plots of n=4 are shown. **(D)** Immunofluorescence in the splenic red pulp identifies IRA-B cells as B220$^+$ CD11b$^-$ PAX5$^+$ and CD19$^+$. Representatives of >100 cells examined are shown.

Figure S2. IRA B cells can be detected in response to infection and in humans. (A) Identification of IRA-B cells in a model of sepsis (cecal ligation and puncture, CLP). **(B)** Quantification of IRA-B cells in response to CLP in bone marrow and spleen (means ± SEM, n = 4). *P<0.05. **(C)** Identification of IRA-B cells in response to *E. coli* infection. **(D)** Identification of IRA-like B cells in human spleens from patients undergoing splenectomies for non-infectious diseases and conditions such as trauma or cancer. **(E)** Quantification of IRA-like B cells retrieved from 4 individuals undergoing splenectomy. **(F)** Expression of CD284 (TLR4) on human IRA-B cells. Data show that ~27% of IRA-B cells, but not other B cells, are TLR4$^+$. Representative plots of n = 4 are shown.

Figure S3. IRA-B cells represent a distinct subset with a unique phenotypic signature. (A) Phenotype of IRA-B cells. Representative plots show B cell phenotypes retrieved from spleens during steady state and inflammation. The majority of IRA-B cells are identified as CD93$^+$ IgM^{high} CD23^{low}. **(B)** Phenotype of IRA-B

cells. Representative plots show B cell phenotypes retrieved from spleens during steady state and inflammation. The majority of IRA-B cells are identified as $B220^{+}$ $CD19^{+}$ IgM^{high} $CD23^{low}$ $CD21^{int}$. **(C)** Phenotype of IRA-B cells. Representative plots show that IRA-B cells are VLA-4^{high} LFA-1^{high}, CD284 $(TLR4)^{+}$. **(D)** Representative plots show the IRA-B cells are $CD138^{+}$ $CD43^{high}$ $CD23^{low}$ **(E)** Representative plots show the phenotype for B1a and B1b B cell in steady-state peritoneum. Data show that B1a B cells are $CD5^{high}$ $CD43^{+}$ $CD138^{low/-}$. **(F)** Representative plots show that IRA-B cells are $CD5^{int}$ $CD43^{high}$ and differ from B1a B cells which are $CD5^{high}$ $CD43^{+}$. Most CD5-expressing B cells in the inflamed spleen are $CD138^{+}$ and are thus B1a-plasma (PC)-like. The dotted line highlights the phenotypic similarity of IRA B cells and "B1a-PC" identified in panes D and F. Also refer to fig. S9. Plots are representative of n>10.

Figure S4. Immunoglobulin and cytokine production by IRA-B cells (A) Representative plots show the intracellular immunoglobulin stores of IgM^{+} $CD138^{+}$ cells in the spleen and bone marrow. Data show that ($CD19^{+}$ $CD138^{+}$ GM-CSF^{+}) IRA-B cells in the spleen contain the very high IgM stores among $CD138^{+}$ cells. Splenic $CD19^{+}$ $CD138^{+}$ GM-CSF^{-} cells, but not IRA-B cells, produce IgG_1. Plots are representative of n=4. **(B)** Representative ELISpot photographs showing IgM and IgG production by 5,000 sorted IRA-B cells, 10,000 sorted myeloid cells, and 10,000 unsorted splenocytes. Data show that IRA-B cells are IgM but not IgG producers. **(C)** Quantification of data shown in panel B. (means ± SEM, n = 3). (**D)** Representative plots show the intracellular inflammatory cytokine production profile. Data show that (IgM^{high} $CD23^{low}$ $CD43^{high}$ $CD93^{+}$) IRA-B cells produce IL-3 but not pro-IL-1β, IL-6 and TNFα. Plots are representative of n=4.

Figure S5. IRA-B cells have a distinct transcriptome. (A) Gating scheme for the isolation of IRA-B cells. After doublets were excluded, $CD23^{low}$ IgM^{high} $CD43^{high}$ $CD93^{+}$ IRA-B cells were sorted. Also refer to Figure 2. A representative plot of n > 10 is shown. **(B)** The transcriptional signature of IRA-B cells was defined using the Genepattern comparative marker selection tool as the 350 selectively top ranking genes against the combined FO, B1a, T1, MZ and PC B cell expression values. Signatures for B1a and PC cells were defined accordingly. **(C)** GSEA of the 350 top ranking IRA-B signature genes comparing B1a and plasma cells against IRA-B cells. IRA-B and B1a cells show virtually no overlap among their signature genes, while some genes overlap between IRA-B cells and plasma cells. **(C)** Transcriptional signatures as defined in panel A of IRA-B, B1a and PC. **(D)** Relative expression of genes known to be important in B cell biology. IRA-B cells are compared to T1, FO, MZ, B1, and PC B cells.

Figure S6. The origin of IRA-B cells. (A) Percent chimerism is shown in spleens of $CD45.1^{+}$ mice that had been in parabiosis with $CD45.2^{+}$ mice for 3 weeks prior to LPS injection. Mice were sacrificed 2 days after LPS. Data show that T1 and FO B cells have high chimerism whereas T2/FO-II/MZP B cells and MZ B cells have low chimerism. Representative plots from n=4-5 are shown. **(B)** B cell phenotypes in the steady state peritoneum. B1a, B1b and B2 B cells are identified. **(C)** Adoptive transfer of $CD45.2^{+}$ cells into $CD45.1^{+}$ cells allows retrieval of $CD45.2^{+}$ $CD45.1^{-}$ cells in the recipient spleen 3 days later. **(D)** Adoptive transfer of splenic T1, FO, MZ, B1 and peritoneal B2, B1b and B1a B cells reveals that B1a B cells give rise to IRA-B cells. B cell subsets from $CD45.2^{+}$ mice were transfered to $CD45.1^{+}$ mice and recipient animals were analyzed 3 days later. The gating schemes for sorting splenic B cell subsets for adoptive transfer are shown in fig. S3, A and B whereas the gating schemes for sorting peritoneal B cell subsets are shown in panel B of this figure. Representative plots from n=4-5 are shown. **(E)** IRA-B cell development is associated with proliferation. Evaluation of DAPI and BrdU on IRA-B cells retrieved from recipient spleens after transfer of naive $CD45.2^{+}$ B1a B cells into $CD45.1^{+}$ mice. Data show that IRA B cells proliferate. **(F)** Proliferation of endogenous B cells in the animal shown in E. Data show a range of proliferation among B cells. Representative plots from n=4-5 are shown.

Figure S7. IRA-B cells in the peritoneum. **(A)** The peritoneum contains a small number of IRA-B cells. Plots show recipient $CD45.1^{+}$ peritoneum in mice that received $CD45.2^{+}$ cells and LPS 3 days earlier. **(B)** B cells adoptively transferred i.p. do not become IRA-B cells in the peritoneum but relocate to the spleen to become IRA-B cells. Plots show $CD45.2^{+}$ B cells retrieved from the peritoneum and spleen of $CD45.1^{+}$ recipients that received LPS. A representative of 3 independent experiments is shown.

Figure S8. The origin of IRA-B cells in vitro. (A) Peritoneal B1a B cells were sorted and placed in vitro for 48 h. Representative plots show the B1a B cell phenotype immediately after sorting and after 48h of culture with LPS. Data show that B1a B cells convert to two discrete cell populations. IRA-B cells upregulate CD138, CD43, GM-CSF and have high stores of intracellular IgM, as shown in vivo in fig. S4. The second B1a B cell-derived population upregulates CD138, slightly downregulates CD43 and does not make GM-CSF. Representative plots of n=4 are shown. **(B)** IRA-B cells spontaneously secrete GM-CSF in vitro. Splenic T cells and peritoneal B1a B cells were sorted from steady state mice. IRA-B cells were sorted from spleens of mice receiving LPS. HUVECs were used as non-leukocyte controls. The cells were placed in medium alone (unstimulated) and ELISA for GM-CSF was performed on media. The graph shows that IRA-B cells, but not other cells, secrete GM-CSF. The ELISA was performed on pooled wells of n =2.

Figure S9. The origin and fate of IRA-B cells in vivo. (A) Peritoneal B1a B cells were sorted from $EGFP^+$ mice and adoptively transferred i.v. to C57BL/6 mice that then received LPS for 4 consecutive days. After 7 days the animals were sacrificed and the presence and phenotype of $EGFP^+$ cells was assessed in the spleen. Data show that B1a B cells give rise to several phenotypically distinct cells, including IRA-B cells. Representative plots from two experiments are shown. **(B and C)** $CD138^+$ $CD43^{high}$ IRA-B cells and $CD138^+$ $CD43^+$ non-IRA B cells were sorted from the spleens of LPS-injected $EGFP^+$ mice and adoptively transferred i.v. to C57BL/6 mice that then received LPS for 3 consecutive days. Cells were sorted according to the gates shown in fig. S3D and resemble the subsets that B1a B cells generate in vitro, as shown in fig. S8. After 3 days the animals were sacrificed and the presence and phenotype of $EGFP^+$ cells was assessed in the spleen. Data show that IRA-B cells and $CD138^+$ $CD43^+$ non-IRA B cells do not give rise to each other under these conditions: IRA-B cell remain $GM\text{-}CSF^+$ (at ~90%), are $CD138^+$ $CD43^{high}$ $CD5^{int}$ and contain high intracellular IgM stores. $CD138^+$ $CD43^+$ cells become $CD138^-$ $CD43^-$ cells. Representative plots from two experiments are shown.

Figure S10. In vivo and in vitro generation of IRA-B cells in response to various TLR ligands. (A) Ligands against TLR1/2 (Pam3CSK4), TLR2/6 (FSL-1), TLR7/8 (R848), TLR3 (Poly(I:C)), TLR5 (FLA-ST), TLR9 (CpG ODN1668), and TLR4 (LPS) were injected to C57BL/6 mice on 4 consecutive days. The graph shows the number of IRA-B cells retrieved from spleen after 4 days. (means ± SEM, n = 4-5). **(B)** Peritoneal B1a B cells were sorted and placed in culture for 48 h with various TLR ligands. Representative plots show that in medium alone B1a B cells do not give rise to IRA-B cells but in the presence of LPS, Pam3CSK4 and R848 they give rise to IRA-B cells. Representatives of n=3 are shown.

Figure S11. IRA-B cells express and utilize the common □ subunit of the GM-CSF receptor, Csf2R□. (A) Surface expression of Csf2Rβ (CD131) on peritoneal B1a B cells an on other splenic leukocytes in the steady state spleen. Reresentative plots show that B1a B cells express CD131. Representative of n = 3 are shown. **(B)** The role of Csf2Rβ on IRA-B cells. Peritoneal B1a B cells were sorted and placed in culture for 2 days with an antibody against CD131 or with an isotype control. Representative plots show that IRA-B cells do not develop when the receptor is blocked, indicating that IRA-B cells utilize GM-CSF as an autocrine factor. Representatives of n =3 are shown. **(C)** T cells were similarly treated as in panel B. The data show that the antibodies do not kill cells indiscriminately. Representatives of n =3 are shown.

Figure S12. Mixed chimeras have a normal leukocyte profile in the blood, bone marrow and peritoneum. (A) PCR of the csf2 gene (codes for GM-CSF) in wt C57BL/5 mice and in *Csf2*$^{-/-}$ mice. **(B)** PCR on sorted IgM^+ cells and IgM^- cells from mixed chimeric GM/μMT mice and control chimeras wt/μMT. Data show that the chimeric mice lack csf2 in B cells. **(C)** The cell profile in the blood and bone marrow of wild type mice that had been lethally irradiated and reconstituted either with bone marrow from wt and μMT mice (50:50, control) or with bone marrow from *Csf2*$^{-/-}$ and μMT mice (50:50, GM/μMT) 10 weeks earlier. Data show that the leukocyte profile in these mice is normal. **(D)** Mixed chimeric mice contain B1a B cells in their peritoneum. **(E)** IRA-B cells can be detected in the peritoeum, spleen and bone marrow 20 h after CLP. (means ± SEM, n = 4-5).

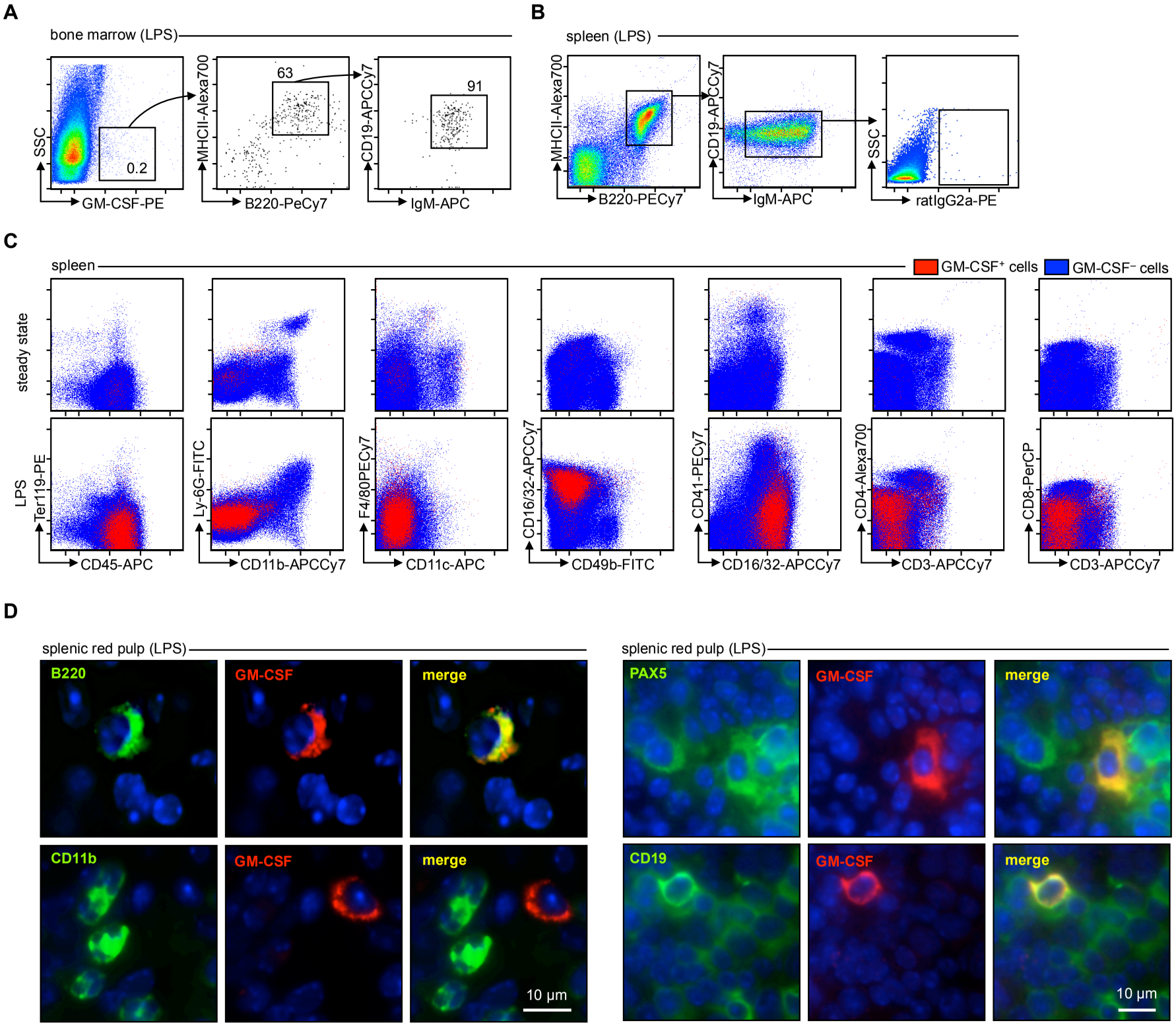
A
bone marrow (LPS)
SSC
GM-CSF-PE
0.2
MHCII-Alexa700
B220-PeCy7
63
CD19-APCCy7
IgM-APC
91
B
spleen (LPS)
MHCII-Alexa700
B220-PECy7
CD19-APCCy7
IgM-APC
SSC
ratIgG2a-PE
C
spleen
GM-CSF+ cells
GM-CSF− cells
steady state
LPS
Ter119-PE
CD45-APC
Ly-6G-FITC
CD11b-APCCy7
F4/80PECy7
CD11c-APC
CD16/32-APCCy7
CD49b-FITC
CD41-PECy7
CD16/32-APCCy7
CD4-Alexa700
CD3-APCCy7
CD8-PerCP
CD3-APCCy7
D
splenic red pulp (LPS)
B220
GM-CSF
merge
CD11b
GM-CSF
merge
10 µm
splenic red pulp (LPS)
PAX5
GM-CSF
merge
CD19
GM-CSF
merge
10 µm

A

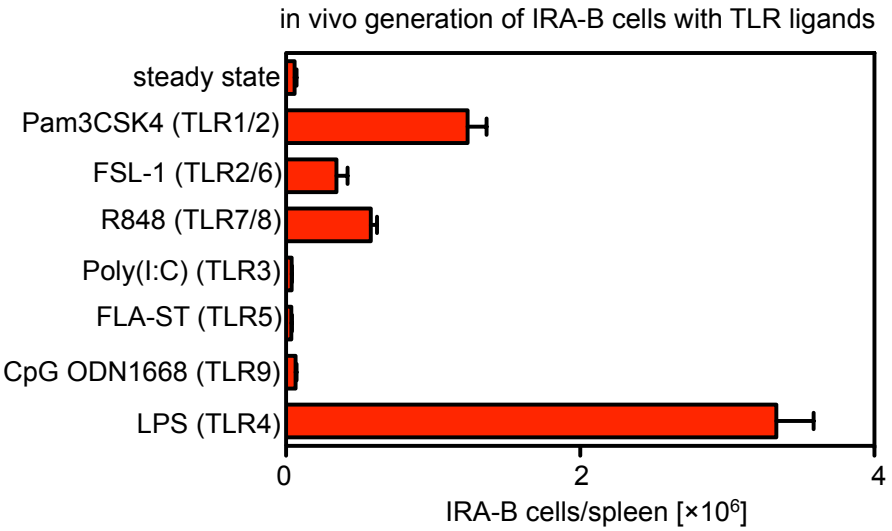
in vivo generation of IRA-B cells with TLR ligands
steady state
Pam3CSK4 (TLR1/2)
FSL-1 (TLR2/6)
R848 (TLR7/8)
Poly(I:C) (TLR3)
FLA-ST (TLR5)
CpG ODN1668 (TLR9)
LPS (TLR4)
0
2
4
IRA-B cells/spleen [×10^6]

B

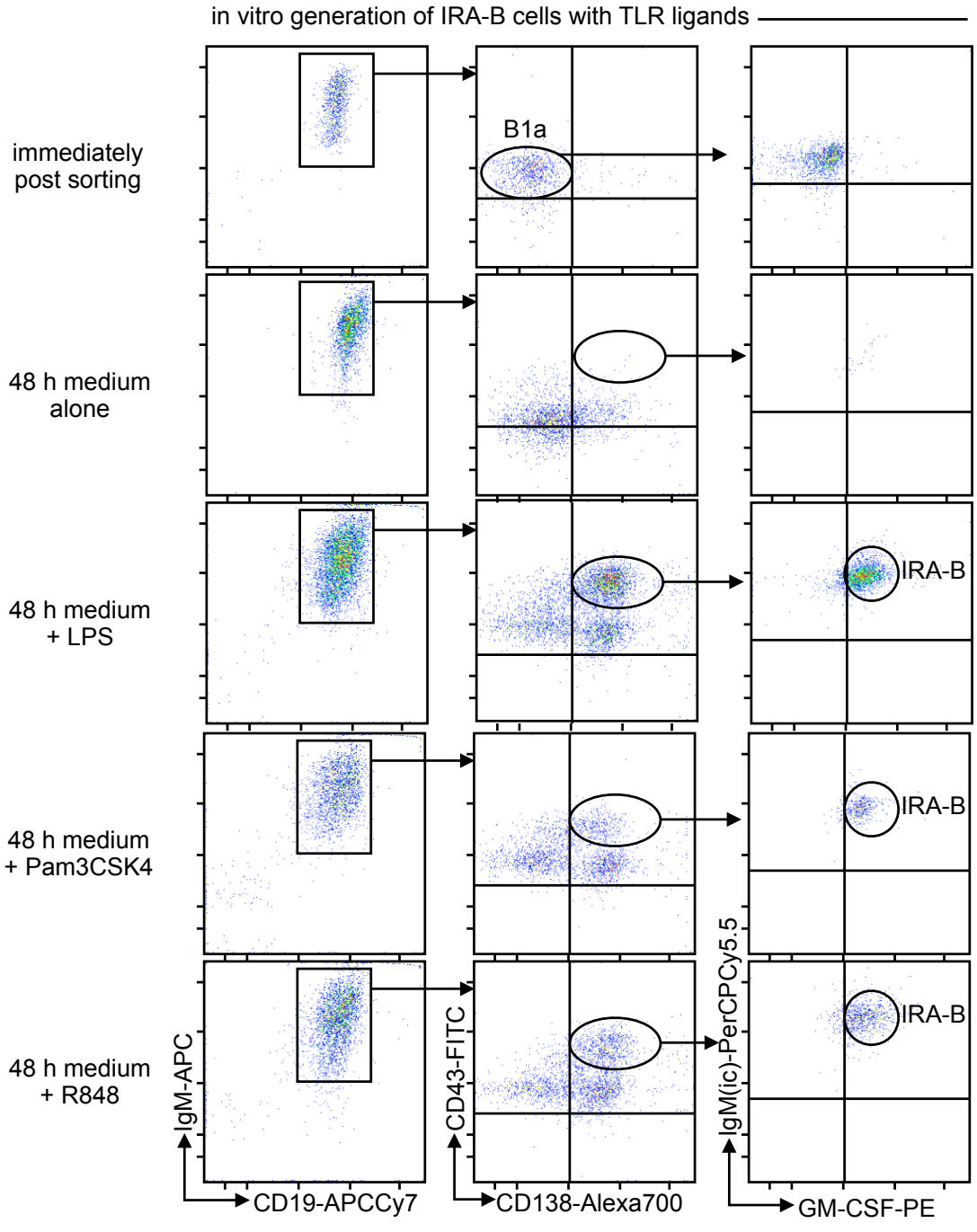
in vitro generation of IRA-B cells with TLR ligands
immediately post sorting
48 h medium alone
48 h medium + LPS
48 h medium + Pam3CSK4
48 h medium + R848
B1a
IRA-B
IgM-APC
CD19-APCCy7
CD43-FITC
CD138-Alexa700
IgM(ic)-PerCPCy5.5
GM-CSF-PE

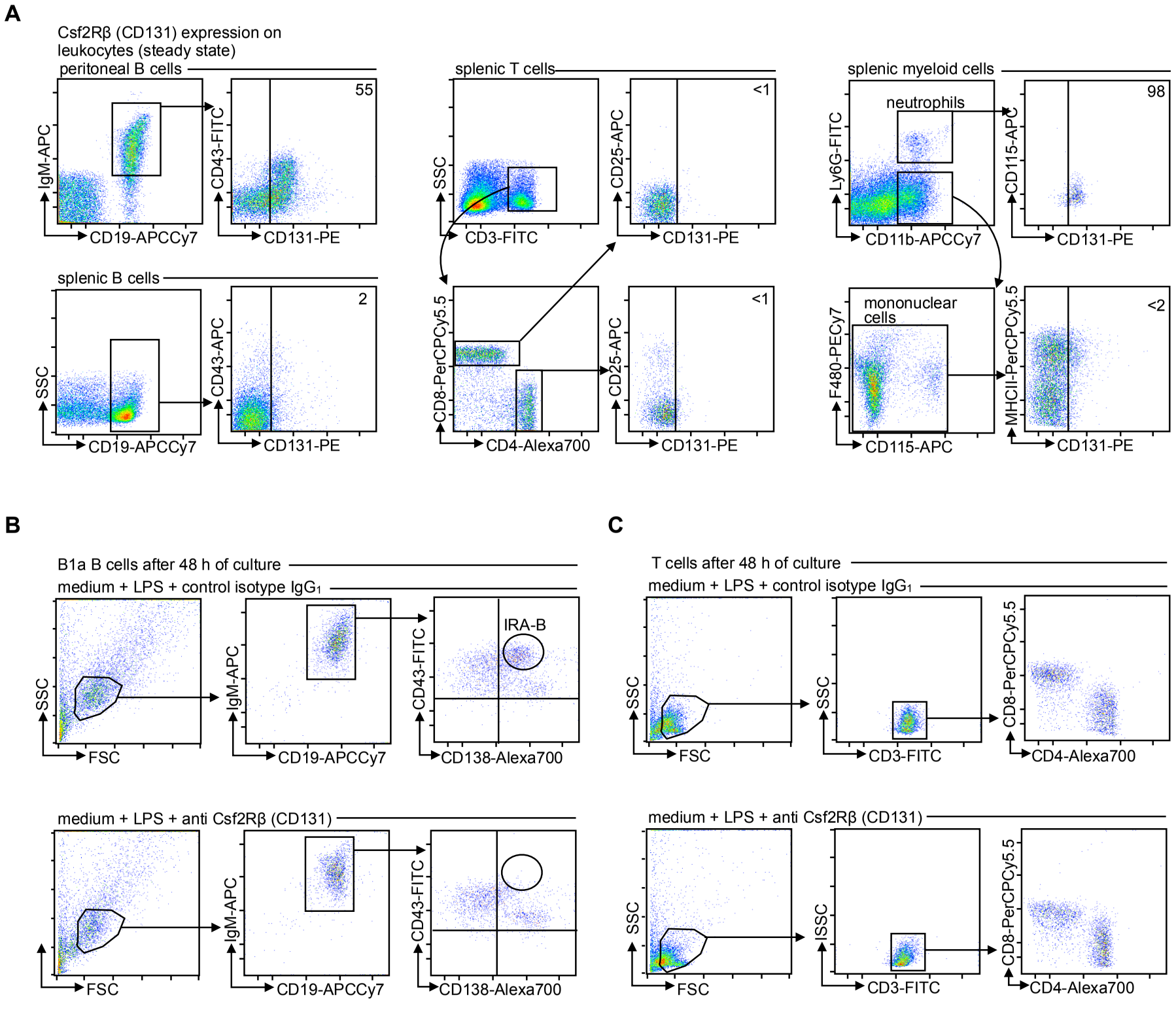
A
Csf2Rβ (CD131) expression on leukocytes (steady state)
peritoneal B cells
IgM-APC
CD19-APCCy7
CD43-FITC
CD131-PE
55
splenic B cells
SSC
CD19-APCCy7
CD43-APC
CD131-PE
2
splenic T cells
SSC
CD3-FITC
CD25-APC
CD131-PE
<1
CD8-PerCPCy5.5
CD4-Alexa700
CD25-APC
CD131-PE
<1
splenic myeloid cells
neutrophils
Ly6G-FITC
CD11b-APCCy7
CD115-APC
CD131-PE
98
mononuclear cells
F480-PECy7
CD115-APC
MHCII-PerCPCy5.5
CD131-PE
<2
B
B1a B cells after 48 h of culture
medium + LPS + control isotype IgG1
SSC
FSC
IgM-APC
CD19-APCCy7
CD43-FITC
CD138-Alexa700
IRA-B
medium + LPS + anti Csf2Rβ (CD131)
FSC
IgM-APC
CD19-APCCy7
CD43-FITC
CD138-Alexa700
C
T cells after 48 h of culture
medium + LPS + control isotype IgG1
SSC
FSC
SSC
CD3-FITC
CD8-PerCPCy5.5
CD4-Alexa700
medium + LPS + anti Csf2Rβ (CD131)
SSC
FSC
ISSC
CD3-FITC
CD8-PerCPCy5.5
CD4-Alexa700

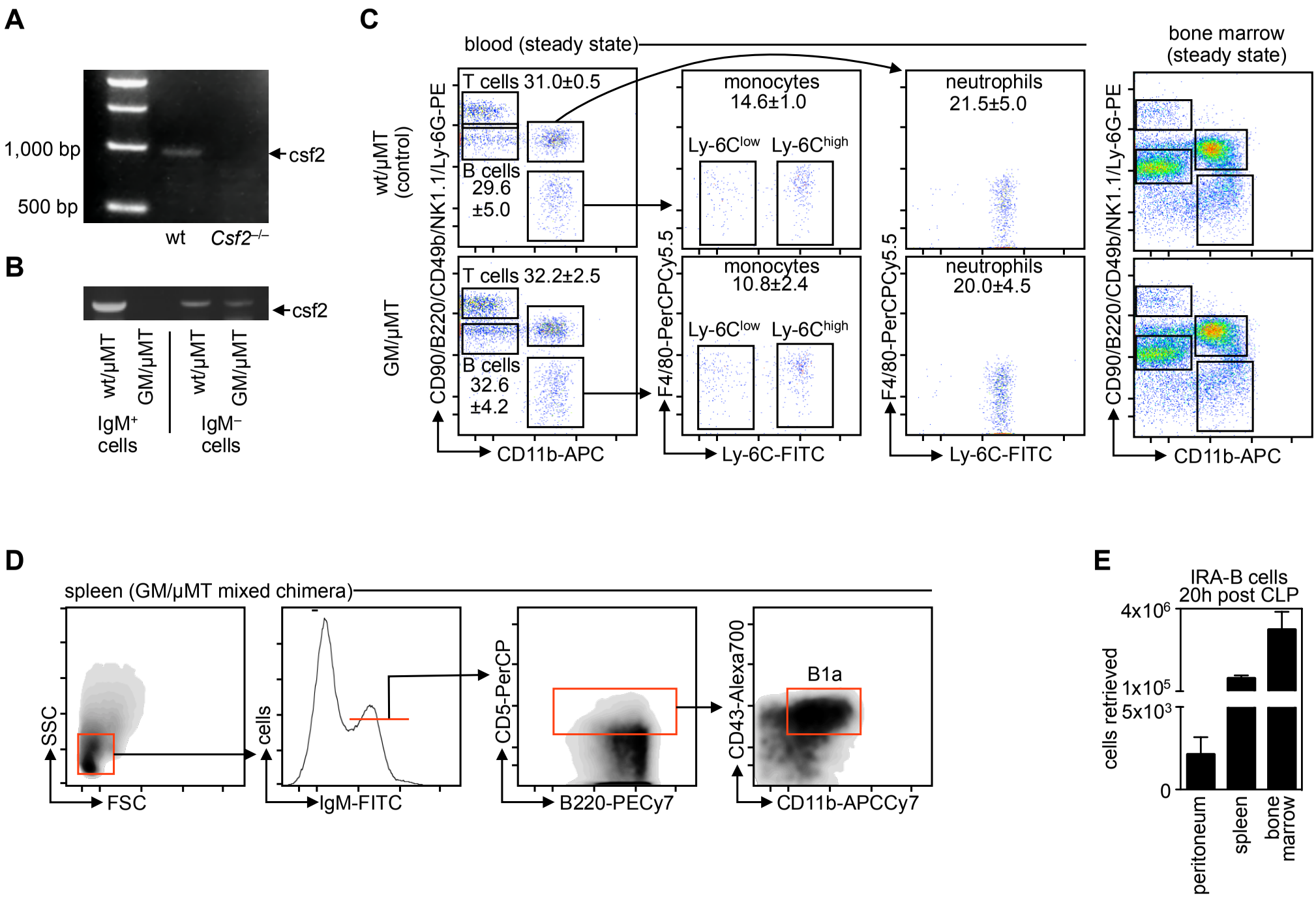
A
1,000 bp
500 bp
csf2
wt
Csf2−/−
B
csf2
wt/µMT
GM/µMT
wt/µMT
GM/µMT
IgM+ cells
IgM− cells
C
blood (steady state)
bone marrow (steady state)
wt/µMT (control)
GM/µMT
T cells 31.0±0.5
B cells 29.6 ±5.0
T cells 32.2±2.5
B cells 32.6 ±4.2
monocytes 14.6±1.0
monocytes 10.8±2.4
neutrophils 21.5±5.0
neutrophils 20.0±4.5
Ly-6Clow
Ly-6Chigh
CD90/B220/CD49b/NK1.1/Ly-6G-PE
F4/80-PerCPCy5.5
Ly-6C-FITC
CD11b-APC
D
spleen (GM/µMT mixed chimera)
SSC
FSC
cells
IgM-FITC
CD5-PerCP
B220-PECy7
CD43-Alexa700
CD11b-APCCy7
B1a
E
IRA-B cells 20h post CLP
cells retrieved
4x10^6
1x10^5
5x10^3
0
peritoneum
spleen
bone marrow

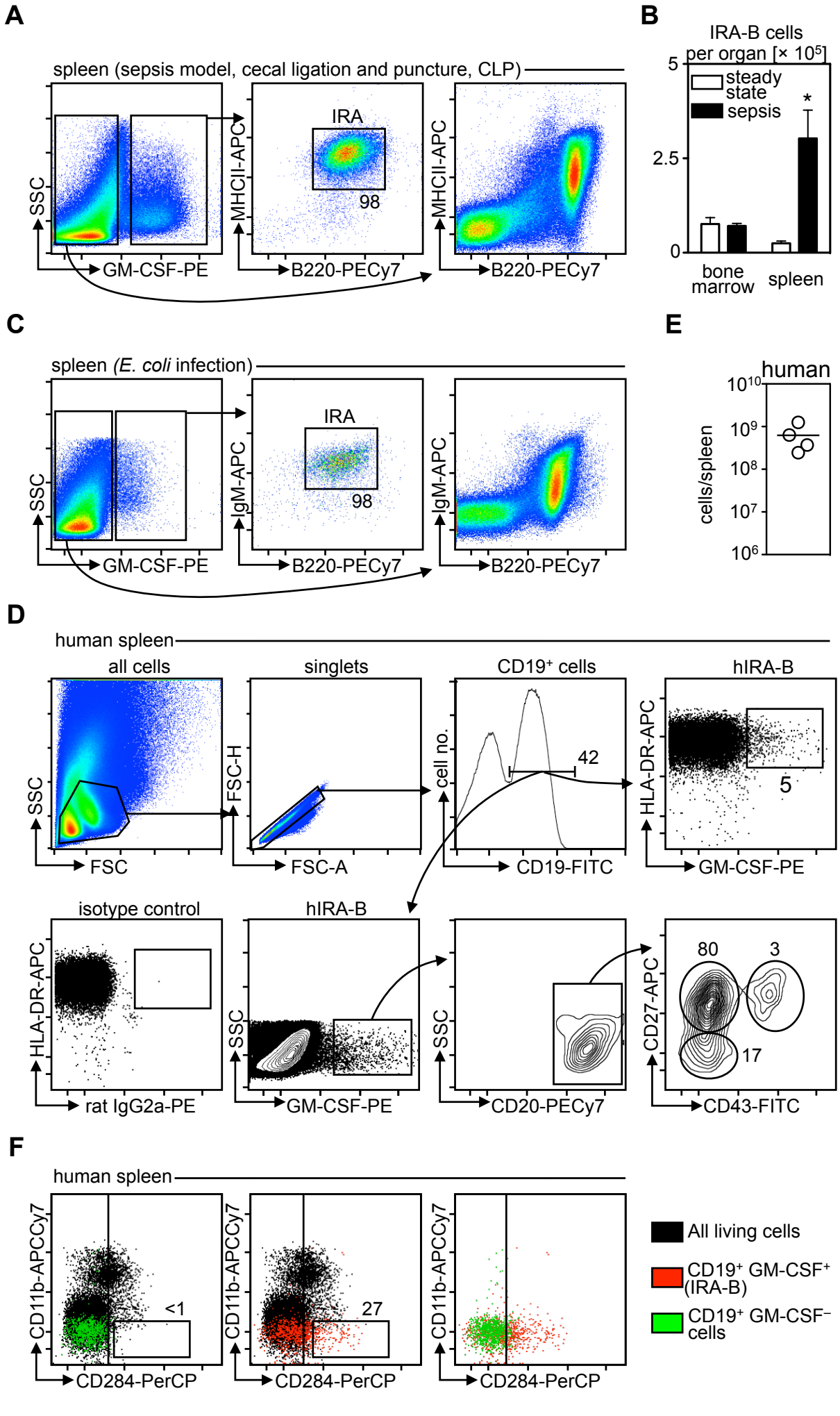
A
spleen (sepsis model, cecal ligation and puncture, CLP)
SSC
GM-CSF-PE
IRA
98
MHCII-APC
B220-PECy7
B
IRA-B cells
per organ [× 10^5]
steady state
sepsis
*
bone marrow
spleen
C
spleen (E. coli infection)
IgM-APC
E
human
cells/spleen
D
human spleen
all cells
singlets
CD19+ cells
hIRA-B
FSC
FSC-A
FSC-H
cell no.
CD19-FITC
42
HLA-DR-APC
5
GM-CSF-PE
isotype control
rat IgG2a-PE
SSC
CD20-PECy7
80
3
17
CD27-APC
CD43-FITC
F
CD11b-APCCy7
CD284-PerCP
<1
27
All living cells
CD19+ GM-CSF+ (IRA-B)
CD19+ GM-CSF− cells

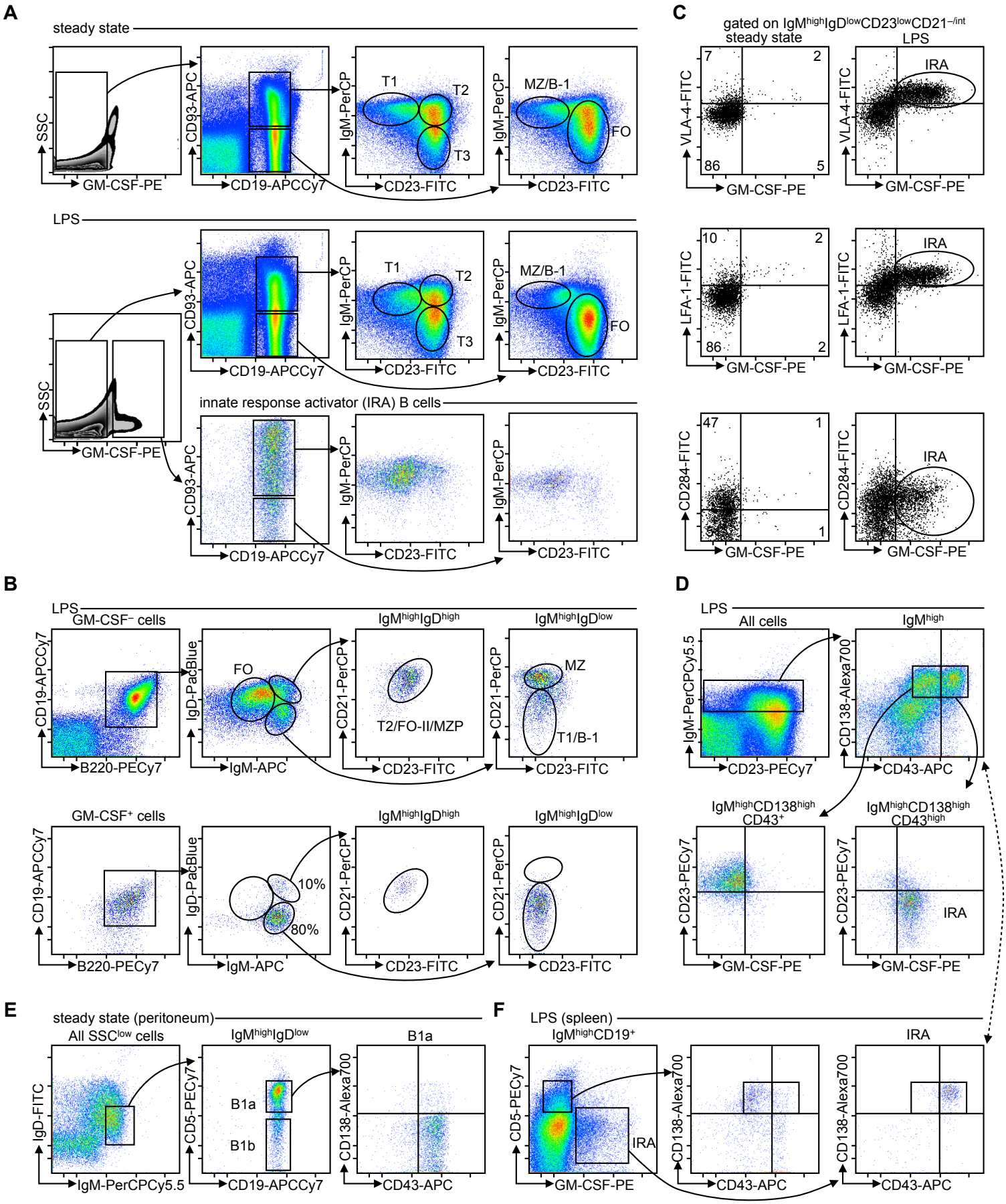
A
steady state
SSC
GM-CSF-PE
CD93-APC
CD19-APCCy7
IgM-PerCP
T1
T2
T3
CD23-FITC
MZ/B-1
FO
LPS
innate response activator (IRA) B cells
C
gated on IgM^high IgD^low CD23^low CD21^−/int
steady state
LPS
IRA
VLA-4-FITC
LFA-1-FITC
CD284-FITC
7
2
86
5
10
47
1
B
GM-CSF⁻ cells
GM-CSF⁺ cells
IgM^high IgD^high
IgM^high IgD^low
CD19-APCCy7
B220-PECy7
IgD-PacBlue
IgM-APC
CD21-PerCP
FO
T2/FO-II/MZP
MZ
T1/B-1
10%
80%
D
All cells
IgM^high
IgM-PerCPCy5.5
CD23-PECy7
CD138-Alexa700
CD43-APC
IgM^high CD138^high CD43⁺
IgM^high CD138^high CD43^high
E
steady state (peritoneum)
All SSC^low cells
IgM^high IgD^low
B1a
IgD-FITC
CD5-PECy7
B1b
F
LPS (spleen)
IgM^high CD19⁺

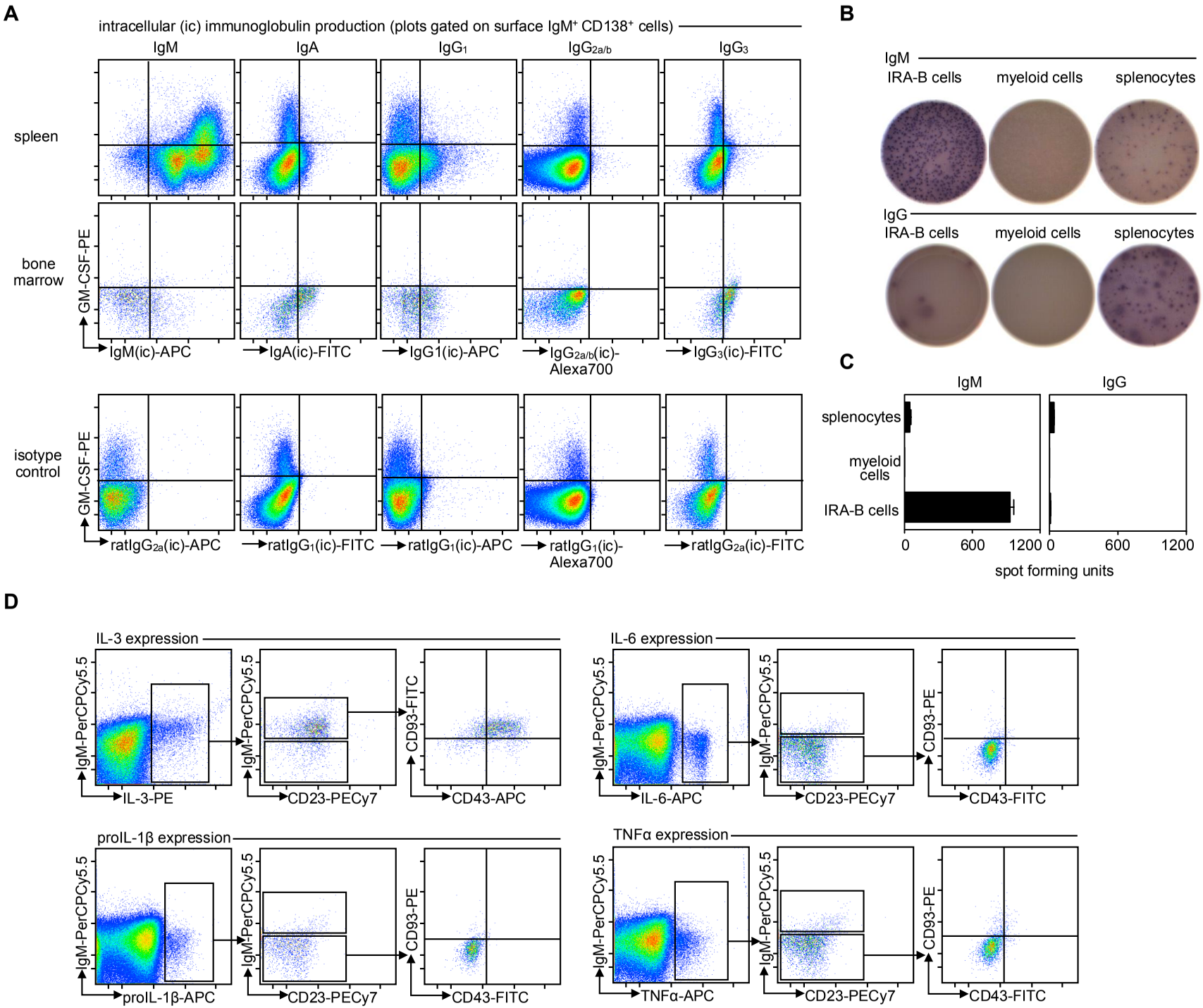
A
intracellular (ic) immunoglobulin production (plots gated on surface IgM+ CD138+ cells)
IgM
IgA
IgG1
IgG2a/b
IgG3
spleen
bone marrow
GM-CSF-PE
IgM(ic)-APC
IgA(ic)-FITC
IgG1(ic)-APC
IgG2a/b(ic)-Alexa700
IgG3(ic)-FITC
isotype control
ratIgG2a(ic)-APC
ratIgG1(ic)-FITC
ratIgG1(ic)-APC
ratIgG1(ic)-Alexa700
ratIgG2a(ic)-FITC
B
IgM
IRA-B cells
myeloid cells
splenocytes
IgG
C
IgM
IgG
splenocytes
myeloid cells
IRA-B cells
0
600
1200
spot forming units
D
IL-3 expression
IgM-PerCPCy5.5
IL-3-PE
CD23-PECy7
CD93-FITC
CD43-APC
IL-6 expression
IL-6-APC
CD93-PE
CD43-FITC
proIL-1β expression
proIL-1β-APC
TNFα expression
TNFα-APC

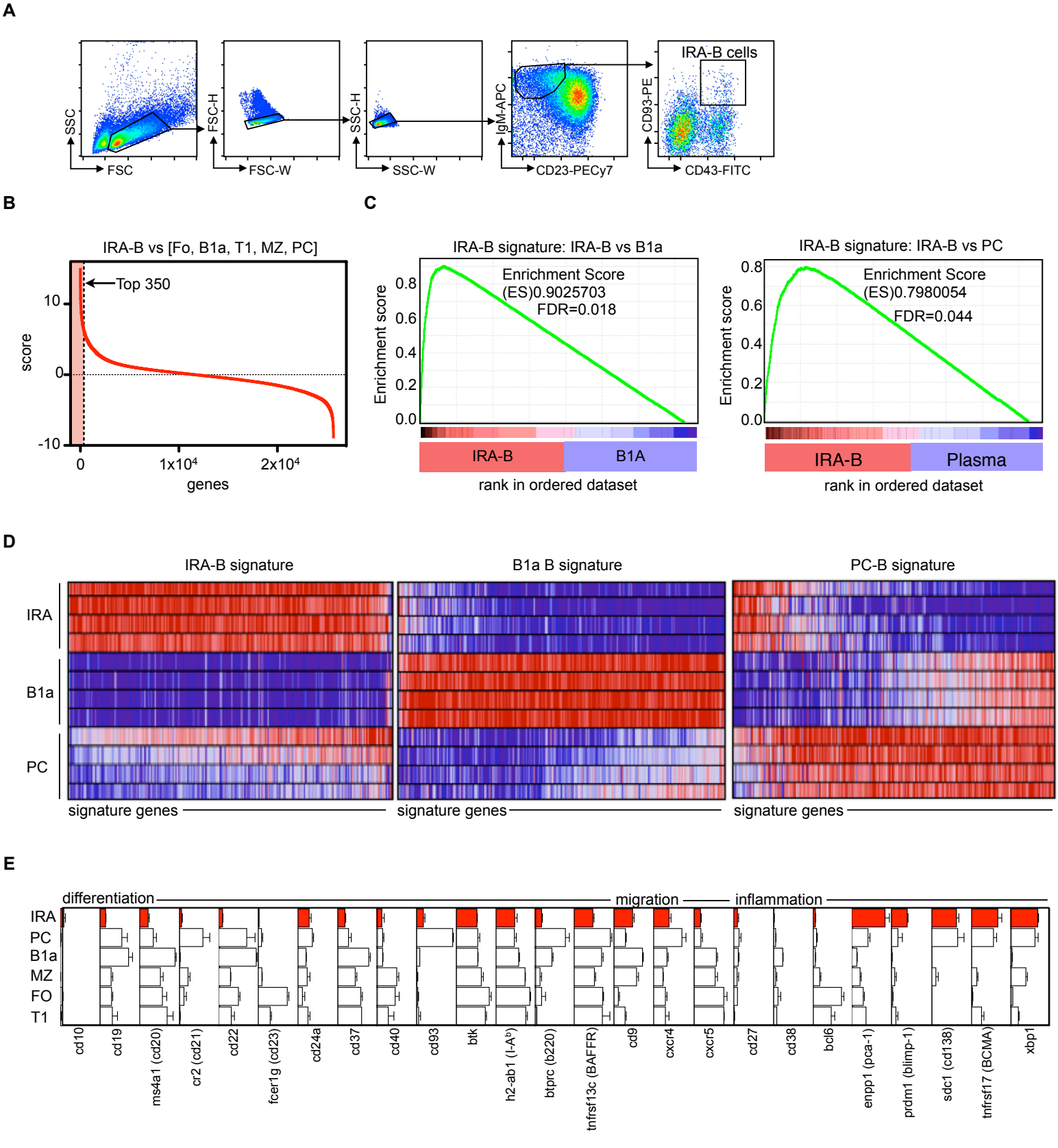
A
SSC
FSC
FSC-H
FSC-W
SSC-H
SSC-W
IgM-APC
CD23-PECy7
IRA-B cells
CD93-PE
CD43-FITC
B
IRA-B vs [Fo, B1a, T1, MZ, PC]
Top 350
score
10
0
-10
0
1x10⁴
2x10⁴
genes
C
IRA-B signature: IRA-B vs B1a
Enrichment score
Enrichment Score
(ES)0.9025703
FDR=0.018
0.8
0.6
0.4
0.2
0.0
IRA-B
B1A
rank in ordered dataset
IRA-B signature: IRA-B vs PC
Enrichment score
Enrichment Score
(ES)0.7980054
FDR=0.044
0.8
0.6
0.4
0.2
0.0
IRA-B
Plasma
rank in ordered dataset
D
IRA-B signature
B1a B signature
PC-B signature
IRA
B1a
PC
signature genes
signature genes
signature genes
E
differentiation
migration
inflammation
IRA
PC
B1a
MZ
FO
T1
cd10
cd19
ms4a1 (cd20)
cr2 (cd21)
cd22
fcer1g (cd23)
cd24a
cd37
cd40
cd93
btk
h2-ab1 (I-Aᵇ)
btprc (b220)
tnfrsf13c (BAFFR)
cd9
cxcr4
cxcr5
cd27
cd38
bcl6
enpp1 (pca-1)
prdm1 (blimp-1)
sdc1 (cd138)
tnfrsf17 (BCMA)
xbp1

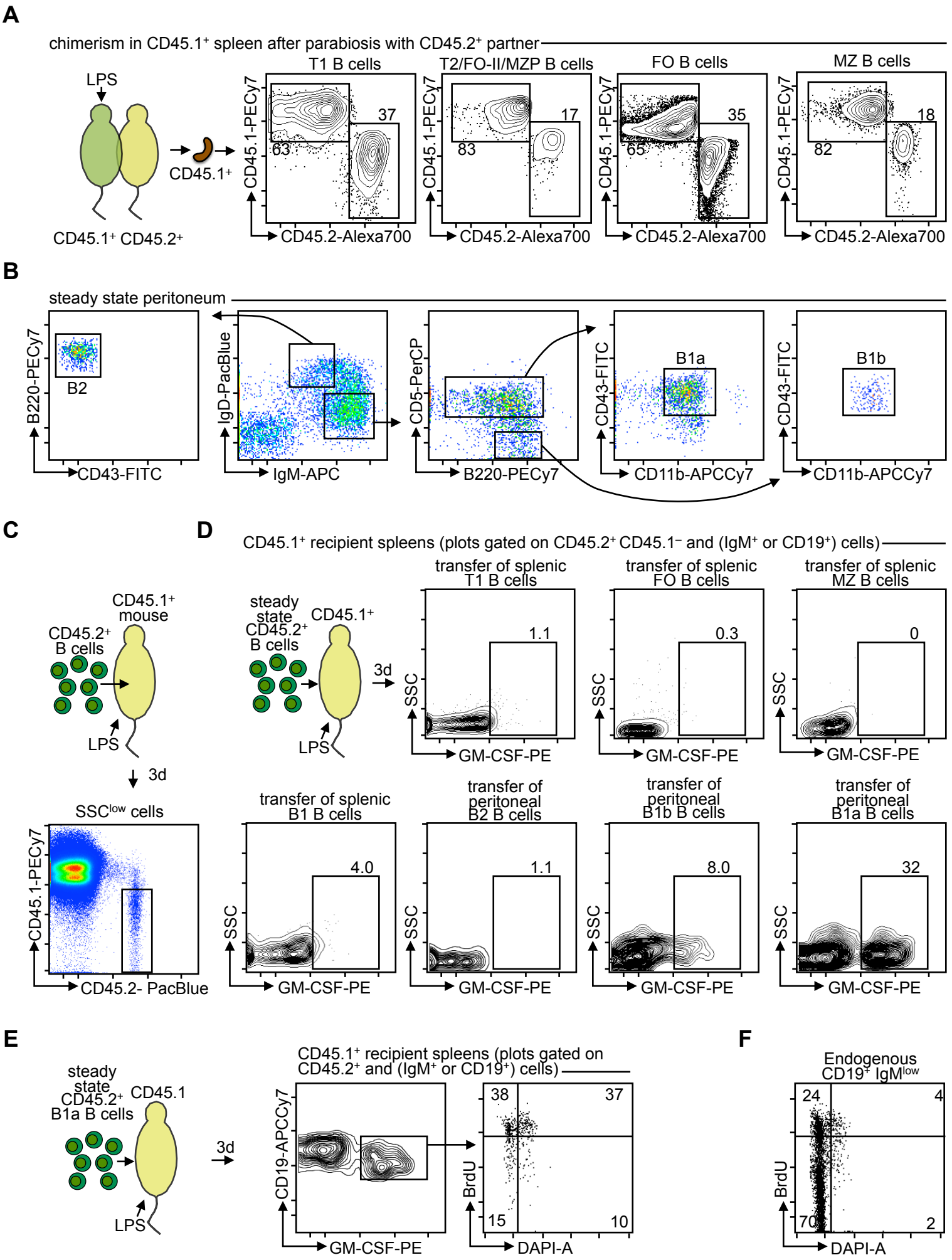
A
chimerism in CD45.1+ spleen after parabiosis with CD45.2+ partner
LPS
CD45.1+
CD45.1+ CD45.2+
T1 B cells
T2/FO-II/MZP B cells
FO B cells
MZ B cells
CD45.1-PECy7
CD45.2-Alexa700
37
63
17
83
35
65
18
82
B
steady state peritoneum
B220-PECy7
B2
CD43-FITC
IgD-PacBlue
IgM-APC
CD5-PerCP
B220-PECy7
B1a
CD11b-APCCy7
B1b
C
CD45.1+ mouse
CD45.2+ B cells
LPS
3d
SSClow cells
CD45.1-PECy7
CD45.2- PacBlue
D
CD45.1+ recipient spleens (plots gated on CD45.2+ CD45.1− and (IgM+ or CD19+) cells)
steady state CD45.1+ CD45.2+ B cells
transfer of splenic T1 B cells
transfer of splenic FO B cells
transfer of splenic MZ B cells
1.1
0.3
0
SSC
GM-CSF-PE
transfer of splenic B1 B cells
transfer of peritoneal B2 B cells
transfer of peritoneal B1b B cells
transfer of peritoneal B1a B cells
4.0
1.1
8.0
32
E
steady state CD45.2+ B1a B cells
CD45.1
LPS
3d
CD45.1+ recipient spleens (plots gated on CD45.2+ and (IgM+ or CD19+) cells)
CD19-APCCy7
GM-CSF-PE
BrdU
DAPI-A
38
37
15
10
F
Endogenous CD19+ IgMlow
24
4
70
2

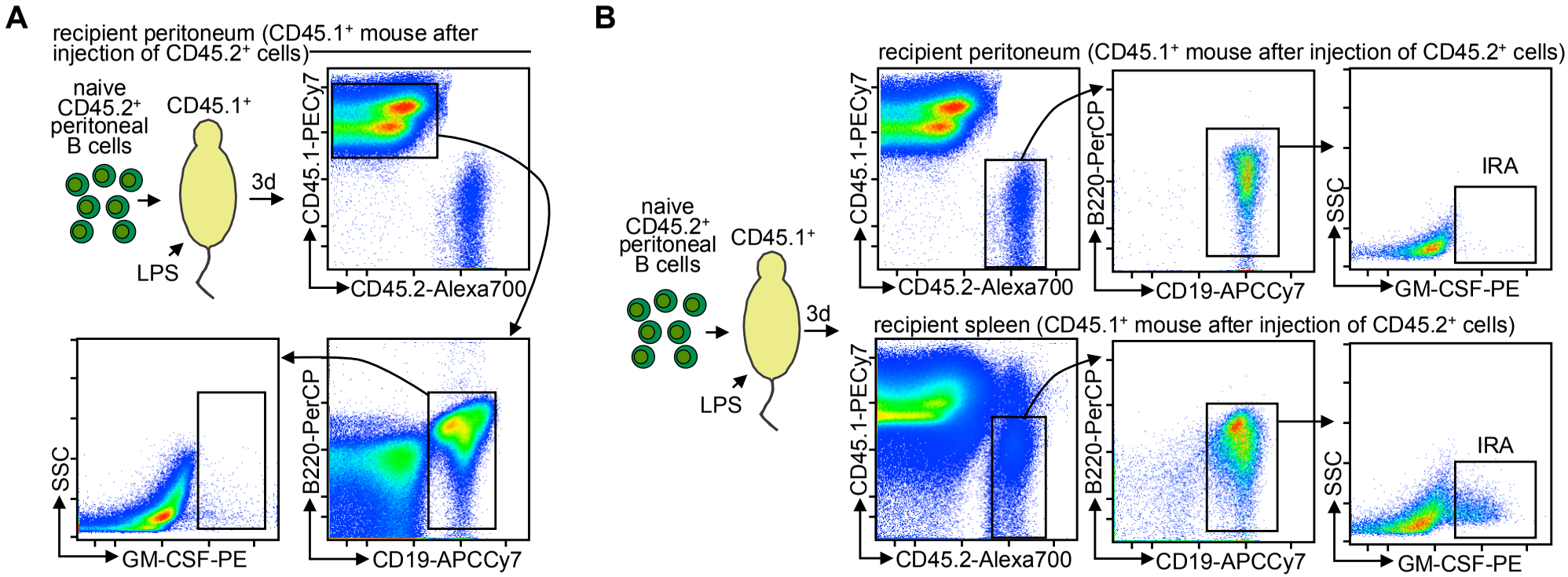
A
recipient peritoneum (CD45.1+ mouse after injection of CD45.2+ cells)
naive CD45.2+ peritoneal B cells
CD45.1+
3d
LPS
CD45.1-PECy7
CD45.2-Alexa700
SSC
GM-CSF-PE
B220-PerCP
CD19-APCCy7
B
recipient peritoneum (CD45.1+ mouse after injection of CD45.2+ cells)
naive CD45.2+ peritoneal B cells
CD45.1+
3d
LPS
CD45.1-PECy7
CD45.2-Alexa700
B220-PerCP
CD19-APCCy7
SSC
IRA
GM-CSF-PE
recipient spleen (CD45.1+ mouse after injection of CD45.2+ cells)
CD45.1-PECy7
CD45.2-Alexa700
B220-PerCP
CD19-APCCy7
SSC
IRA
GM-CSF-PE

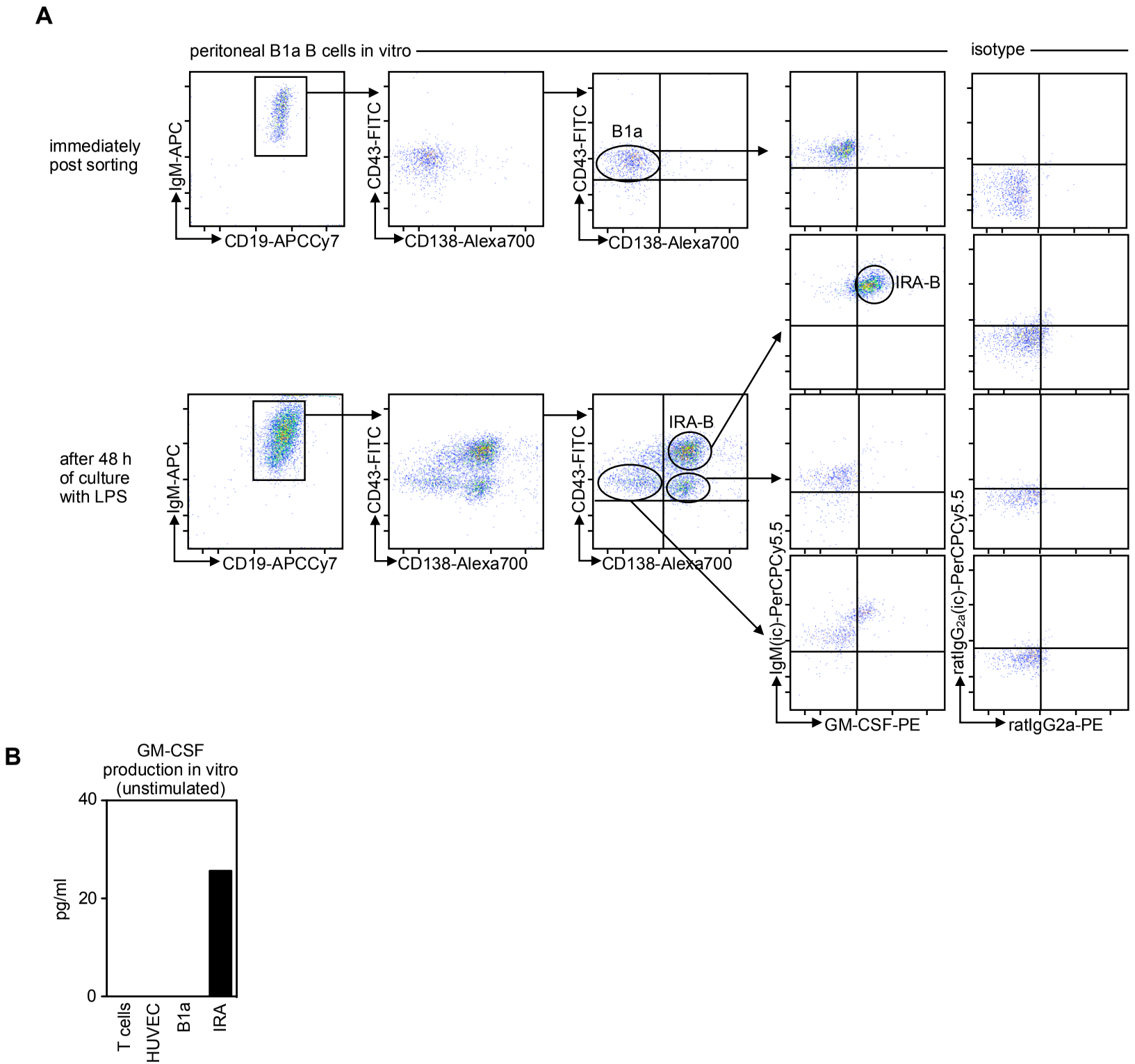
A
peritoneal B1a B cells in vitro
isotype
immediately post sorting
after 48 h of culture with LPS
IgM-APC
CD19-APCCy7
CD43-FITC
CD138-Alexa700
B1a
IRA-B
IgM(ic)-PerCPCy5.5
ratIgG2a(ic)-PerCPCy5.5
GM-CSF-PE
ratIgG2a-PE
B
GM-CSF production in vitro (unstimulated)
pg/ml
40
20
0
T cells
HUVEC
B1a
IRA

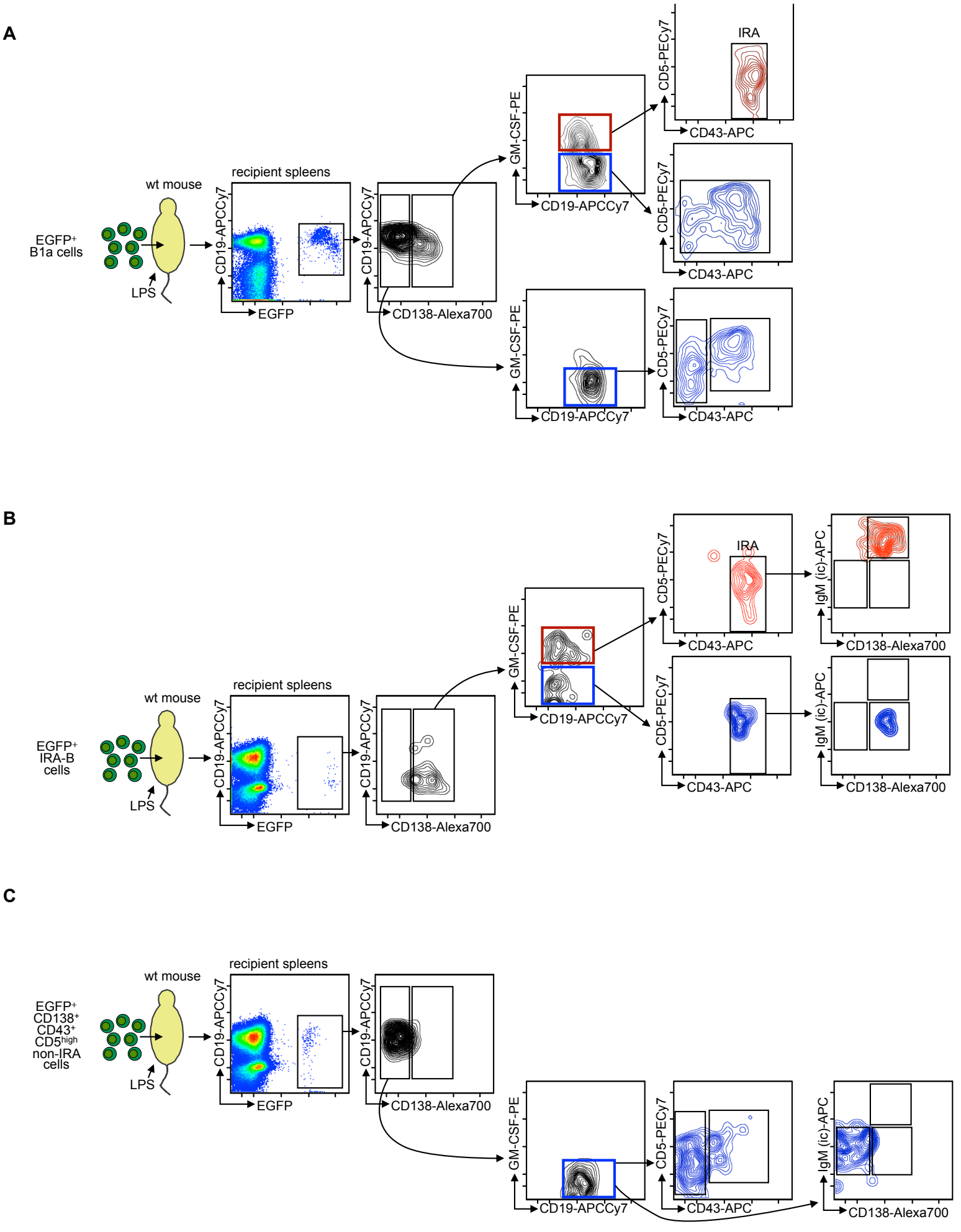
A
EGFP+
B1a cells
wt mouse
LPS
recipient spleens
CD19-APCCy7
EGFP
CD138-Alexa700
GM-CSF-PE
CD5-PECy7
CD43-APC
IRA
B
EGFP+
IRA-B
cells
IgM (ic)-APC
C
EGFP+
CD138+
CD43+
CD5high
non-IRA
cells

Table 1- The IRA-B cell transcriptome signature

The values show the 350 genes that are expressed at levels higher than other B cells

	ID	Gene Name	Score	FDR
1	ILMN_1239397	LOC1000479	15.1042382	0.07143651
2	ILMN_1232184	GGCX	14.12256402	0.07143651
3	ILMN_2854962	SGOL1	13.79331562	0.07143651
4	ILMN_2888552	SLC1A4	13.60149638	0.07143651
5	ILMN_1237518	DGKG	13.49869288	0.07143651
6	ILMN_2949021	AADACL1	13.41660506	0.07143651
7	ILMN_1258376	KCNK6	13.37436313	0.07143651
8	ILMN_2645090	ST7L	13.12264757	0.07143651
9	ILMN_2755973	POMT2	12.54304963	0.07143651
10	ILMN_2999818	1700019H03	12.52987856	0.07143651
11	ILMN_2931095	IGF2R	12.28876404	0.07143651
12	ILMN_2508745	ZFYVE21	12.23740623	0.07143651
13	ILMN_3117650	NT5DC3	12.01630748	0.07143651
14	ILMN_3162476	SEC61A1	11.89479458	0.07143651
15	ILMN_2648618	ARFGAP3	11.73449444	0.07143651
16	ILMN_1221067	NME1	11.55332109	0.07143651
17	ILMN_2949266	RPN2	11.5164747	0.07143651
18	ILMN_2731974	FOXM1	11.38635825	0.07143651
19	ILMN_1233076	PRKCSH	11.38087235	0.07143651
20	ILMN_1216388	UBA5	11.35286378	0.07143651
21	ILMN_2596970	TMEM39A	11.24170366	0.07143651
22	ILMN_1233455	OLFML3	11.15664327	0.07143651
23	ILMN_1230444	TXNDC11	11.01441828	0.07143651
24	ILMN_2833596	ABCB6	10.97036286	0.07143651
25	ILMN_3139405	HBS1L	10.92280229	0.07143651
26	ILMN_2752618	SLC35E1	10.85698656	0.07143651
27	ILMN_2805339	HSPB6	10.84806924	0.07143651
28	ILMN_2825109	ZFP330	10.80757646	0.07143651
29	ILMN_2742667	C1GALT1	10.77027615	0.07143651
30	ILMN_2667971	CUGBP1	10.58744075	0.07143651
31	ILMN_3111298	MCFD2	10.57652659	0.07143651
32	ILMN_2667972	CUGBP1	10.57298931	0.07143651
33	ILMN_2661107	ATL2	10.55134819	0.07143651
34	ILMN_2604643	TBL2	10.49761403	0.07143651
35	ILMN_3161906	EG432879	10.49026292	0.07143651
36	ILMN_2440803	SND1	10.4516721	0.07143651
37	ILMN_1256875	TICAM1	10.36523773	0.07143651
38	ILMN_1248860	DPM3	10.35471939	0.07143651
39	ILMN_2432508	SLC39A13	10.20140735	0.07143651

40	ILMN_2435079	ZMPSTE24	10.18611319	0.07143651
41	ILMN_2652971	DEB1	10.13209147	0.07143651
42	ILMN_1246201	CACNA1H	10.08805521	0.07143651
43	ILMN_2603781	D17WSU104	10.04467729	0.07143651
44	ILMN_2884610	PPAPDC1B	10.03013298	0.07143651
45	ILMN_2699624	2310008H09	9.953125955	0.07143651
46	ILMN_1213725	NUDT5	9.934721327	0.07143651
47	ILMN_3114998	BC043301	9.931413428	0.07143651
48	ILMN_2891573	RAI12	9.910132705	0.07143651
49	ILMN_2759770	NPLOC4	9.813950637	0.07143651
50	ILMN_2610234	IL15	9.779250872	0.07143651
51	ILMN_3142273	VKORC1L1	9.719216971	0.07143651
52	ILMN_2730714	TMBIM4	9.678559796	0.07143651
53	ILMN_2792268	TIRAP	9.656299965	0.07143651
54	ILMN_1228783	LOC1000439	9.648897385	0.07143651
55	ILMN_1254437	SLC31A1	9.647217566	0.07143651
56	ILMN_1241035	2010311D03	9.625051199	0.07143651
57	ILMN_2607786	FADS1	9.609926364	0.07143651
58	ILMN_2611874	PTPLAD1	9.565215688	0.07143651
59	ILMN_1239314	FOXM1	9.554797496	0.07143651
60	ILMN_1255416	LY6A	9.474051526	0.07143651
61	ILMN_1237963	ALG8	9.451940977	0.07143651
62	ILMN_2593774	1190002H23	9.436077317	0.07143651
63	ILMN_1246694	DUS1L	9.348603493	0.07143651
64	ILMN_2627217	PI4K2B	9.322270466	0.07143651
65	ILMN_2713471	METTL9	9.305137346	0.07143651
66	ILMN_1244768	SRPRB	9.303263757	0.07143651
67	ILMN_1245789	CCNE2	9.261683005	0.07143651
68	ILMN_1237197	NRP1	9.253577341	0.07143651
69	ILMN_1249301	BCKDK	9.251641186	0.07143651
70	ILMN_2664628	DAD1	9.221609388	0.07143651
71	ILMN_1222602	2410014A08	9.199288248	0.07143651
72	ILMN_1259488	MGEA6	9.163693522	0.07143651
73	ILMN_2711948	LOC1000476	9.134715119	0.07143651
74	ILMN_1215493	COPS4	9.003816509	0.07143651
75	ILMN_2491301	USP16	8.995139234	0.07143651
76	ILMN_2795792	TMEM38B	8.99511225	0.07143651
77	ILMN_2922942	3000004C01	8.967053197	0.07143651
78	ILMN_2698430	BCL2L1	8.96478306	0.07143651
79	ILMN_1216213	INCENP	8.929259783	0.07143651
80	ILMN_2677595	NCAPG2	8.878209823	0.07143651
81	ILMN_2833985	RILPL2	8.857907148	0.07143651
82	ILMN_3104928	CENPM	8.857006332	0.07143651

83	ILMN_2686132	ADA	8.856865987	0.07143651
84	ILMN_2914010	DMWD	8.855076718	0.08935787
85	ILMN_1250947	TXNDC5	8.837336875	0.07143651
86	ILMN_2694917	SAP30	8.830597778	0.07143651
87	ILMN_2733472	CENPM	8.818169058	0.07143651
88	ILMN_3078327	BCL2L11	8.793691838	0.07143651
89	ILMN_2747641	KIF4	8.785605681	0.07143651
90	ILMN_2685133	1700034H14	8.745253558	0.07143651
91	ILMN_1255513	CDR2	8.741295943	0.07143651
92	ILMN_1214811	PSEN1	8.726757512	0.07143651
93	ILMN_2657844	CDC2A	8.716281491	0.07143651
94	ILMN_2512043	LOC1000470	8.713301866	0.07143651
95	ILMN_2910106	ALG3	8.713214551	0.08935787
96	ILMN_1237761	STRA13	8.708797421	0.07143651
97	ILMN_1245467	CCDC127	8.695858987	0.07143651
98	ILMN_2732877	1700034H14	8.695581201	0.07143651
99	ILMN_2630641	SRM	8.656788285	0.07143651
100	ILMN_2512216	TUBGCP2	8.650186012	0.07143651
101	ILMN_2819951	LRP12	8.623508129	0.07143651
102	ILMN_2765407	LUC7L2	8.623282969	0.07143651
103	ILMN_3155342	RAB43	8.616345382	0.07143651
104	ILMN_2658878	TG	8.5770917	0.07143651
105	ILMN_3163029	VKORC1L1	8.567197534	0.07143651
106	ILMN_1216285	CREB3	8.566184658	0.07143651
107	ILMN_2669172	4930547N16	8.550132383	0.07143651
108	ILMN_1247156	APOA2	8.531452532	0.08935787
109	ILMN_2838645	SSR3	8.530194699	0.07143651
110	ILMN_2868987	SMPD1	8.520695969	0.07143651
111	ILMN_2795359	HDLBP	8.493511141	0.07143651
112	ILMN_2902228	CORO2B	8.472037855	0.07143651
113	ILMN_2702233	CCNG1	8.44048799	0.07143651
114	ILMN_2717569	UFSP2	8.425006084	0.07143651
115	ILMN_2596230	2410014A08	8.413551136	0.07143651
116	ILMN_2592093	IFT20	8.390060659	0.07143651
117	ILMN_1223624	HRAS1	8.388244892	0.07143651
118	ILMN_1224651	2810405J04F	8.376138958	0.07143651
119	ILMN_2595597	ANLN	8.364359345	0.07143651
120	ILMN_1234641	6720463M24	8.360777564	0.07143651
121	ILMN_2656871	TMEM97	8.355906203	0.07143651
122	ILMN_1246495	TMEM9B	8.349016554	0.07143651
123	ILMN_2962606	PSMA5	8.345025198	0.07143651
124	ILMN_2791121	AK3	8.329414407	0.07143651
125	ILMN_2885293	2310016E02I	8.324815222	0.07143651

126	ILMN_2870443	FPGS	8.319250574	0.07143651
127	ILMN_2605694	KRTCAP2	8.291941428	0.07143651
128	ILMN_1256334	ATP6V0A1	8.287282392	0.07143651
129	ILMN_2619491	ARFIP2	8.263577151	0.07143651
130	ILMN_2682970	BC030307	8.242088388	0.08935787
131	ILMN_3153207	LAMP2	8.239983917	0.07143651
132	ILMN_1233857	MCM6	8.224971025	0.07143651
133	ILMN_2639809	NUCB1	8.219021326	0.07143651
134	ILMN_2767187	MRPL53	8.21791799	0.07143651
135	ILMN_1259198	GLT8D1	8.210413186	0.07143651
136	ILMN_3030148	DNAJC19	8.199140221	0.07143651
137	ILMN_2797642	NCAPH	8.197512824	0.07143651
138	ILMN_2859978	PAPSS1	8.197100845	0.07143651
139	ILMN_2689731	DUSP4	8.181407446	0.07143651
140	ILMN_2681057	PHCA	8.180835117	0.07143651
141	ILMN_2668706	SLC39A11	8.165693004	0.07143651
142	ILMN_2732896	OGFOD2	8.143822548	0.07143651
143	ILMN_2484707	TYMS	8.130620114	0.07143651
144	ILMN_1260378	CSRP1	8.119428944	0.07143651
145	ILMN_1243030	ZFAND6	8.114841516	0.07143651
146	ILMN_2978533	TRABD	8.095453504	0.07143651
147	ILMN_2598374	CCDC92	8.065544696	0.07143651
148	ILMN_2949632	PSMB2	8.064680941	0.07143651
149	ILMN_1224678	GLT8D1	8.041390119	0.07143651
150	ILMN_1245425	ATP2A2	8.039715005	0.07143651
151	ILMN_2972755	CPOX	8.027318123	0.08935787
152	ILMN_1223029	RAB8B	8.024697274	0.07143651
153	ILMN_1252437	4933407N01	7.945202721	0.07143651
154	ILMN_2653735	4933407N01	7.943409753	0.07143651
155	ILMN_2597923	PRDM1	7.94097703	0.08935787
156	ILMN_1221936	COX19	7.928741559	0.07143651
157	ILMN_2968907	TIPIN	7.921998896	0.07143651
158	ILMN_2761472	LRPAP1	7.904235476	0.07143651
159	ILMN_2789321	RC3H1	7.882440837	0.07143651
160	ILMN_2812935	ATP6V1H	7.870595992	0.07143651
161	ILMN_2617425	CLPTM1	7.86508833	0.07143651
162	ILMN_2715661	PEX11C	7.859498128	0.08935787
163	ILMN_2757125	PRC1	7.851750998	0.07143651
164	ILMN_1235363	GSG2	7.849969693	0.07143651
165	ILMN_2600339	GOSR2	7.844179405	0.07143651
166	ILMN_2845272	KLHDC2	7.818997269	0.07143651
167	ILMN_2976601	TFG	7.818006607	0.07143651
168	ILMN_1228328	POU2AF1	7.813825315	0.07143651

169	ILMN_1213958	SEC23A	7.813380212	0.07143651
170	ILMN_3147112	MAPK6	7.8011704	0.07143651
171	ILMN_2626389	NOMO1	7.7889212	0.07143651
172	ILMN_2641111	DPAGT1	7.775550563	0.10798193
173	ILMN_2617228	AURKA	7.77512495	0.08935787
174	ILMN_1225520	2310008H09	7.768648163	0.07143651
175	ILMN_2986393	TUBA1B	7.72750211	0.10798193
176	ILMN_3125363	FXN	7.723836199	0.07143651
177	ILMN_2594477	PAPSS1	7.723712517	0.07143651
178	ILMN_2929896	PBK	7.71124409	0.08935787
179	ILMN_2883907	LSM8	7.704075785	0.07143651
180	ILMN_2493067	ZRANB3	7.690784872	0.07143651
181	ILMN_2631813	GEMIN6	7.686761023	0.07143651
182	ILMN_2692124	ATP5G3	7.673501849	0.07143651
183	ILMN_2643455	TRABD	7.669791947	0.07143651
184	ILMN_2705166	ST6GAL1	7.664915198	0.07143651
185	ILMN_2417316	LOC1000443	7.662722429	0.07143651
186	ILMN_1258732	CRYBA4	7.629837442	0.07143651
187	ILMN_2998020	SPCS1	7.601467066	0.08935787
188	ILMN_2632712	BIRC5	7.596870632	0.07143651
189	ILMN_2634169	CLDN19	7.570423758	0.07143651
190	ILMN_1220943	NUP37	7.549160223	0.07143651
191	ILMN_1247682	ATP6V0A1	7.547524405	0.07143651
192	ILMN_3132223	C630004H02	7.545282807	0.07143651
193	ILMN_1242013	UCK2	7.5435587	0.07143651
194	ILMN_2876629	LOC654426	7.521299529	0.07143651
195	ILMN_1229964	GSTZ1	7.512986407	0.07143651
196	ILMN_2791578	GSPT1	7.511771755	0.07143651
197	ILMN_1260175	GOLGA3	7.498958703	0.08935787
198	ILMN_2803334	ALG2	7.47742941	0.07143651
199	ILMN_2637845	DHDDS	7.466634506	0.08935787
200	ILMN_2943849	ZBTB45	7.458974703	0.07143651
201	ILMN_1254734	MRPS12	7.457370831	0.07143651
202	ILMN_2651389	BHLHB8	7.446018662	0.08935787
203	ILMN_1242233	NDUFB6	7.430623368	0.07143651
204	ILMN_2723058	PLOD3	7.401713134	0.08935787
205	ILMN_2649172	ZCCHC18	7.400532358	0.07143651
206	ILMN_2962632	ATP5J	7.395572399	0.07143651
207	ILMN_2780915	PRMT7	7.388327394	0.07143651
208	ILMN_1213855	EXTL2	7.382194638	0.07143651
209	ILMN_2883414	CENPL	7.340750152	0.07143651
210	ILMN_2653619	CTAGE5	7.333379004	0.07143651
211	ILMN_2757445	CCDC41	7.327681993	0.07143651

212	ILMN_2751054	ATF2	7.326952401	0.07143651
213	ILMN_2687908	ALG9	7.31982267	0.07143651
214	ILMN_2821092	STX5A	7.319014469	0.07143651
215	ILMN_2731989	EXT1	7.319007853	0.07143651
216	ILMN_2660414	ALG5	7.310254713	0.07143651
217	ILMN_1227723	NUDT22	7.305443557	0.08935787
218	ILMN_3151503	C130032J12F	7.300270724	0.07143651
219	ILMN_2636685	MCPH1	7.29966902	0.10798193
220	ILMN_1215469	DBI	7.290238061	0.07143651
221	ILMN_2741726	LSM2	7.290183801	0.07143651
222	ILMN_1213914	ATP5J2	7.283179736	0.07143651
223	ILMN_2715546	GPX3	7.281135069	0.07143651
224	ILMN_2732419	METTL1	7.272055466	0.07143651
225	ILMN_1238497	CLIP1	7.263718669	0.07143651
226	ILMN_1253323	D5WSU178E	7.246261994	0.07143651
227	ILMN_2701851	NCAPD3	7.241077049	0.07143651
228	ILMN_2678200	GARS	7.215800991	0.07143651
229	ILMN_1233838	DOM3Z	7.214668897	0.07143651
230	ILMN_2599487	NMT1	7.204693739	0.07143651
231	ILMN_2471634	ZMPSTE24	7.191064546	0.07143651
232	ILMN_2635348	IQCB1	7.188911285	0.07143651
233	ILMN_1239921	MAN1B1	7.182310204	0.07143651
234	ILMN_2694074	GINS4	7.175242306	0.07143651
235	ILMN_1237089	GANAB	7.168846494	0.07143651
236	ILMN_2721894	EIF2B4	7.164691393	0.07143651
237	ILMN_2967528	RPL36AL	7.156775487	0.08935787
238	ILMN_2970345	SLC35A2	7.146615817	0.07143651
239	ILMN_1220362	NDUFA12	7.13209191	0.07143651
240	ILMN_2736875	PDIA3	7.120501102	0.07143651
241	ILMN_2761247	CAD	7.106769871	0.07143651
242	ILMN_1217506	DPF1	7.078850459	0.07143651
243	ILMN_1255220	ATP9A	7.073465993	0.07143651
244	ILMN_1225594	1110008P14I	7.069685528	0.07143651
245	ILMN_2657694	NDUFA9	7.067378579	0.07143651
246	ILMN_1226325	CNNM2	7.053052544	0.07143651
247	ILMN_2830661	TOP2A	7.050297172	0.07143651
248	ILMN_2695181	SMTN	7.036178683	0.08935787
249	ILMN_1251890	LOC1000454	7.0150566	0.07143651
250	ILMN_3041056	MED22	7.011393196	0.07143651
251	ILMN_3148175	PUS10	7.010992309	0.07143651
252	ILMN_2439813	SLC16A10	7.002452661	0.07143651
253	ILMN_2666108	SSBP3	6.99828403	0.07143651
254	ILMN_1231503	OXCT1	6.996442998	0.07143651

255	ILMN_1228287	CALU	6.995058092	0.08935787
256	ILMN_2603568	OBRGRP	6.979369656	0.07143651
257	ILMN_1222503	ALG5	6.97507253	0.08935787
258	ILMN_2592779	KLHL9	6.973260127	0.07143651
259	ILMN_2715802	HMGA1	6.973241673	0.07143651
260	ILMN_1220284	PSMD7	6.971346977	0.07143651
261	ILMN_2780454	S100PBP	6.961517898	0.08935787
262	ILMN_1255736	VCP	6.957897991	0.07143651
263	ILMN_2931384	LRRC59	6.95747367	0.08935787
264	ILMN_1225923	S100PBP	6.956498814	0.07143651
265	ILMN_2740176	LOC1000480	6.943973502	0.07143651
266	ILMN_2512206	WSB2	6.937131806	0.07143651
267	ILMN_2844316	DDX1	6.927261415	0.10798193
268	ILMN_2939424	ATP6AP2	6.926963588	0.07143651
269	ILMN_2591217	RARS	6.919072305	0.07143651
270	ILMN_2599618	MORF4L2	6.902649088	0.07143651
271	ILMN_2904961	2310008M10	6.895279943	0.07143651
272	ILMN_2745433	ERGIC1	6.894078399	0.07143651
273	ILMN_2790512	1110039B18	6.893913937	0.08935787
274	ILMN_2850753	MDM2	6.891278712	0.07143651
275	ILMN_3005441	PPA1	6.889586642	0.07143651
276	ILMN_2648080	KNTC1	6.88503302	0.07143651
277	ILMN_1244409	CMTM4	6.876666311	0.07143651
278	ILMN_2647590	SAMD8	6.875087805	0.07143651
279	ILMN_2588362	CDCA8	6.87399254	0.07143651
280	ILMN_1227824	JOSD1	6.86952237	0.07143651
281	ILMN_2614895	NUS1	6.864729667	0.07143651
282	ILMN_2838317	PQLC3	6.852384446	0.10798193
283	ILMN_2679464	MCM10	6.841623812	0.07143651
284	ILMN_3133489	A730035I17R	6.833667619	0.10798193
285	ILMN_2617071	NSL1	6.827775913	0.07143651
286	ILMN_2768026	GUSB	6.825630393	0.07143651
287	ILMN_1236574	CENPA	6.816088887	0.07143651
288	ILMN_2923463	KIF23	6.809926218	0.13399012
289	ILMN_1239181	NMRAL1	6.792451512	0.07143651
290	ILMN_2697433	TMEM184B	6.787962826	0.07143651
291	ILMN_2617478	PSIP1	6.781163294	0.07143651
292	ILMN_2712557	H47	6.778555538	0.07143651
293	ILMN_2884416	GALNT2	6.769382122	0.08935787
294	ILMN_2429025	WBP5	6.764253874	0.08935787
295	ILMN_1233693	SLC30A7	6.7607801	0.07143651
296	ILMN_2908070	GTSE1	6.754293048	0.08935787
297	ILMN_2870549	DNAJC3	6.748935463	0.08935787

298	ILMN_2740523	COPS2	6.73551819	0.07143651
299	ILMN_1255423	GPAA1	6.733540792	0.07143651
300	ILMN_2648746	BCKDK	6.72855879	0.07143651
301	ILMN_1224117	UHRF2	6.725582347	0.08935787
302	ILMN_2885982	TRPT1	6.723845901	0.07143651
303	ILMN_2889313	5730419I09R	6.717874989	0.07143651
304	ILMN_2722902	AMFR	6.709029849	0.07143651
305	ILMN_2974945	COG6	6.704860093	0.07143651
306	ILMN_2612079	RRBP1	6.682038084	0.08935787
307	ILMN_1245272	INSIG1	6.680894523	0.07143651
308	ILMN_2793616	LIN54	6.670535757	0.07143651
309	ILMN_1230765	TPST1	6.669566539	0.07143651
310	ILMN_2998548	PYCR2	6.664393884	0.13399012
311	ILMN_2648397	ANAPC5	6.653067591	0.10798193
312	ILMN_1251876	SRPK2	6.64806762	0.07143651
313	ILMN_2614778	SLC30A5	6.633974615	0.07143651
314	ILMN_3161617	FANCD2	6.632931528	0.10798193
315	ILMN_2812084	RCBTB2	6.620119373	0.08935787
316	ILMN_2700354	DENND5B	6.60244882	0.07143651
317	ILMN_2703563	STAC2	6.593282421	0.07143651
318	ILMN_1240387	G430055L02I	6.583620938	0.08935787
319	ILMN_1228366	CDKN2C	6.567666405	0.07143651
320	ILMN_2667234	MGAT1	6.560245653	0.07143651
321	ILMN_2759289	SLK	6.553393228	0.07143651
322	ILMN_2894245	SFMBT1	6.546467039	0.07143651
323	ILMN_2997998	SAR1B	6.528940685	0.08935787
324	ILMN_3161263	FZD5	6.528412788	0.07143651
325	ILMN_2792267	TIRAP	6.518864726	0.07143651
326	ILMN_2921303	TYMS-PS	6.515049784	0.08935787
327	ILMN_2795040	HIST1H2AD	6.511534332	0.14745975
328	ILMN_2643883	BRIP1	6.499735779	0.12248697
329	ILMN_2661125	MAGED1	6.499495095	0.08935787
330	ILMN_2861176	CALR	6.485041215	0.07143651
331	ILMN_2672325	LOC1000461	6.47478936	0.07143651
332	ILMN_2671411	KLC1	6.474523694	0.07143651
333	ILMN_2753226	RAD51AP1	6.469323914	0.08935787
334	ILMN_1237621	E430028B21I	6.451739223	0.07143651
335	ILMN_2603699	BIRC5	6.450188855	0.10798193
336	ILMN_3152241	SLC16A6	6.448071066	0.07143651
337	ILMN_2952661	DBF4	6.442283749	0.08935787
338	ILMN_2684732	HNRPLL	6.432390554	0.07143651
339	ILMN_1259473	FEN1	6.430362409	0.07143651
340	ILMN_2630769	COPE	6.425551176	0.07143651

341	ILMN_2632153	CDCA2	6.414456523	0.13399012
342	ILMN_1226712	CCDC134	6.412257709	0.07143651
343	ILMN_2795791	TMEM38B	6.403351099	0.08935787
344	ILMN_2769680	RETSAT	6.402532276	0.07143651
345	ILMN_1238246	1810074P20I	6.39412072	0.07143651
346	ILMN_2706057	2610204L23F	6.390819742	0.08935787
347	ILMN_2661287	AKP2	6.387195569	0.07143651
348	ILMN_2431237	XBP1	6.380885693	0.12248697
349	ILMN_1225035	CARHSP1	6.379195688	0.07143651
350	ILMN_2729743	SLC38A10	6.379171548	0.07143651